RE-EVALUATION OF THE SCO2 AND SC SEISMIC REFLECTION DATASETS, EASTERN SOUTH CAROLINA: IMPLICATIONS FOR TECTONIC EVOLUTION AND SEISMICITY

By

MICHAEL ROHRER

Bachelor of Science in Geophysics

Millsaps College

Jackson, Mississippi

2018

Submitted to the Faculty of the
Graduate College of the
Oklahoma State University
in partial fulfillment of
the requirements for
the Degree of
MASTER OF SCIENCE
May, 2020

RE-EVALUATION OF THE SCO2 AND SC SEISMIC REFLECTION DATASET, EASTERN SOUTH CAROLINA: IMPLICATIONS FOR TECTONIC EVOLUTION AND SEISMOGENIC ORIGIN

Thesis Approved:

Dr. James H. Knapp

Thesis Adviser

Dr. Camelia Knapp

Dr. Mohamed Abdelsalam

ACKNOWLEDGEMENTS

The completion of any large-scale project is never the result of a single person's efforts. Thus, I would like to take a moment to thank Dr. James Knapp who has consistently been a great source of advice and guidance. His genuine consultation in matters related to this project, to my career as a geophysicist, and as a friend will always be remembered. My committee members, Dr. Mohamed Abdelsalam and Dr. Camelia Knapp were incredibly helpful throughout my entire graduate career as well. Their willingness to provide feedback and mold me into a better scientist will be something I am always thankful for. I would also like to thank my wife, Kinsey Rohrer, for providing a constant source of support and encouragement. None of this would be possible without her helping me along in more ways than I can list. I would also like to thank my colleagues, Ruoshi Cao and Zachery Tunin for their listening ear and constructive criticism. Lastly, thank you Boone Pickens School of Geology and Oklahoma State University for providing all of the opportunities possible to become a better geophysicist and better person.

Name: MICHAEL ROHRER

Date of Degree: MAY, 2020

Title of Study: RE-EVALUATION OF THE SCO2 AND SC SEISMIC REFLECTION DATASET, EASTERN SOUTH CAROLINA: IMPLICATIONS FOR TECTONIC EVOLUTION AND SEISMOGENIC ORIGIN

Major Field: GEOLOGY

Abstract: Identification and characterization of the Paleozoic Suwanee basin sedimentary sequence and the associated Pangea supercontinent transcurrent fault are critical in furthering our present understanding of tectonic history and its impacts today. However, explicit bounding of the Suwannee basin has manifested itself as difficult to delineate due to thick coastal plain cover, lack of well control and petrophysical analysis, and sparse seismic reflection data. The objective of this study is to present the results and analysis of two 2D seismic reflection datasets: 1) SC reflection profiles (collected 1979) and 2) SCO2 reflection profiles (collected December 2010 to January 2011) that demonstrate the prominent regional presence of a previously uninterpreted Paleozoic sedimentary section, the Suwannee basin sequence, near the Middleton Place Summerville Seismic Zone (MPSSZ) in onshore Eastern South Carolina, as well as associated structural deformation. Previously identified offshore, this package of low-frequency, near horizontal, laterally continuous reflectors are clearly separate and distinct from overlying Jurassic/Triassic sequences above the post-rift unconformity (PRU). The interpreted base of the Paleozoic sequence is defined by the lack of laterally continuous seismic reflectors marked by crystalline basement presence. It is believed that the Suwannee basin sequence can be mapped continuously over the entire study area, which is roughly 7,010 km^2. Similar sedimentary sequences recognized from onshore exploration wells in Florida have been identified as part of the Suwannee basin sequence of Gondwanan origin. Identification of the presence and extent of these Gondwanan strata onshore implies: (1) the position of the Pangea supercontinent transcurrent fault lies roughly <40 km further northwest of the study area; (2) previously identified terranes (Brunswick, Charleston, Suwannee, Northern Florida) combine to represent Gondwana based on the size and presence of stable platform stratigraphy; (3) intraplate seismicity that occurs within the MPSSZ may be attributed to faulting observed within the study area.

TABLE OF CONTENTS

LIST OF TABLES

Table Page

LIST OF FIGURES

Figure Page

Figure Page

CHAPTER I

INTRODUCTION

Observation of a Paleozoic strata presence of Gondwanan (non-Laurentian) origin within the subsurface of southeastern United States was central in leading to Wilson's (1966) influential work on the opening and closing of ocean basins (Boote and Knapp, 2016). Denoted as the Suwannee basin by King (1961), the sequence of early- to mid- Paleozoic strata was first identified from onshore petroleum exploration wells during the early 20th century in northern Florida, southern Alabama, and southern Georgia (Applin, 1951; Barnett, 1975) (Fig. 1a). However, continued identification of the Suwannee basin's regional extent and associated boundaries of the Suwannee terrane (Fig. 1) have been challenging due to thick coastal plain cover, little analysis of deep well penetrations, and sparse onshore seismic reflection data (Williams and Hatcher, 1983; Tauvers and Muehlberger, 1987; Horton et al., 1989; Mueller at al., 2014).

1.1 Suwannee Basin

Extensive petroleum exploration during the early 20th century led to the discovery of Paleozoic age sedimentary rocks within the subsurface of the southeastern United States (Boote and Knapp, 2016). First termed as the "Suwannee River Basin," the Paleozoic sequence was found to be prominent in Florida, Georgia, and Alabama (Braunstein, 1957). The name was later shortened to the "Suwannee basin" (King, 1961). Given the continuous use of the term "Suwannee basin" to identify the region that contains the Paleozoic sedimentary sequence, this study will hold that convention in referencing the area containing the Paleozoic sedimentary sequence of Gondwanan terrane (Nelson et al., 1985; Poppe et al., 1995; Pollock et al., 2012, Boote and Knapp, 2016). Suwannee basin strata are distinct, both lithologically and faunally, from age-equivalent Appalachian foreland sequences (Boote and Knapp, 2016). Instead, the strata are closer related to similar age and faunal assemblage sedimentary rocks within the West Africa basins, such as the Bove Basin near Senegal and Guinea (Chowns and Williams, 1983; Boote and Knapp 2016). Furthermore, detrital zircon dating performed on the Suwannee basin sedimentary rocks revealed ages tying it to Gondwanan orogenic events not associated with those observed in southeastern Laurentian zircon records (Mueller et al., 1994; Mueller et al., 2014).

The Paleozoic strata is characterized by Lower Ordovician quartzites, which are likely the result of sandstone exposure to partial, low-grade metamorphism, and Middle Ordovician to Middle Devonian fossiliferous shales and sandstones that overlie complex pre-Cambrian felsic volcanic and intrusive rocks (Applin, 1951; Barnett, 1975; Chowns and Williams, 1983) (Fig. 2).

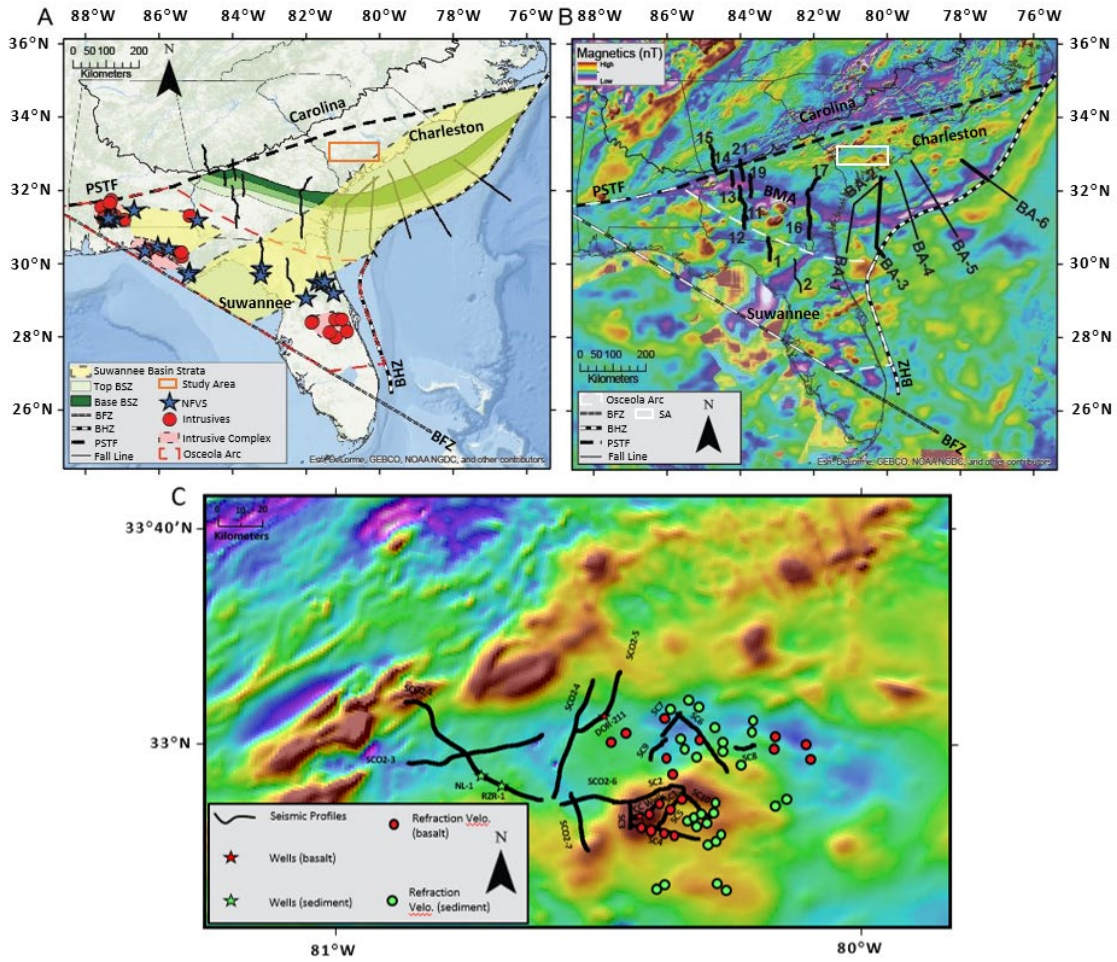

Fig. 1. (a) Map of southeastern North America (modified from Boote and Knapp, 2018) showing extent of Osceola arc (OA) constrained by Neoproterozoic intrusive (red dots) and extrusive (blue stars) rocks in the subsurface in relation to the Brunswick suture zone (BSZ; green bands) (Boote and Knapp, 2018). Subcrop of younger Paleozoic Suwannee Basin strata (SBS) lying unconformably above both the OA and BSZ shown in yellow (Boote and Knapp, 2018). Preserved lateral extent of the OA, BSZ, and SBS are limited by the younger Pangea supercontinent transcurrent fault (PSTF), Basement Hinge zone (BHZ), and Bahamas Fracture zone (BFZ). Black lines indicate seismic profiles used in (Boote and Knapp, 2018). Black stars represent the two wells in figure 1. (b) Magnetic anomaly map (modified from Boote and Knapp, 2018) in same area as figure 2a and seismic reflection profiles. Note spatial coincidence of Brunswick Magnetic anomaly (BMA) with BSZ locus. (c) Enlarged magnetic anomaly map of study area. Black lines indicate SCO2 and SC reflection seismic datasets used in this study, red stars indicate wells utilized that encountered Jurassic basalt, green stars indicate wells utilized that did encounter Jurassic basalt, red circles indicate refraction velocities greater than or equal to 5.4 km/s from (Ackermann, 1983) refraction velocity survey which indicate the presence of Jurassic basalt, green circles indicate refraction velocities less than 5.4 km/s which indicate no basalt presence.

Through the correlation of seismic refraction and reflection data alongside gravity and magnetic data, the Paleozoic sequence thickness onshore is expected to be 2.5-3 km, but wells drilled have penetrated only the upper 600 m of the sequence (Arden, 1974; Chowns and Williams, 1983; Thomas et al., 1989; Pollock et al., 2012). Further supporting Gondwanan deposition, the

Suwannee basin strata appear to represent a typical continental platform sequence with a mixed source of continental derived sands and marine muds that we expect to see in Gondwanan continental crust (Arden, 1974; Duncan, 1998).

While previous studies have used the mappable extent of Suwannee basin rocks and associated Gondwanan affinity basement to attempt to delineate the boundaries of the Suwannee terrane onshore, there is a lack of constraint as far north as the Middleton Place Summerville Seismic Zone (MPSSZ). Our method of using seismic reflection data in correlation with well data provides additional, better defined constraints on the Suwannee basin boundaries within the study area. Based on the definition provided by previous authors, we will use the term "Suwannee basin" to define the last terrane sutured onto Laurentia that consists of Suwannee basin rocks overlying Gondwanan basement.

1.2 Previous Alleghanian/Suwannee Suture Interpretations

The Alleghanian/Suwannee suture in southeast North America represents the segregation of Laurentian terrane from Gondwanan terrane, associated with the formation of the supercontinent Pangea. It may have a different tectonic history than previously thought. Previous studies that have attempted to define the exotic terrane boundaries through the use of geophysical and

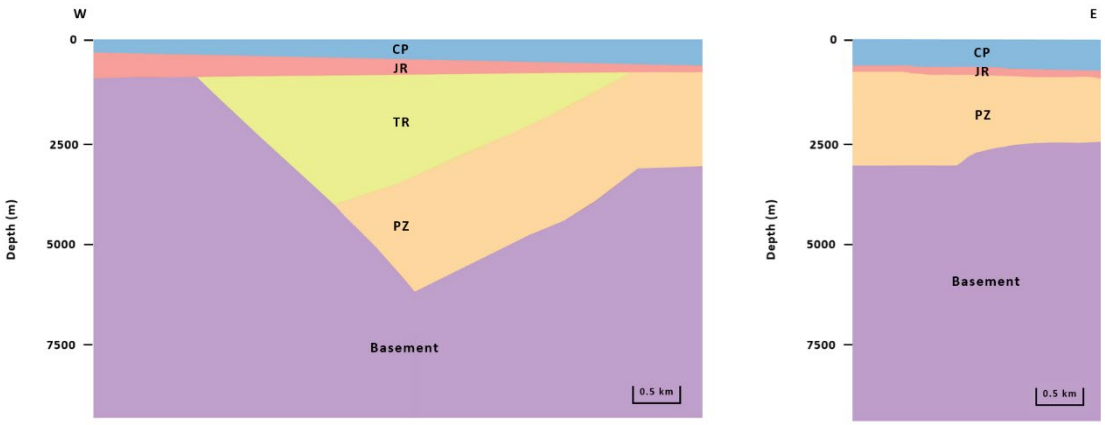

Fig. 2. Cross-section demonstrating regional geology within the study area. Two types of stratigraphic relationships are encountered. Within the asymmetric Triassic Ehrhardt basin, the presence of Triassic sediment is observed along with slight deformation (left). Outside of the Ehrhardt basin, the Triassic sediment is not present and all sequences remain relatively flat-lying (right).

geologic data have provided locations for the Alleghanian suture (Boote and Knapp, 2016). The current interpretations for the suture are well constrained in western Georgia and Alabama, but fail to continue northward into the Carolinas (Fig. 1). Previous interpretations of the suture's position, with the exception of Boote and Knapp (2016; 2018), are primarily constrained by onshore data.

With the use of aeromagnetic data, Higgins and Zeitz (1983) proposed the Alleghanian suture position along the northern boundary of the Charleston terrane as a NE-SW dextral strike-slip fault known as the Carolina-Mississippi fault (Boote and Knapp, 2016). At the same time, Chowns and Williams (1983) proposed a further south location, between Savannah and Charleston, Georgia, for the suture by mapping the subsurface extent of Gondwanan affinity sedimentary rocks using drill holes (Boote and Knapp, 2016). Then, Nelson et al. (1985) utilized seismic reflection data from the Consortium for Continental Reflection Profiling (**COCORP**) program to correlate the Alleghanian suture with a package of southward dipping reflectors and diffractions to suggest one location of the probable suture in western Georgia which coincides with the Brunswick Magnetic Anomaly (BMA) (Boote and Knapp, 2016).

There have been numerous instances in which authors suggest the BMA to closely define the Alleghanian suture (Tauvers and Muelhberger, 1987; McBride and Nelson, 1988; Horton et al., 1989) (Fig. 1). However, Suwannee basin sedimentary sequences are found north of the anomaly onshore (Boote and Knapp, 2016). Subsequent studies found that the BMA was an unlikely candidate for the Alleghanian suture (Austin et al., 1990; Oh et al., 1991; Holbrook et al., 1994; Lizarralde et al., 1994) and a correlation for its existence still did not exist (Boote and Knapp, 2016). However, (Boote and Knapp, 2018) confirmed the BMA's presence to be related to the Brunswick suture zone (BSZ) and the presence of volcanic igneous rocks which are unrelated to the suturing of Gondwana and Laurentia (Figs. 2a and 2b).

One of the more recent suture interpretations, termed the Suwannee suture instead of the Alleghanian suture, (PSTF; Fig. 1) is defined by both Mueller et al. (2014) and Thomas (2010) as overlying crustal scale dipping reflections, as seen in the COCORP profiles by Nelson et al. (1985), and conforming to the proposed dextral strike-slip stress regime of Hatcher (2010) (Boote and Knapp, 2016). While the proposed Suwannee suture zone remained largely coincident with the BMA, it could not account for the presence of Paleozoic Suwannee basin rocks found onshore north of the anomalous magnetic low (Boote and Knapp, 2016). Thus, Boote and Knapp (2016; 2018) utilized legacy Atlantic margin seismic reflection data integrated with refraction studies and well data to determine the extent of the Suwannee basin sequence offshore and provide constraints of the last sutured Suwannee terrane onshore. Due to its consistent 4-6 km presence up to the coastline, Boote and Knapp (2016;2018) proposed an interpreted Suwannee suture zone to be slightly northwest of the study area described in this investigation (PSTF; Fig. 1a).

Given the importance of understanding the extent of the Suwannee basin onshore in order to constrain the suture zone, the purpose of this study is to provide additional insight into the Suwannee basin's characteristics onshore and to gain insight as to if the Suwannee suture zone experienced post-suture dextral strike-slip motion. By utilizing an integrated dataset consisting of

unpublished SCO2 seismic reflection data collected by the Department of Energy (**DOE**) during December 2010-January 2011, previously collected SC seismic reflection data (1979 vintage) (Hamilton et al., 1983), previously collected refraction velocity data (Ackermann, 1983), and well data (Fig. 1c) we are able to analyze the Suwannee basin's characteristics in great detail.

1.3 MPSSZ Seismicity

The current focus of seismic activity within the MPSSZ, near Charleston, South Carolina, is a northwest trending zone that is active within a depth range of 2 to 12 km on a nearly vertical plane (Yantis et al., 1983). The shaking effects of the 1886 Charleston earthquake estimate that its Moment magnitude rage from Mw 6.9 to 7.3 (Johnston, 1996; Bakun and Hopper, 2004). The strongest shaking occurred in the area containing the town of Summerville which is located about 25 km to the northwest of Charleston (Dutton, 1889).

In the spring of 1974, the USGS undertook a multidisciplinary study of the 1886 Charleston earthquake region to investigate the cause of the earthquake, evaluate future seismicity, and better understand subsurface stratigraphy. Part of this study involved the acquisition of multichannel seismic reflection data that consisted of 10 seismic profiles (the same SC reflection dataset used in this study) (Hamilton et al., 1983). The resulting interpretation proposed 3 northeast trending fault planes (see Fig. 1 from Hamilton et al., 1983): (1) Drayton Fault; (2) Cooke Fault; (3) Gants Fault. The faults are interpreted where local dip of reflections are anomalously steep, disrupted laterally, and offset (Hamilton et al., 1983). Thus, the configurations of these reflections suggest tectonic significance (Hamilton et al., 1983). It is also important to note that the fault plane trends of the Drayton, Cooke, and Gants faults parallel that of the Helena Banks fault which has been significantly substantiated (see Fig. 1 from Behrendt et al., 1983).

Later, Weems and Lewis (2002) and Chapman and Beale (2008, 2010) aimed to describe the geologic setting of the epicentral area and find evidence for the source of seismicity within the

MPSSZ region. Utilizing well data, seismic reflection data, and potential field data, they found that the Coastal Plain and early Mesozoic sediments comprised most of the near surface stratigraphy. Furthermore, Cretaceous and Cenozoic marine sediments provided thick cover beneath the Coastal Plain and early Mesozoic sediment. Chapman and Beale (2010) also documented evidence for extensive faulting within the early Mesozoic rocks. Seismic profiles imaged associated folding and faulting of Cretaceous and Cenozoic Coastal Plain sediments at five locations in the 1886 epicentral region (Chapman and Beale, 2010). They proposed that, given its spatial association with the seismogenic activity that occurs in the region, these faults were likely related to the earthquakes that are occurring (Chapman and Beale, 2010).

In an additional study, Chapman and Beale (2016) utilized data from an eight-station temporary seismic network that operated for one year in the Summerville area alongside the previously mentioned shallow crustal reprocessed seismic reflection profiles and analogies drawn from their recent study on the 2011 Mineral, Virginia earthquake (Chapman, 2013; Wu et al., 2015) to propose yet another hypothesis as to the cause of the 1886 Charleston event. It is in this study that they propose that modern seismicity in the region is the result of later-term aftershock activity of the 1886 earthquake (Chapman and Beale, 2016). Furthermore, they present evidence suggesting that the earthquakes are originating in a single, extensive tabular zone that trends south and dips to the west (Chapman and Beale, 2016).

Various tectonic models have been suggested to explain the origin of seismogenic activity that occurs within the MPSSZ. These models have consisted of everything from compressional stepovers, restraining bends, and intersections of major strike-slip and reverse faults (Chapman and Beale, 2016). The fault source for the major 1886 earthquake has been a challenging problem to solve. Previous studies have utilized geophysical, geological, and geomorphological data in an attempt to find the source of these events (Chapman and Beale, 2016). The motivation behind this study is to see if any new discoveries may further substantiate or refute previously proposed

hypotheses, particularly under the framework of the Suwannee basin's presence within this region.

CHAPTER II

STUDY AREA

Previous analyses of the study area, which covers roughly 7,010 km^2 within onshore Eastern South Carolina (Fig. 1), have concluded that the region is a Triassic rift basin, correlated with the South Georgia Rift basin (SGR), with earthquake focal depths varying from 2-12 km and focal mechanisms trending N60E (Heffner et al., 2011). Previous interpretation of subsurface geology has denoted that regional stratigraphy consists of (shallow to deep): (a) Cenozoic to Cretaceous Coastal Plain sedimentary sequence; (b) Jurassic Basaltic layer; (c) Late Triassic Redbed sequence; (d) Early to Mid-Triassic Crystalline basement (Gohn, 1983; Hamilton et al., 1983; Schilt et al., 1983; Chapman and Beale, 2008). However, analysis and interpretation from this study revises the previous subsurface geology to include the Suwannee basin sedimentary sequence overlying Gondwanan basement, both of which were previously interpreted as Triassic crystalline basement (Figs. 1 and 3).

Regional structure outside of Triassic basins consists of generally flat-lying, laterally extensive sedimentary sequences with some near vertical faulting apparent. However, within the Triassic basin present in the study area, known as the Ehrhardt basin, we see slight deformation occurring within both the Paleozoic Suwannee basin sequence as well as the Triassic basin sequence while Coastal Plain and Jurassic sedimentary sequences remain relatively flat lying (Fig. 3).

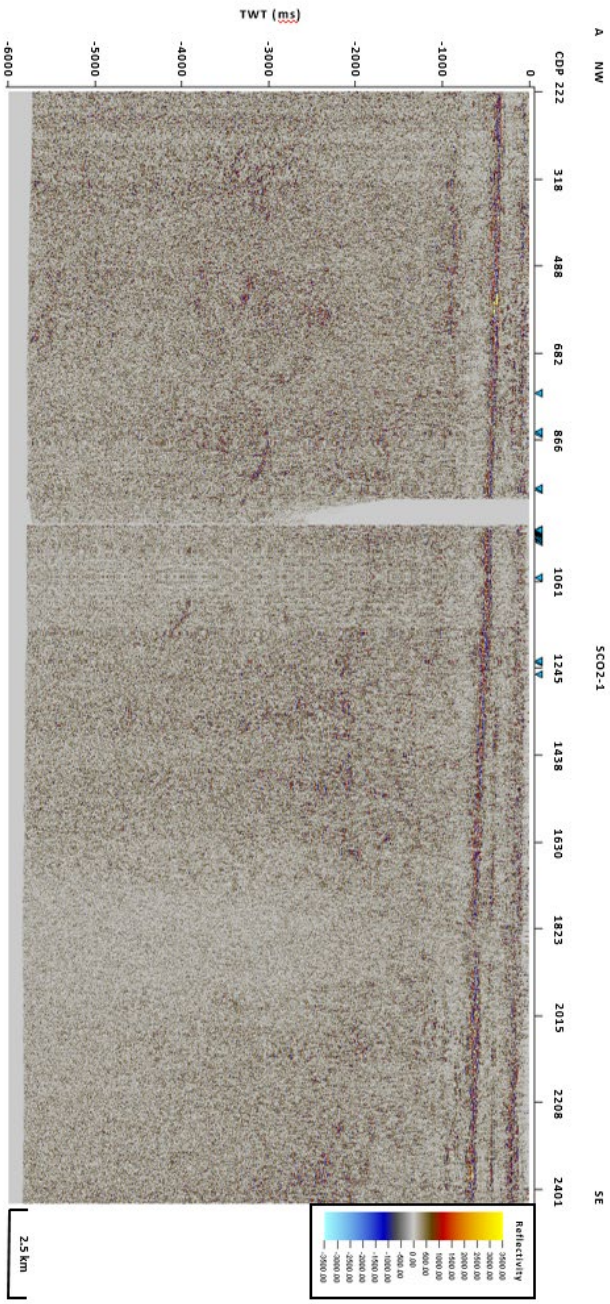
A NW
SE
SCO2-1
TWT (ms)
0
-1000
-2000
-3000
-4000
-5000
-6000
CDP 222
318
488
682
866
1061
1245
1438
1630
1823
2015
2208
2401
Reflectivity
2.5 km

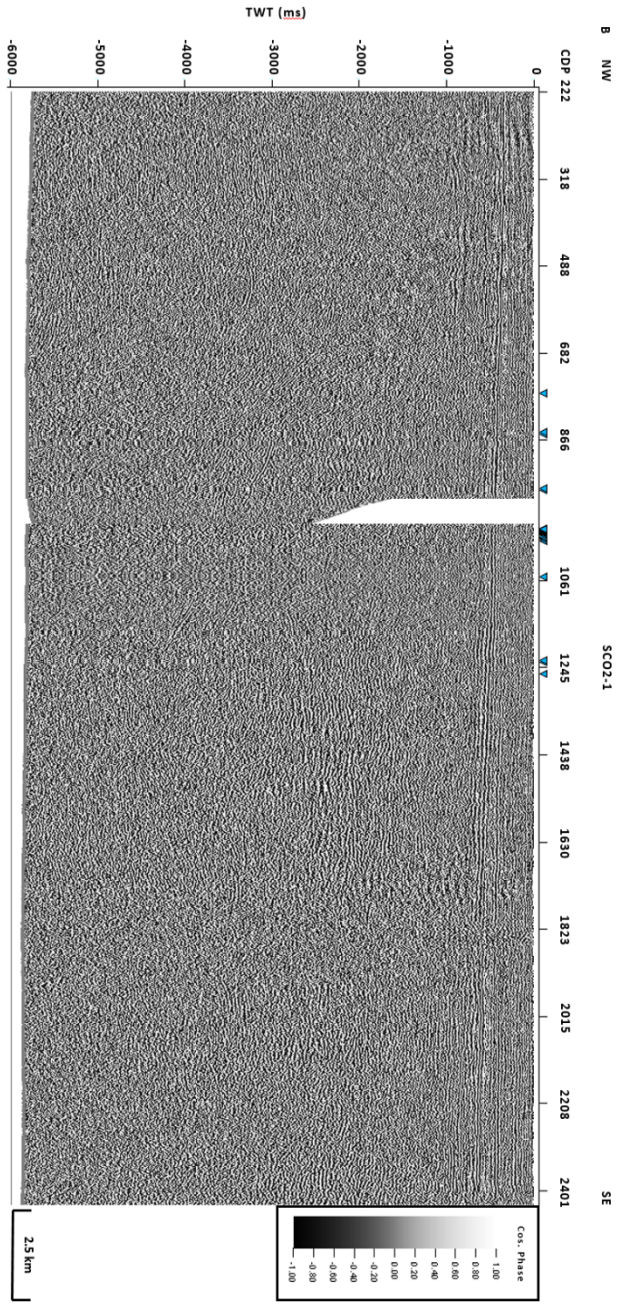
B
NW
SCO2-1
SE
CDP 222
318
488
682
866
1061
1245
1438
1630
1823
2015
2208
2401
TWT (ms)
0
-1000
-2000
-3000
-4000
-5000
-6000
Cos. Phase
1.00
0.80
0.60
0.40
0.20
0.00
-0.20
-0.40
-0.60
-0.80
-1.00
2.5 km

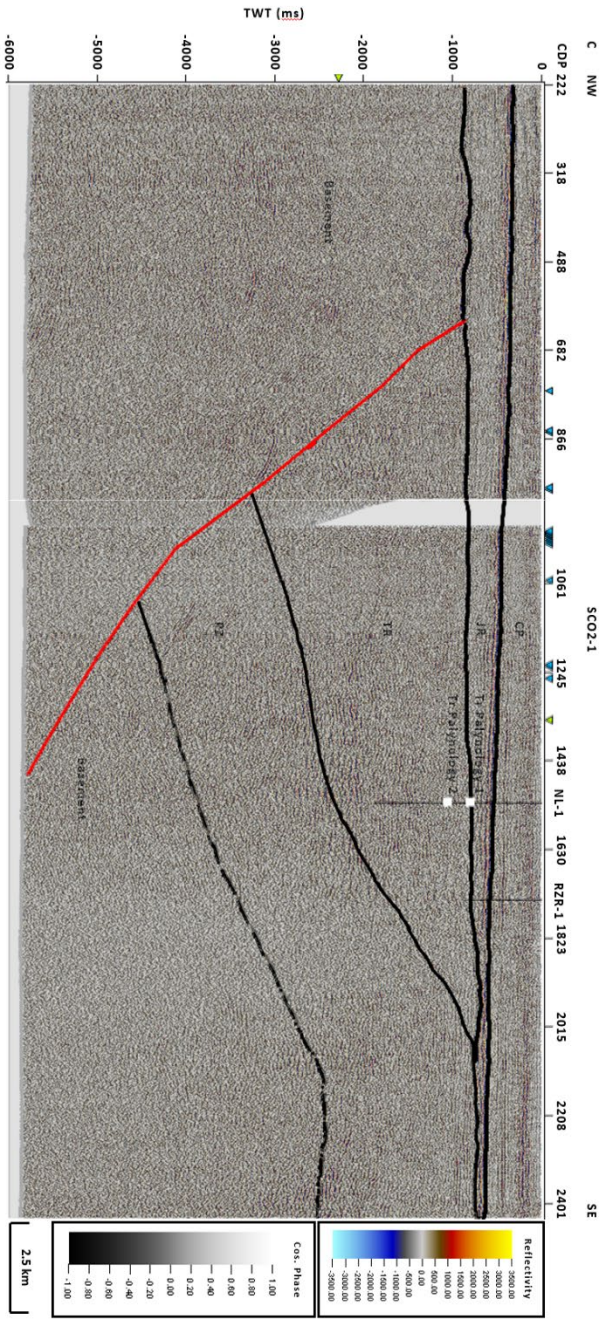

Fig. 3. SCO2-1 reflectivity seismic profile uninterpreted (a), cosine of phase profile uninterpreted (b), and interpreted reflectivity co-rendered with cosine of phase (c). SCO2-1's location (Fig. 1c) lies within an asymmetrical Triassic rift basin within the study area. It demonstrates the stratigraphic relationships of the Cretaceous Coastal Plain sedimentary sequence (CP), Jurassic sedimentary sequence (JR), Triassic sedimentary sequence (Tr), Paleozoic Suwannee basin sedimentary sequence (PZ), and basement. SCO2-1 shows the slight deformation we see within both the Triassic and Paleozoic sequences when located within a Triassic rift basin. The deformation is highlighted by the disruption of lateral consistency and abrupt dip change within reflector packages in both the reflectivity and cosine of phase profiles. The Norris-Lightsey #1 well contains palynology samples reinforcing the Triassic basin's presence (Traverse, 1987).

CHAPTER III

METHODS

The purpose of this study is to build upon the formerly mentioned work of Thomas (2010), Mueller et al. (2014), Boote and Knapp (2016), and Boote and Knapp (2018) to further constrain the extent of the Suwannee basin such that the location of the Suwannee suture zone can be better refined as the Pangea supercontinent transcurrent fault and its location further north, near eastern onshore South Carolina, can be better defined. By utilizing an integrated data set consisting of seismic reflection data (SCO2 and SC datasets), refraction velocities, and well data, we can better constrain our observations. Furthermore, due to the study location's presence near the MPSSZ, structural deformation is observed to see if it has any correlation to known seismicity within the region.

3.1 SCO2 Seismic Data

The SCO2 seismic reflection data was collected from Dec. 2010 to Jan. 2011 (Fig 2c). Acquisition parameters (summarized in Table 1) consist of rolling into a split spread followed by a rollout utilizing a vibroseis source sweeping from 10-72 Hz for 8000 ms while 240 stations record. Each station is comprised of 12 geophones (10 Hz) over a 52 m spread such that the 12 geophones could be stacked into a single station and improve the signal to noise ratio of the acquisition. The geophones record for 6000 ms at a 2 ms sample rate. Shot points are halfway between station locations (or 26 m from each station).

Table 1	
Generalized Acquisition Parameters for SCO2 Seismic Reflection Survey	
Polarization	P-wave
Energy Source	Vibroseis Unit (8-72 Hz Sweep for 8000 ms)
No. of Stations	240 (12 geophones spaced across 52 m - per station)
Geophone Frequency	10 Hz
Shot Offset	26 m (shot point in between stations spaced 52 m apart)
Station Spacing	52 m
Sample Rate	2 ms
Maximum Fold	240
Spread Configuration	Roll into split spread and roll out

3.2 SC Seismic Data

In 1979 the U.S. Geological Survey (USGS) acquired 140 km of multichannel seismic reflection data along ten profiles termed SC1-SC10 (Fig. 1c). The profiles were collected to obtain regional coverage throughout the area of Charleston, SC to investigate features related to seismogenic activity, particularly the 1886 earthquake that occurred (Behrendt and Hamilton, 1982). Acquisition parameters (summarized in Table 2) consisted of a split spread with a vibroseis source. The source occurs between stations which are 120 m away. There are 60 m between stations with 48 stations causing as much as 1500 m of separation from the last station to the vibration point, on either side. The source generated a seven-second sweep ranging from 10-60 Hz. The sample rate is 4 ms with a 3 s total recording time.

Table 2	
Generalized Acquisition Parameters for SC Seismic Reflection Survey	
Polarization	P-wave
Energy Source	Vibroseis Unit (10-60 Hz Sweep for 7000 ms)
No. of Stations	48
Geophone Frequency	10 Hz
Shot Offset	60 m (shot point in between stations spaced 120 m apart)
Station Spacing	120 m
Sample Rate	4 ms
Maximum Fold	12 (from paper)
Spread Configuration	Split Spread

3.3 Well Data

Available well data consisted of six wells: (1) Norris-Lightsey #1 (NL-1); (2) Rizer #1 (RZR-1); (3) Dorchester 211 (DOR-211); (4) Clubhouse Crossroads #1 (CC1); (5) Clubhouse Crossroads #2 (CC2); (3) Clubhouse Crossroads #3 (CC3) (Fig 2c.). Both NL-1 and RZR-1 lie on seismic line SCO2-1 with available density and sonic data in LAS file format such that they can be tied into the SCO2-1 profile. DOR-211 lies on seismic line SCO2-5 with available density and sonic data in LAS file format such that it can be tied into the SCO2-5 profile. Wells CC1-3 intersect profile SC1, but only well descriptions are available. Thus, they were not able to be tied into the seismic profile itself. However, the descriptions still aid in interpretation.

NL-1 (Fig. 4) is a deep oil test well drilled ~70 km west of Summerville, South Carolina in Colleton County. It penetrated the base of the Coastal Plain sediment at a depth of ~610 m before it reached a total depth of ~4115 m within Triassic sediment (Heffner, 2013). Pollen collected from cuttings between 1373 m and 2184 m were dated by Traverse (1987) to be Triassic in age.

RZR-1 (Fig. 4) is a scientific well in Colleton County, ~3 km SW of NL-1. It encountered diabase while reaching a total depth of ~1890 m. DOR-211 (Fig. 4) is located in Dorchester County,

South Carolina. It is located ~42 km NE of NL-1 and reached a total depth of ~631 m where it bottomed in basalt.

CC#1 (Fig. 4), located 40 km NW of Charleston, SC drilled through Coastal Plain sediment until it reached a total depth of 792 m where it bottomed in 42 m of Jurassic age basalt. CC#2 (Fig. 4), located just SW of CC#1, encountered similar lithology in which it drilled to a depth of 907 m. CC#3 (Fig. 4), furthest SW from CC#1, also encountered the same lithology and reached a total depth of 1152 m in which it bottomed in redbeds.

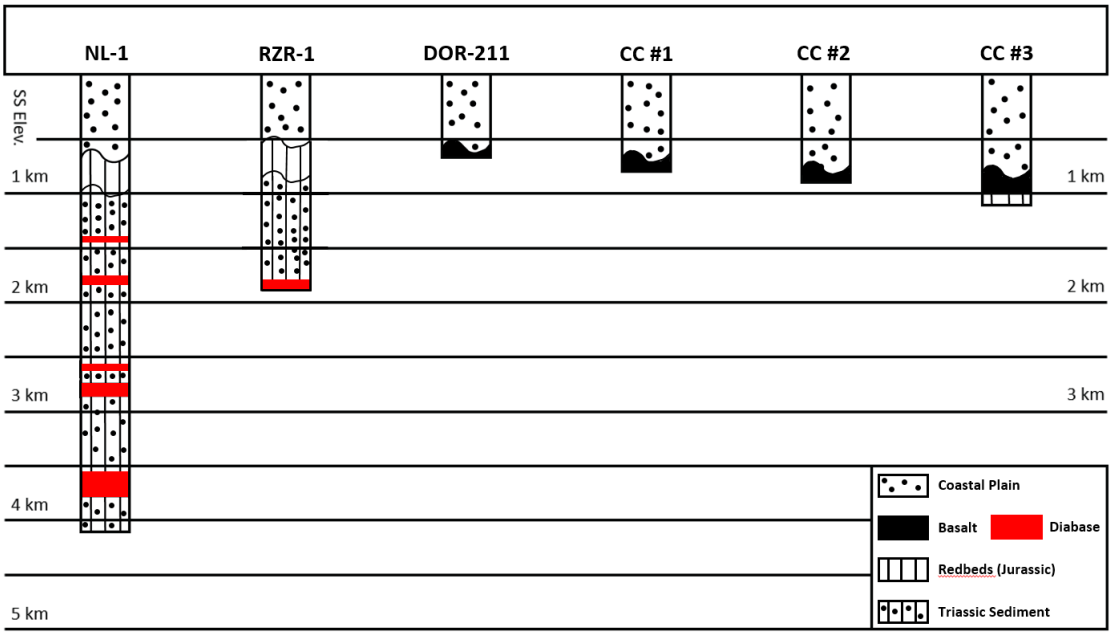

Fig. 4. Generalized stratigraphic columns for all wells used in this study demonstrating Coastal Plain sediment, Jurassic basalt, Jurassic redbeds, diabase and Triassic sediment.

3.4 Pre-Stack Processing (SCO2 Seismic Data)

A traditional pre-stack processing flow was utilized to obtain adequate stacked profiles within the SCO2 seismic dataset. Halliburton's SeisSpace was the software used to process the pre-stack data. The processing flow (summarized in Table 3) began with importing the raw SEGY shot gathers into SeisSpace. Then, a 2D land geometry spreadsheet was created and applied to the raw shot gathers. Next, if necessary, the vibroseis shot gathers were correlated. The following steps consisted of multiple muting methods – trace kills on noisy traces, upper end muting, and spectral analysis to create an ormsby bandpass filter (with a 60 Hz notch filter). Then, automatic gain control was applied to enhance the inherently low amplitude reflection signal. Next, CDP sorted shot gathers were utilized to allow a properly performed velocity analysis. 'Supergather' Semblance Velocity analysis was used to pick optimum stacking velocities. 15 CDPs per panel were used. After velocity analysis was complete, the velocity volume was slightly smoothed. Lastly, datum statics, normal moveout corrections (NMO), and predictive deconvolution were all applied to the CDP gathers. The purpose of the predictive deconvolution was to dissipate any coherency in reflectors that may occur as multiples. The CDPs were then stacked to create a seismic profile.

Table 3
Standard Procedures Used for Processing SCO2 Profiles
1. SEGY Import
2. 2D Land Geometry
2a. If necessary, Correlation of Vibroseis Shot Gathers
3. Muting (Trace Kills, Upper End Muting, Ormsby Bandpass Filtering)
4. Automatic Gain Control
5. CDP Sort
6. Supergather Semblance Velocity Analysis
7. Datum Statics
8. Normal Moveout Correction
9. Predictive Deconvolution
10. CDP Stack

3.5 Post-Stack Analysis (both SCO2 and SC Seismic Data)

Any post-stack analysis, performed in Schlumberger's Petrel software, aided in the interpretation stage of the analysis. By decomposing the reflectivity signal into its individual components, known as attributes, discrepancies within the data can be more easily identified and consistencies within reflector packages become more apparent. Thus, correlation of reflector packages within the 2D profiles become easier. The attributes utilized consist of: Root Mean Square (RMS) amplitude, Instantaneous Phase, and Cosine of Phase.

RMS Amplitude

RMS amplitude (Equation a) computes a scaled rms average of reflectivity on instantaneous trace samples over a specified window. It often resembles a smoother version of a reflectivity volume. As reflectivity is indicative of acoustic impedance and acoustic impedance is the product of density and velocity, RMS amplitude provides the ability to visualize amplitude anomalies (bright spots, dim spots, change in amplitude character) on an absolute scale rather than a relative scale. Hence, it can be helpful in identifying coarse-grained facies, compaction related effects, and unconformities (Koson et al., 2014).

Eq. A:

$$RMS_1[T,i] = \sqrt{\frac{1}{n}\sum_{j=i-n/2}^{j=i+n/2} T[j]^2}$$

Equation representing the RMS Amplitude volume calculation where *T(i)* represents a single trace sample, over a specified vertical window length of *n* samples for each sample in an input trace *T*.

Instantaneous Phase

Instantaneous phase ($\phi(t)$) (Equation b) is given by the arc tangent of the seismic trace (T(t)) and its Hilbert transform (H(t)). It is measured in degrees from -180 to 180. Given its independence from amplitude, it is useful in showing continuity by demonstrating consistency of phase, discontinuity by demonstrating a phase change, and bedding configuration by showing phase characteristic of that bedding.

Eq. B:

$$\phi(t)=\tan^{-1}[H(t)/T(t)]$$

where (T(t)) is the seismic trace and (H(t)) is its Hilbert transform

Cosine of Phase

Cosine of phase (C(t)) is also independent of amplitude and shows bedding very well. It is smoother than instantaneous phase and is helpful when used in conjunction with instantaneous phase. It is derived simply by taking the cosine of phase ($\phi(t)$).

CHAPTER IV

RESULTS AND DISCUSSION

4.1 Suwannee Basin Sequence

Throughout all 15 seismic profiles, we see a consistent presence of near horizontal, low frequency, laterally continuous package of reflectors lying beneath either Triassic or Jurassic sediment (Fig. 5 and 6). This package is interpreted as Suwannee basin sediment. Furthermore, the attributes of this reflector package are maintained throughout all 15 profiles. These attributes can act as a seismic signature for the Suwannee basin sequence reflectors.

When looking at the reflectivity profiles, we see a significant peak marking the top of the Paleozoic Suwannee basin sequence (Fig. 6). This is consistent with what we would expect as the overlying Triassic and Jurassic sediments have lower velocities, but are also likely less compacted which would give them lower elasticity constant values relative to the underlying Suwannee basin sequence. Furthermore, the RMS amplitude of the boundary between the Suwannee basin sequence and overlying sediment is marked by a laterally continuous anomalous high (Fig. 7). As previously mentioned, RMS amplitude is effective for highlighting the facies change that occurs from the presence of the underlying Suwannee basin sequence and compaction related effects. Hence, it is likely picking up these two variables and their impact on the overall reflectivity of the boundary.

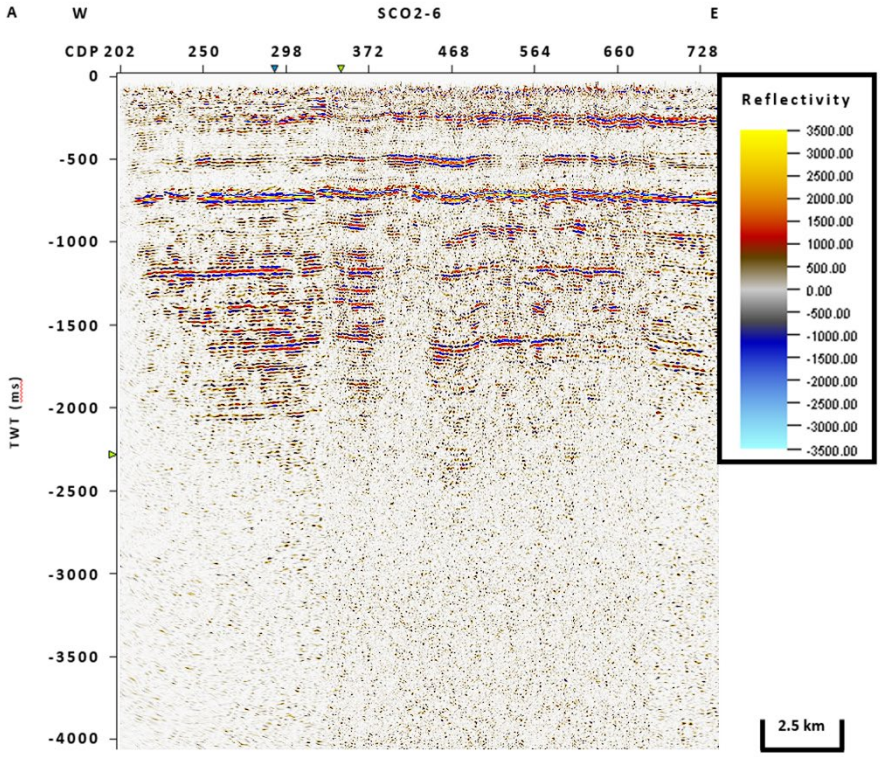
A
W
SCO2-6
E
CDP 202
250
298
372
468
564
660
728
0
-500
-1000
-1500
-2000
-2500
-3000
-3500
-4000
TWT (ms)
Reflectivity
3500.00
3000.00
2500.00
2000.00
1500.00
1000.00
500.00
0.00
-500.00
-1000.00
-1500.00
-2000.00
-2500.00
-3000.00
-3500.00
2.5 km

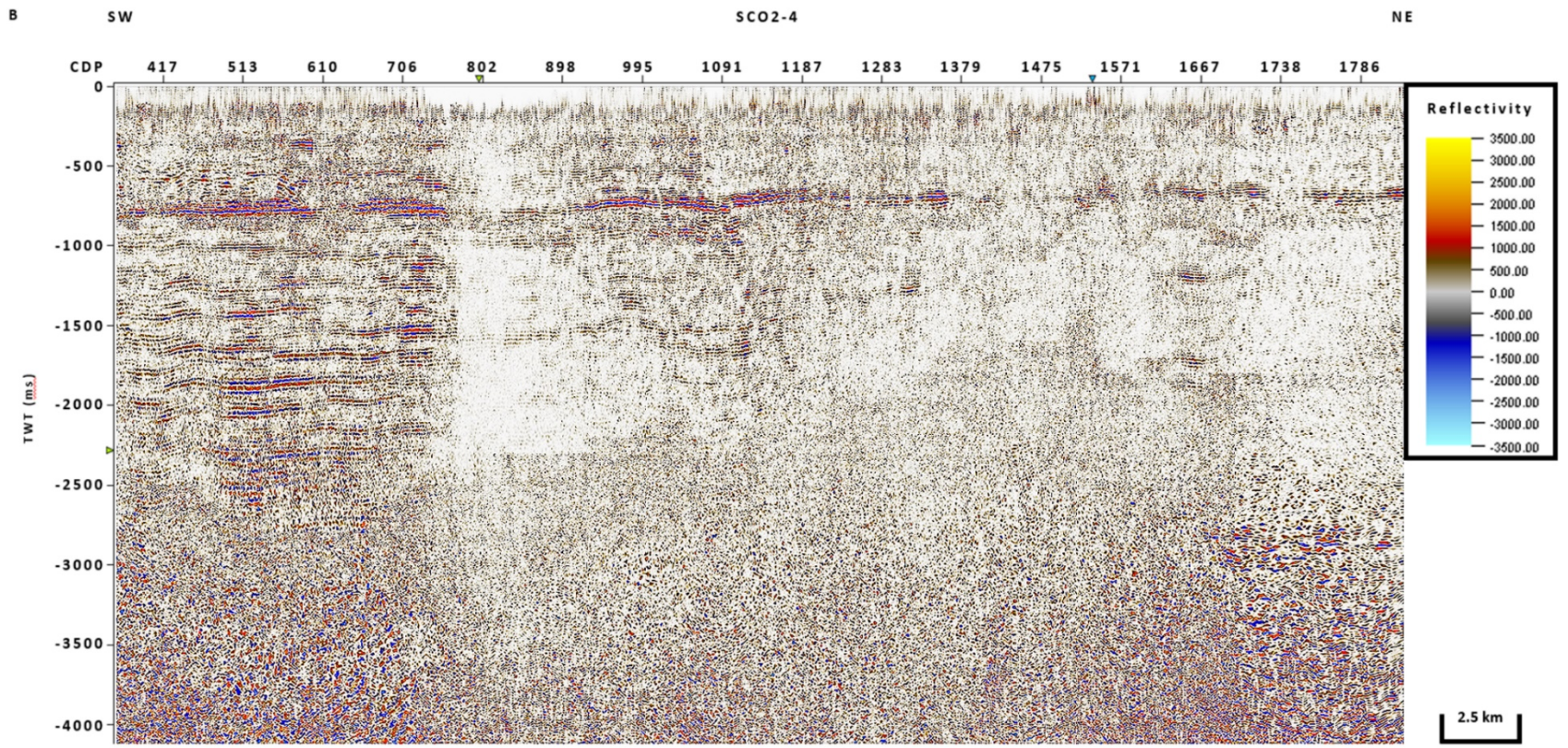
B
SW
SCO2-4
NE
CDP
417
513
610
706
802
898
995
1091
1187
1283
1379
1475
1571
1667
1738
1786
0
-500
-1000
-1500
-2000
-2500
-3000
-3500
-4000
TWT (ms)
Reflectivity
3500.00
3000.00
2500.00
2000.00
1500.00
1000.00
500.00
0.00
-500.00
-1000.00
-1500.00
-2000.00
-2500.00
-3000.00
-3500.00
2.5 km

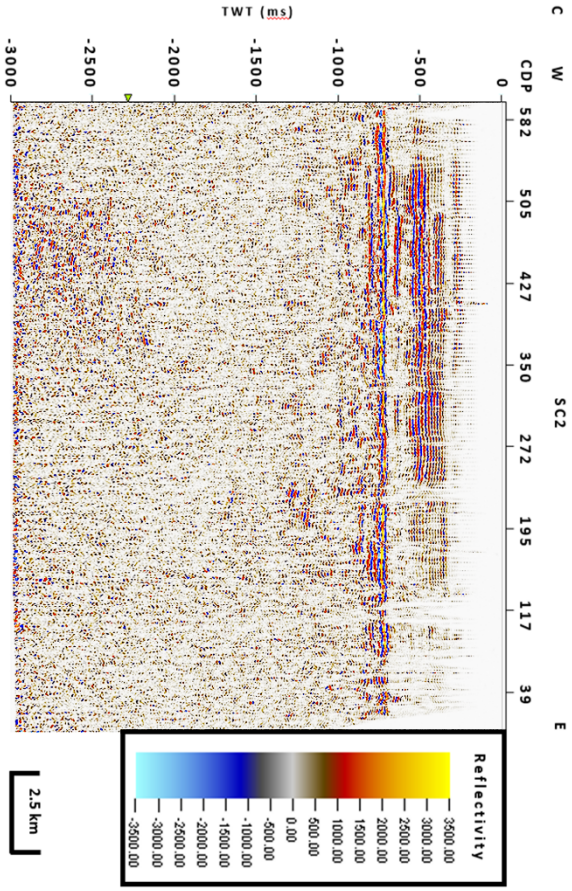
C
W
CDP 582
505
427
350
SC2
272
195
117
39
E
TWT (ms)
0
-500
-1000
-1500
-2000
-2500
-3000
Reflectivity
3500.00
3000.00
2500.00
2000.00
1500.00
1000.00
500.00
0.00
-500.00
-1000.00
-1500.00
-2000.00
-2500.00
-3000.00
-3500.00
2.5 km

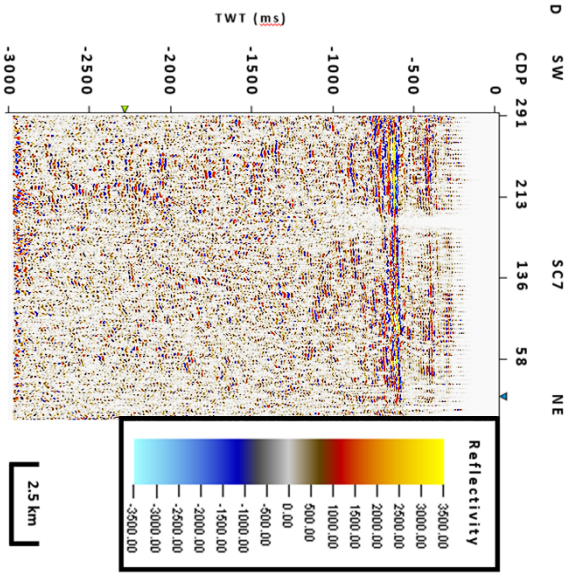

Fig. 5. Uninterpreted reflectivity profiles SCO2-6 (a), SCO2-4 (b), SC2 (c), and SC7 (d) covering the entire stratigraphic section seen in the study area outside of the Triassic rift basin. These profiles were chosen because they provide regional coverage within the study area (Fig. 1c).

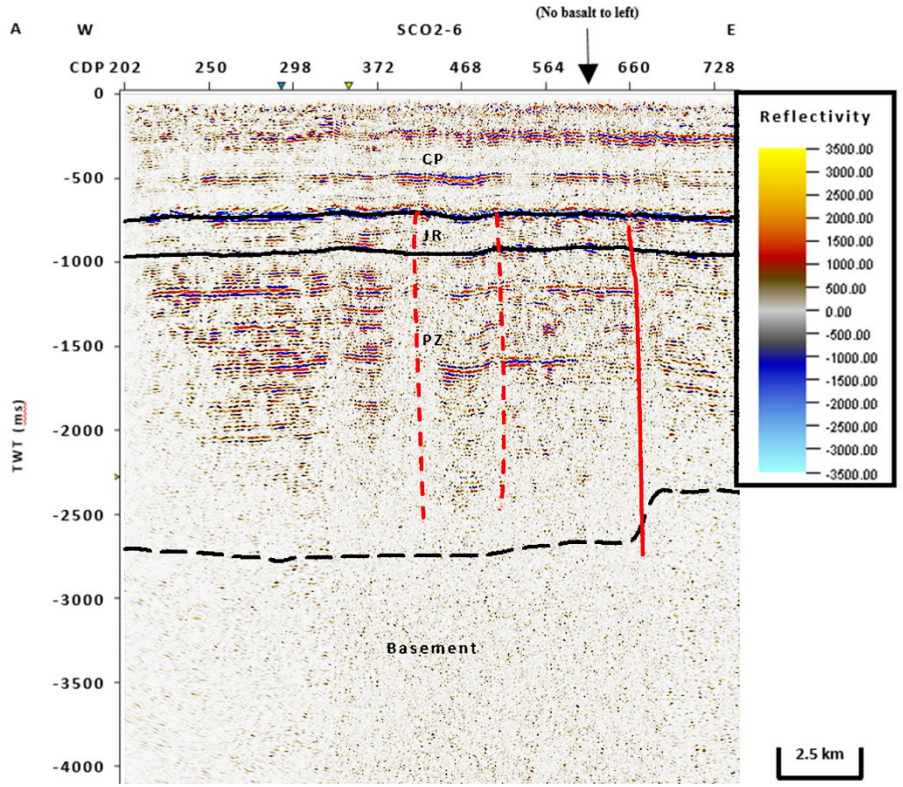
A
W
SCO2-6
E
(No basalt to left)
CDP 202
250
298
372
468
564
660
728
0
-500
-1000
-1500
-2000
-2500
-3000
-3500
-4000
TWT (ms)
CP
JR
PZ
Basement
Reflectivity
3500.00
3000.00
2500.00
2000.00
1500.00
1000.00
500.00
0.00
-500.00
-1000.00
-1500.00
-2000.00
-2500.00
-3000.00
-3500.00
2.5 km

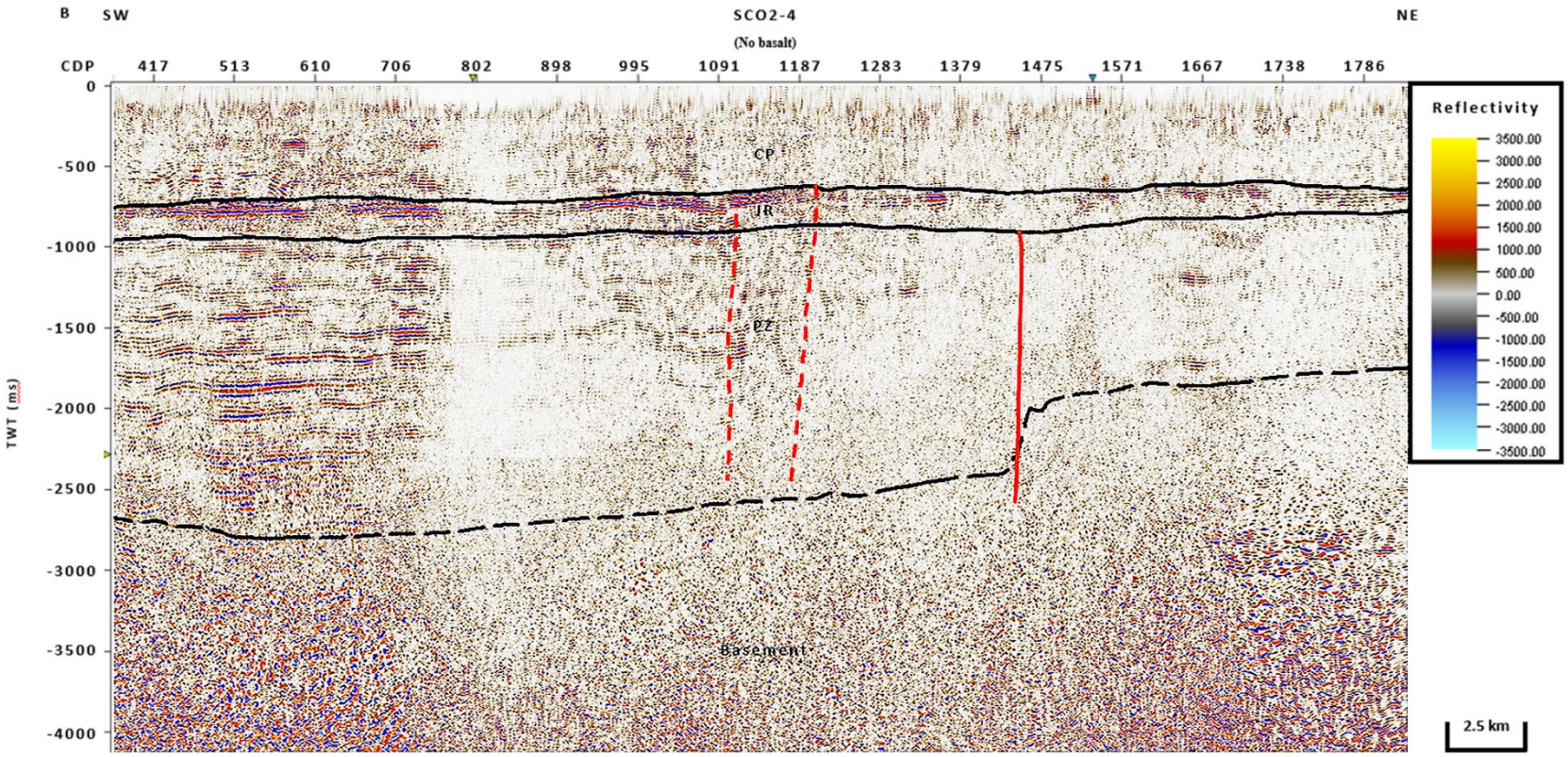
B
SW
SCO2-4
(No basalt)
NE
CDP
417
513
610
706
802
898
995
1091
1187
1283
1379
1475
1571
1667
1738
1786
0
-500
-1000
-1500
-2000
-2500
-3000
-3500
-4000
TWT (ms)
CP
JR
PZ
Basement
Reflectivity
3500.00
3000.00
2500.00
2000.00
1500.00
1000.00
500.00
0.00
-500.00
-1000.00
-1500.00
-2000.00
-2500.00
-3000.00
-3500.00
2.5 km

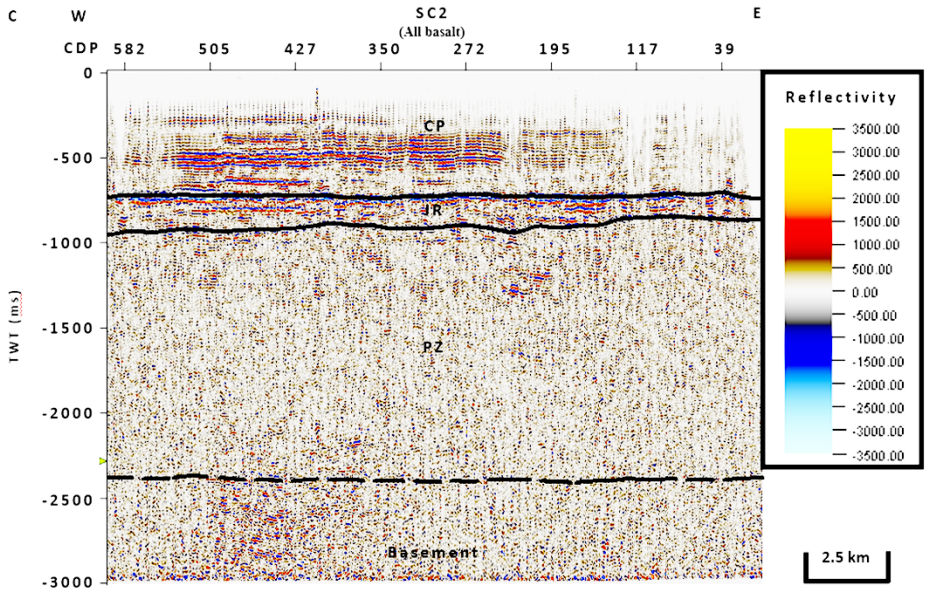
C
W
SC2
(All basalt)
E
CDP 582 505 427 350 272 195 117 39
0
-500
-1000
-1500
-2000
-2500
-3000
TWT (ms)
CP
JR
PZ
Basement
Reflectivity
3500.00
3000.00
2500.00
2000.00
1500.00
1000.00
500.00
0.00
-500.00
-1000.00
-1500.00
-2000.00
-2500.00
-3000.00
-3500.00
2.5 km

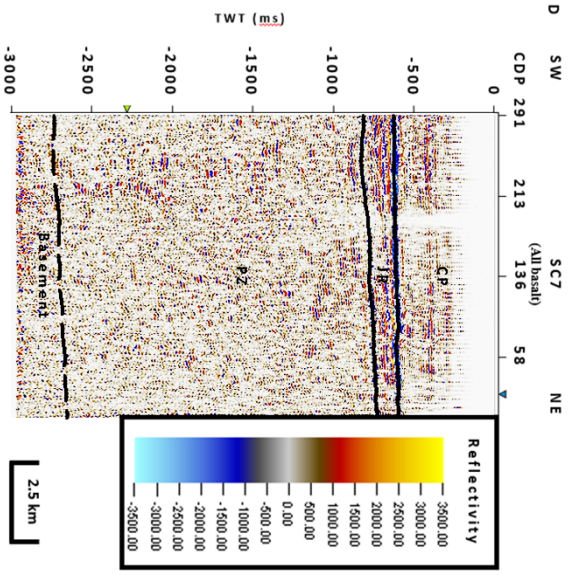

Fig. 6. Interpreted reflectivity profiles SCO2-6 (a), SCO2-4 (b), SC2 (c), and SC7 (d) covering the entire stratigraphic section seen in the study area outside of the Triassic rift basin. These profiles were chosen because they provide regional coverage within the study area (Fig. 1c). Note that all 4 profiles demonstrate near-horizontal dip, lateral continuity, and low frequency within the original seismic trace reflector packages for the sedimentary Paleozoic section. Solid red lines indicate faulting that correlates with magnetic high boundaries (Fig 18) and demonstrate disruption of lateral continuity, amplitude loss, and sudden dip change through the entire Suwannee basin sequence down to basement. Dashed red lines indicate accessory faulting based on disruption of lateral continuity, amplitude loss, and sudden dip change.

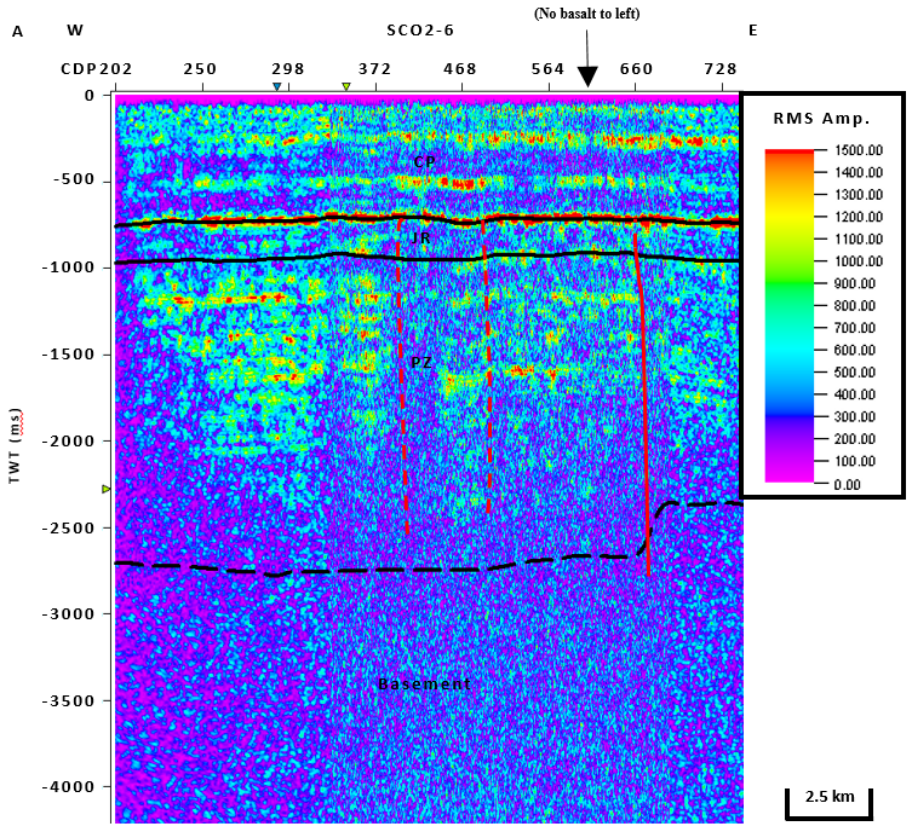
A
W
SCO2-6
(No basalt to left)
E
CDP202
250
298
372
468
564
660
728
0
-500
-1000
-1500
-2000
-2500
-3000
-3500
-4000
TWT (ms)
CP
JR
PZ
Basement
RMS Amp.
1500.00
1400.00
1300.00
1200.00
1100.00
1000.00
900.00
800.00
700.00
600.00
500.00
400.00
300.00
200.00
100.00
0.00
2.5 km

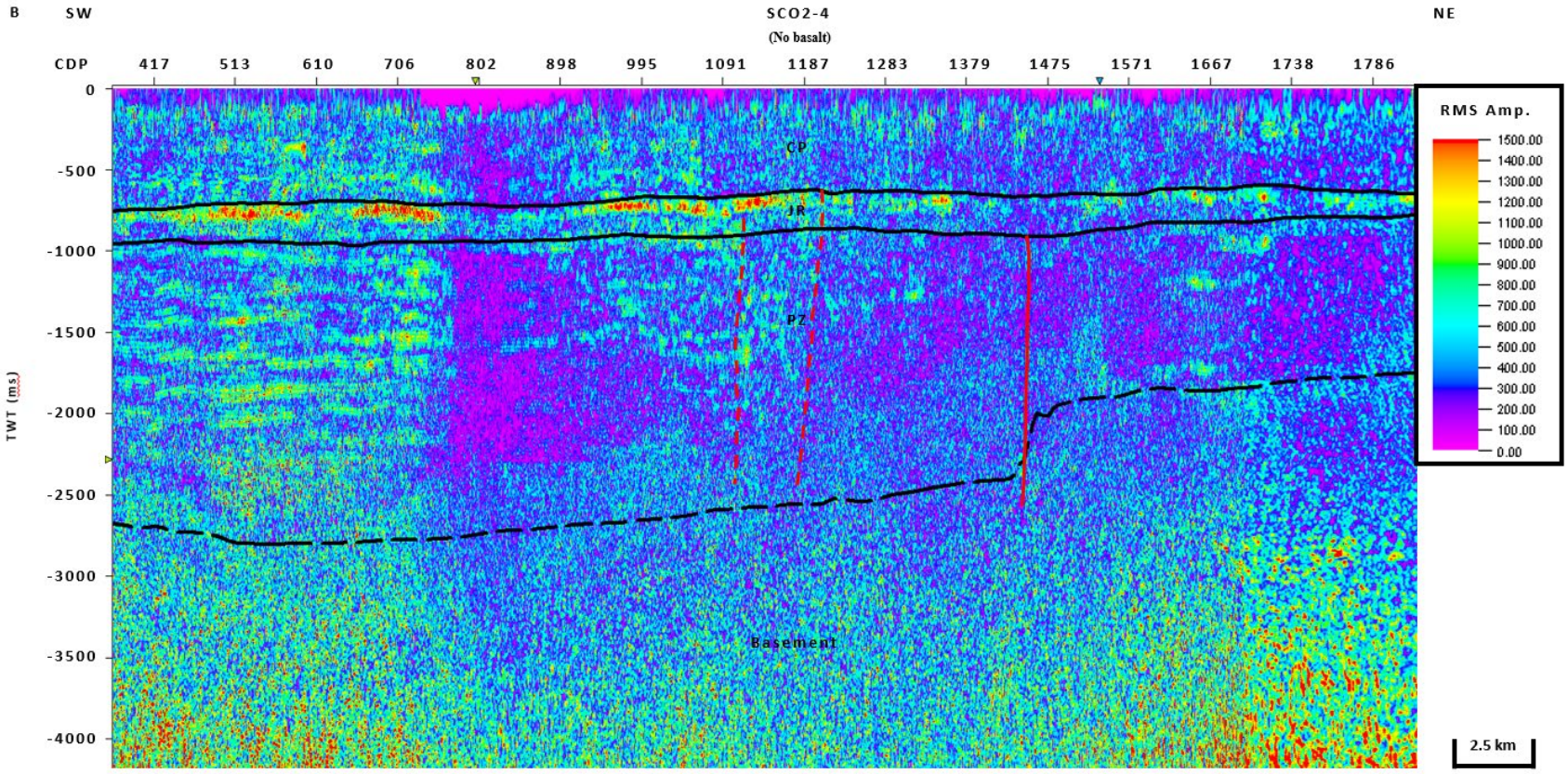
B
SW
SCO2-4
(No basalt)
NE
CDP
417
513
610
706
802
898
995
1091
1187
1283
1379
1475
1571
1667
1738
1786
0
-500
-1000
-1500
-2000
-2500
-3000
-3500
-4000
TWT (ms)
CP
JR
PZ
Basement
RMS Amp.
1500.00
1400.00
1300.00
1200.00
1100.00
1000.00
900.00
800.00
700.00
600.00
500.00
400.00
300.00
200.00
100.00
0.00
2.5 km

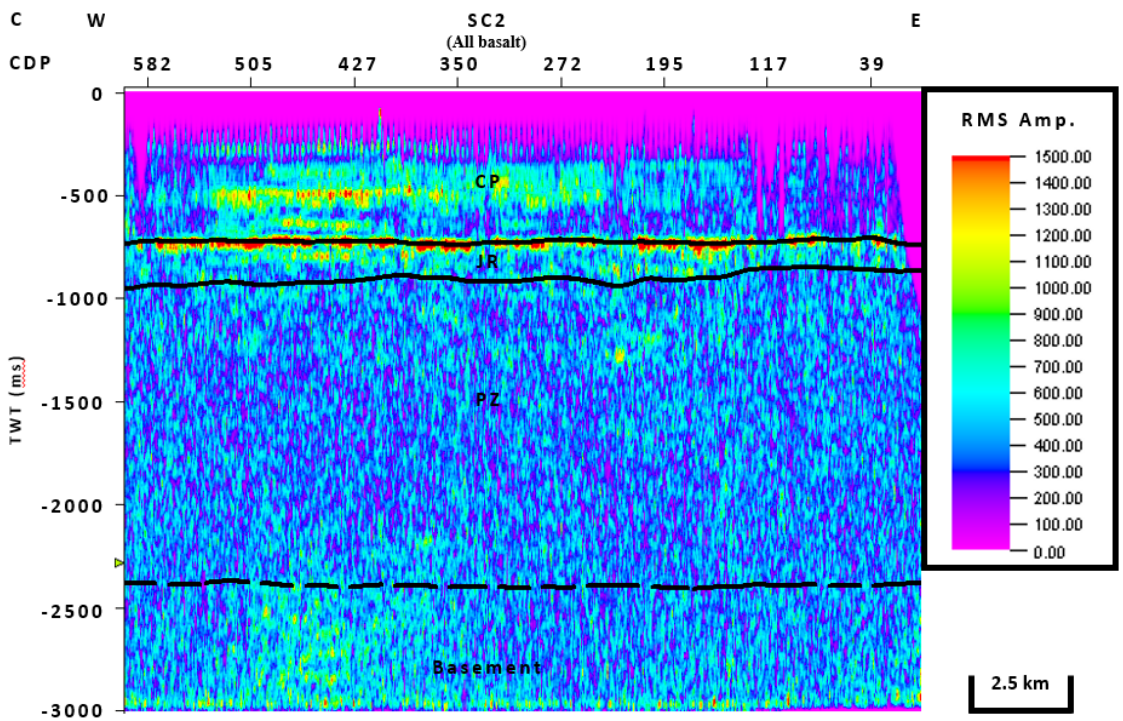
C
W
SC2
(All basalt)
E
CDP
582
505
427
350
272
195
117
39
0
-500
-1000
-1500
-2000
-2500
-3000
TWT (ms)
CP
JR
PZ
Basement
RMS Amp.
1500.00
1400.00
1300.00
1200.00
1100.00
1000.00
900.00
800.00
700.00
600.00
500.00
400.00
300.00
200.00
100.00
0.00
2.5 km

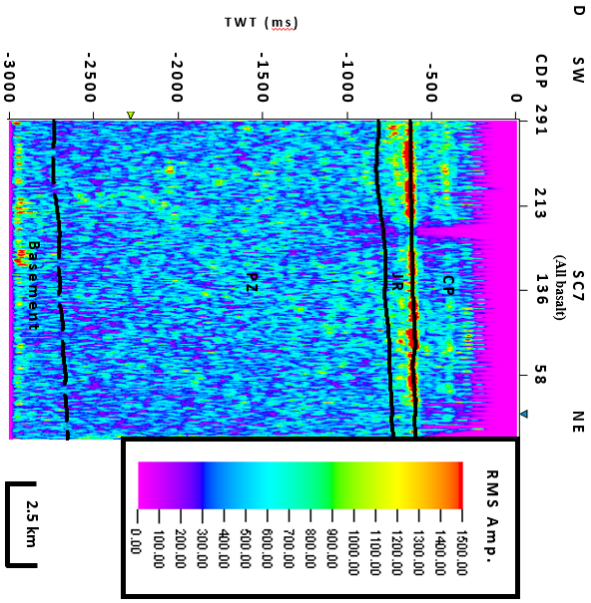

Fig. 7. Interpreted **r**oot mean square (RMS) amplitude profiles SCO2-6 (a), SCO2-4 (b), SC2 (c), and SC7 (d) covering the entire stratigraphic section seen in the study area outside of the Triassic rift basin. These profiles were chosen because they provide regional coverage within the study area (Fig. 1c). Note that all 4 profiles demonstrate a laterally continuous amplitude anomaly at the boundary marking the top of the Paleozoic sequence. Solid red lines indicate faulting that aligns with magnetic high boundaries (Fig 18) and demonstrate amplitude loss through the entire Suwannee basin sequence down to basement. Dashed red lines indicate accessory faulting based on disruption of lateral continuity and amplitude loss.

Both instantaneous phase and cosine of phase were used alongside RMS amplitude and reflectivity to interpret the top of the Paleozoic sequence.

Instantaneous phase and cosine of phase are useful in showing not only lateral continuity, but highlighting unconformities as well. Thus, they are effective for showing the boundary that marks the top of the Paleozoic, the PRU (Figs. 8 and 9), in areas where amplitude may not be quite as effective. When we have the presence of Jurassic aged basalt, constrained by well data, seismic signature, and refraction velocities (Ackermann, 1983), we tend to see lower amplitude values and less bright reflectors beneath the Jurassic top (Figs. 6a, 6c, 6d and 7a, 7c, 7d). This is likely the result of the basalt being such a strong boundary that it returns most of the reflective energy back to the surface. This leaves less energy to propagate deeper into the subsurface than in areas where the basalt is not present. However, both phase calculations are independent of amplitude and allow for improved interpretations as they highlight the lateral continuity of the deeper reflector packages. The top of the Paleozoic demonstrates laterally continuous phase characteristics (Figs. 8 and 9). Furthermore, subtle stratigraphic pinch-outs within the Jurassic sedimentary sequence can be observed (particularly in Figs. 8a and 9a). Lastly, both phase calculations allow us to better qualitatively observe the change in reflector package frequency between the Jurassic sediment and Suwannee basin sediment. This signature is highlighted by the increased vertical gap (change in time) between black and white (degree equivalent) phase within the Paleozoic as opposed to the more frequent vertical occurrence of phase equivalent reflectors within the Jurassic sequence. This type of behavior within the seismic data, when isolated, is very helpful in picking the boundary that marks the top of the Paleozoic.

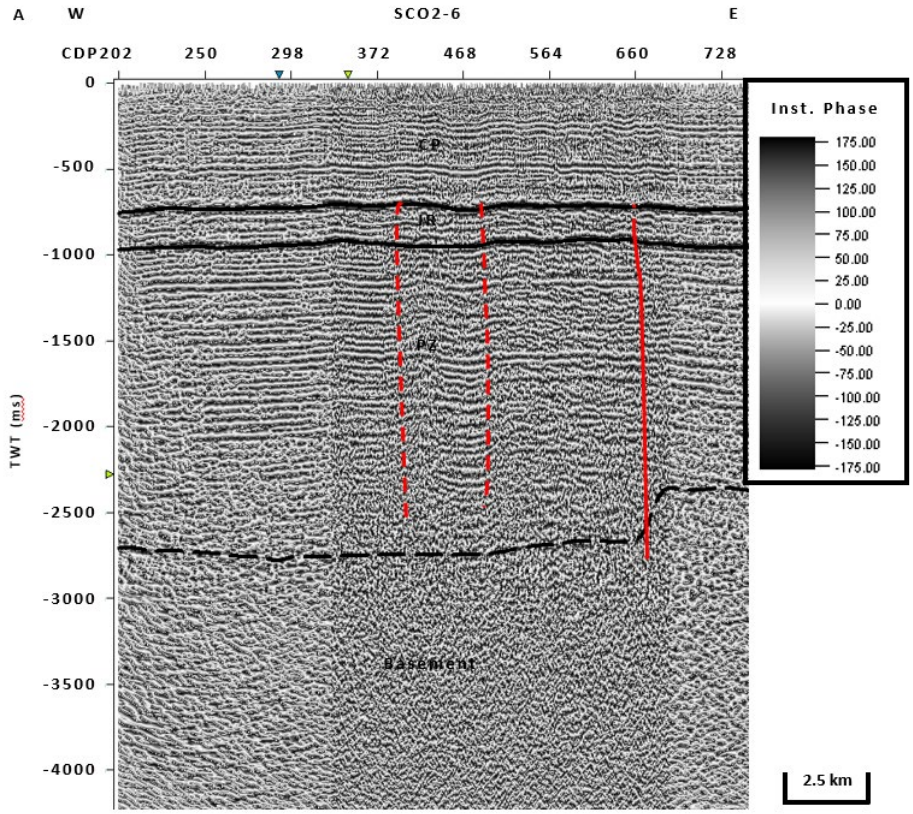
A
W
SCO2-6
E
CDP202
250
298
372
468
564
660
728
0
-500
-1000
-1500
-2000
-2500
-3000
-3500
-4000
TWT (ms)
SP
OB
PZ
Basement
Inst. Phase
175.00
150.00
125.00
100.00
75.00
50.00
25.00
0.00
-25.00
-50.00
-75.00
-100.00
-125.00
-150.00
-175.00
2.5 km

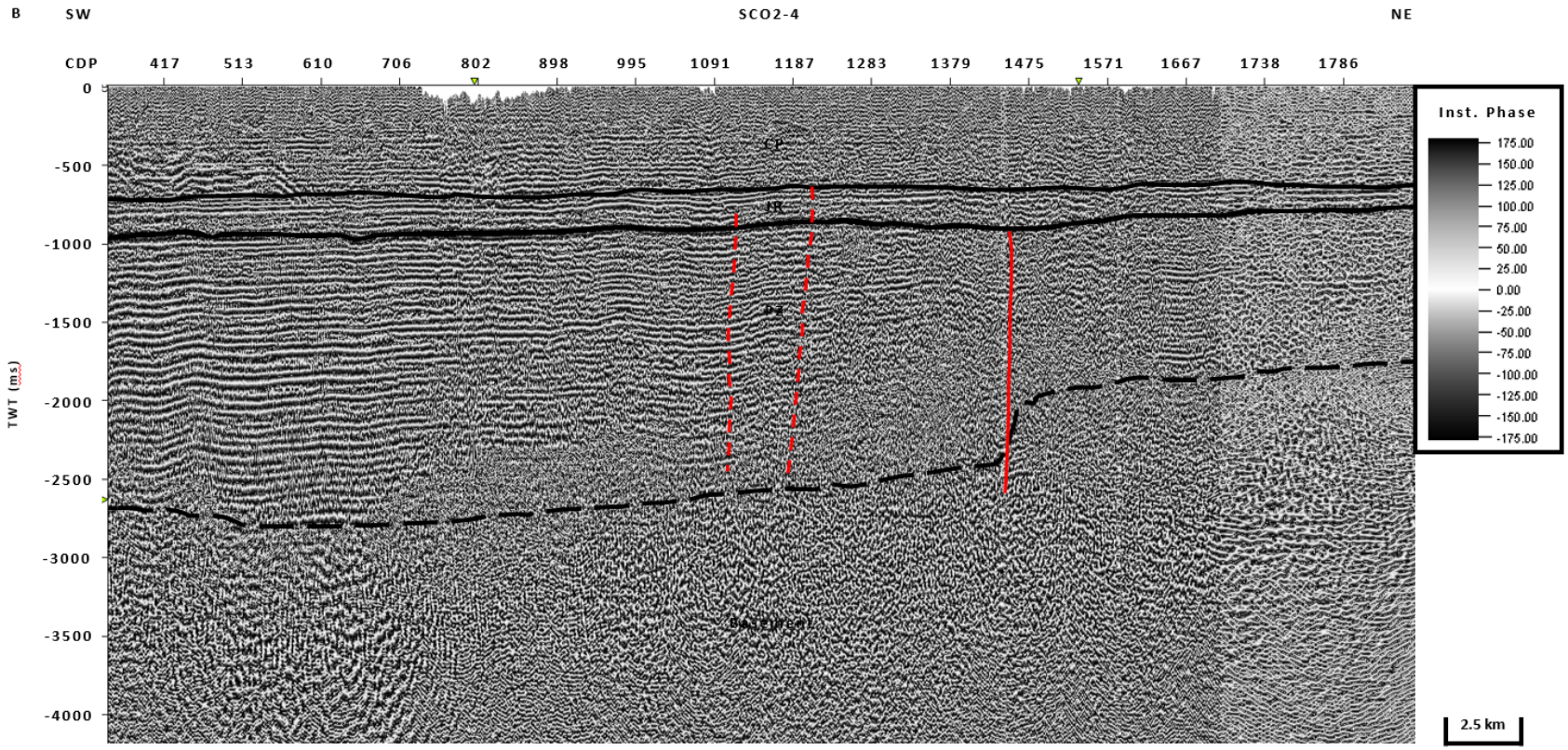
B
SW
SCO2-4
NE
CDP
417
513
610
706
802
898
995
1091
1187
1283
1379
1475
1571
1667
1738
1786
0
-500
-1000
-1500
-2000
-2500
-3000
-3500
-4000
TWT (ms)
CP
KR
P2
BASEMENT
Inst. Phase
175.00
150.00
125.00
100.00
75.00
50.00
25.00
0.00
-25.00
-50.00
-75.00
-100.00
-125.00
-150.00
-175.00
2.5 km

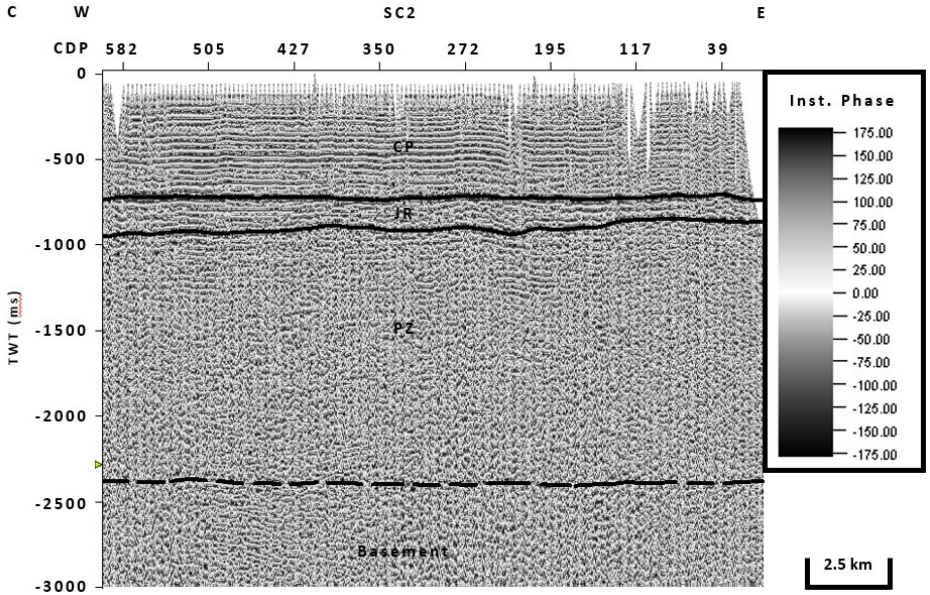
C
W
SC2
E
CDP 582 505 427 350 272 195 117 39
0
-500
-1000
-1500
-2000
-2500
-3000
TWT (ms)
CP
JR
PZ
Basement
Inst. Phase
175.00
150.00
125.00
100.00
75.00
50.00
25.00
0.00
-25.00
-50.00
-75.00
-100.00
-125.00
-150.00
-175.00
2.5 km

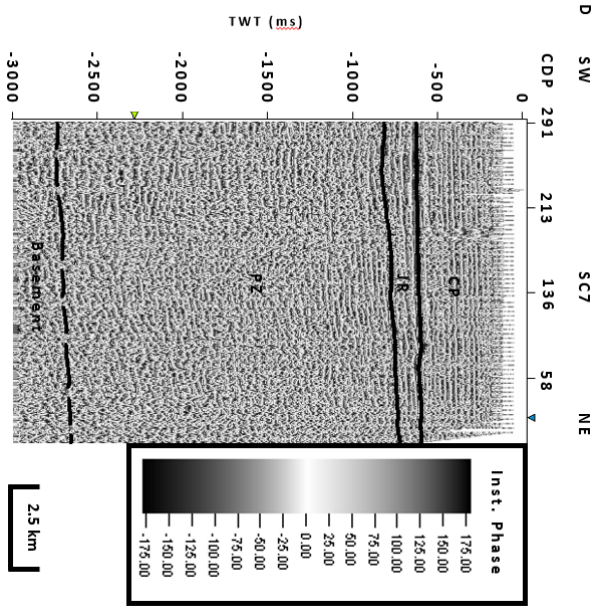

Fig. 8. Instantaneous Phase profiles SCO2-6 (a), SCO2-4 (b), SC2 (c), and SC7 (d) covering the entire stratigraphic section seen in the study area outside of the Triassic rift basin. These profiles were chosen because they provide regional coverage within the study area (Fig. 1c). Note that all 4 profiles demonstrate lateral continuity at the boundary marking the top and throughout the Paleozoic sequence. Solid red lines indicate faulting that aligns with magnetic high boundaries (Fig 18) and demonstrate disruption of lateral continuity and sudden dip change through the entire Suwannee basin sequence down to basement. Dashed red lines indicate accessory faulting based on disruption of lateral continuity and sudden dip change.

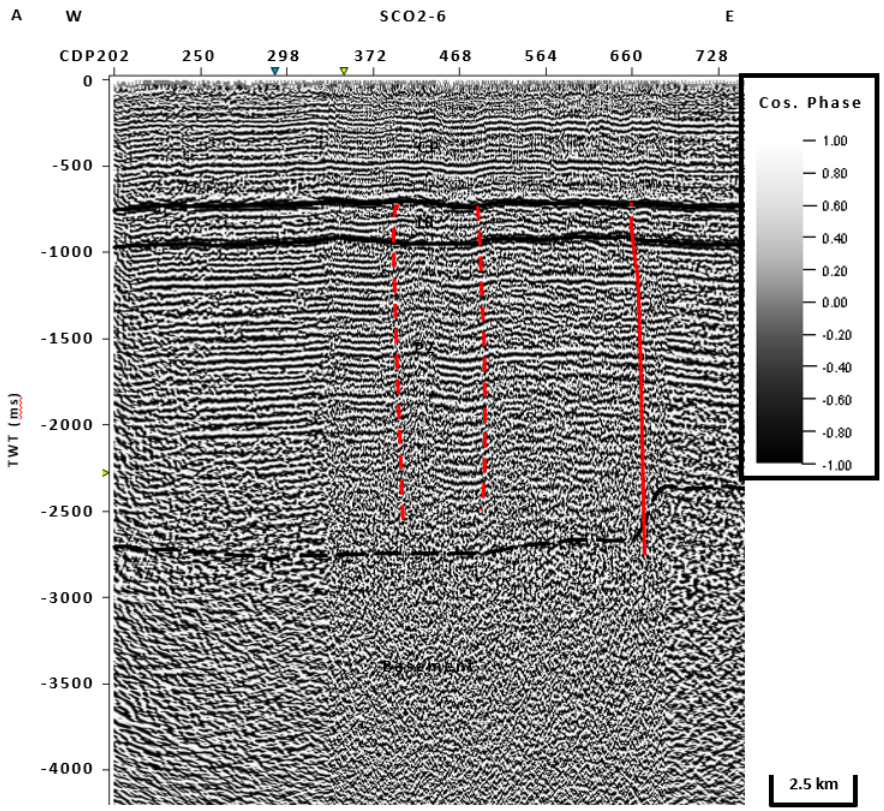
A
W
SCO2-6
E
CDP202
250
298
372
468
564
660
728
0
-500
-1000
-1500
-2000
-2500
-3000
-3500
-4000
TWT (ms)
Cos. Phase
1.00
0.80
0.60
0.40
0.20
0.00
-0.20
-0.40
-0.60
-0.80
-1.00
2.5 km

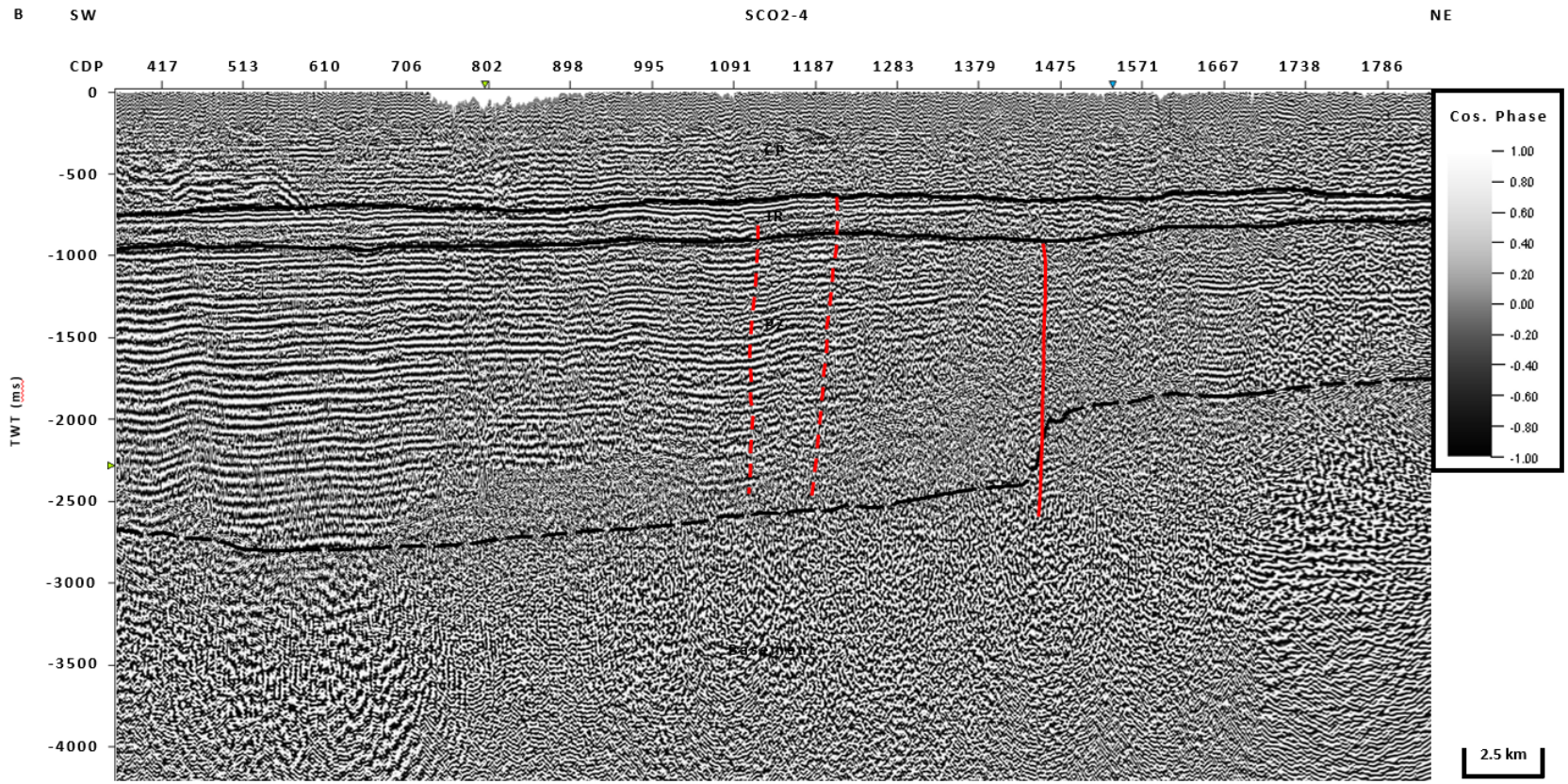
B
SW
SCO2-4
NE
CDP
417
513
610
706
802
898
995
1091
1187
1283
1379
1475
1571
1667
1738
1786
0
-500
-1000
-1500
-2000
-2500
-3000
-3500
-4000
TWT (ms)
Z_b
TR
BZ
Basement
Cos. Phase
1.00
0.80
0.60
0.40
0.20
0.00
-0.20
-0.40
-0.60
-0.80
-1.00
2.5 km

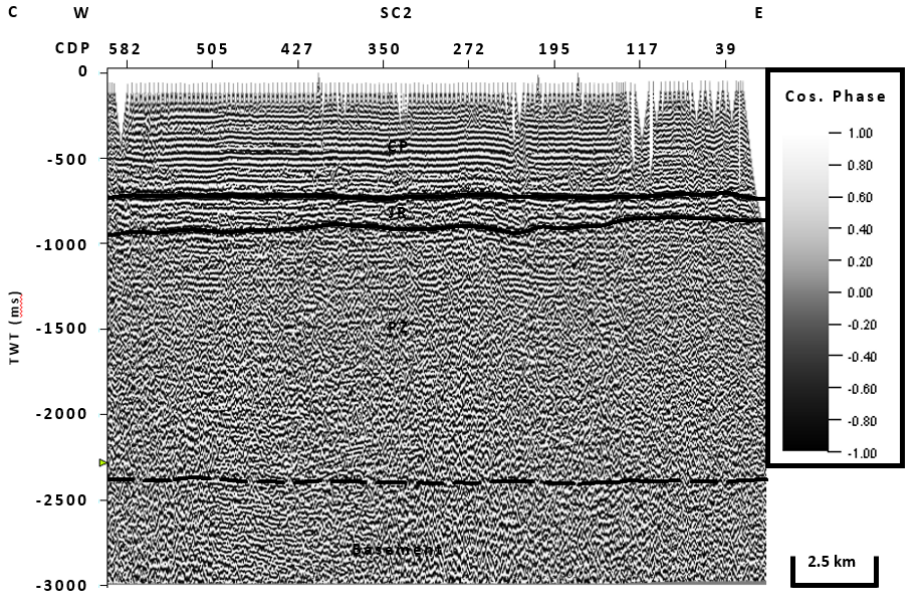
C
W
SC2
E
CDP 582 505 427 350 272 195 117 39
0
-500
-1000
-1500
-2000
-2500
-3000
TWT (ms)
Cos. Phase
1.00
0.80
0.60
0.40
0.20
0.00
-0.20
-0.40
-0.60
-0.80
-1.00
2.5 km

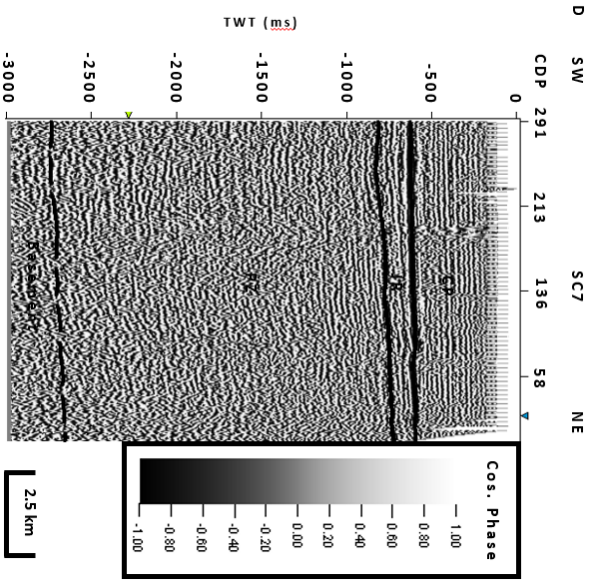

Fig. 9. Cosine of Phase profiles SCO2-6 (a), SCO2-4 (b), SC2 (c), and SC7 (d) covering the entire stratigraphic section seen in the study area outside of the Triassic rift basin. These profiles were chosen because they provide regional coverage within the study area (Fig. 1c). Note that all 4 profiles demonstrate lateral continuity at the boundary marking the top and throughout the Paleozoic sequence. Solid red lines indicate faulting that aligns with magnetic high boundaries (Fig 18) and demonstrate disruption of lateral continuity and sudden dip change through the entire Suwannee basin sequence down to basement. Dashed red lines indicate accessory faulting based on disruption of lateral continuity and sudden dip change.

The consistent presence of the Suwannee basin sequence throughout all 15 seismic profiles, which is confirmed through the correlation of the picked top of Paleozoic boundary utilizing the original reflectivity profiles and the calculated attributes that confirm its presence, suggests that the revised position of the Suwannee Suture Zone (SSZ) proposed in Boote and Knapp (2018) is likely accurate, other than the fact that we believe it is a strike-slip boundary rather than a suture zone. Furthermore, throughout most of the profiles we see little relative deformation of the Suwannee basin sequence which is reiterated by the resulting structure maps produced from our interpretation of the seismic dataset (Figs. 10 and 11).

This suggests that the Gondwanan terrane was not emplaced where we observe it today during the collision of Gondwana and Pangea. Thus, we propose that there must be a component of strike-slip motion present that emplaced the Suwannee basin sequence in its current position today. Otherwise, we would see evidence of collisional deformation present within the sequence. It is our belief that a massive strike slip branch that is 50 km wide separates Gondawanan terrane from Laurentian terrane throughout the Southeast region of present day United States. This strike slip branch is termed the PSTF (Fig. 1c).

The areas where significant deformation is observed within the Suwannee basin all occur as a result of faulting as seen on seismic profiles SCO2-1, SCO2-4, SCO2-5, SCO2-6, SCO2-7, and SC6. At the locality of the faults, we also see a significant amount of thinning of the Suwannee basin (Figs. 12 and 13). When plotted on the magnetic anomaly map (Fig. 14), the faults and their projected planes appear to be spatially coincident with boundaries marking the edge of anomalous magnetic highs that occur within the study area.

Thus, it is our belief that the magnetic highs that occur within the study area are a result of the crystalline basement interacting with the magnetic survey that was taken. Subsequently, the presence of the magnetic highs is a function of the thickness of the Paleozoic Suwannee basin

sequence (Fig. 15). In other words, when the Suwannee basin is significantly thinned, the crystalline basement is able to interact with the magnetic survey and produce the resulting highs. However, when the Suwannee basin thickness is greater than the threshold necessary for the crystalline basement to interact with the magnetic survey, we tend to see lower magnetic values.

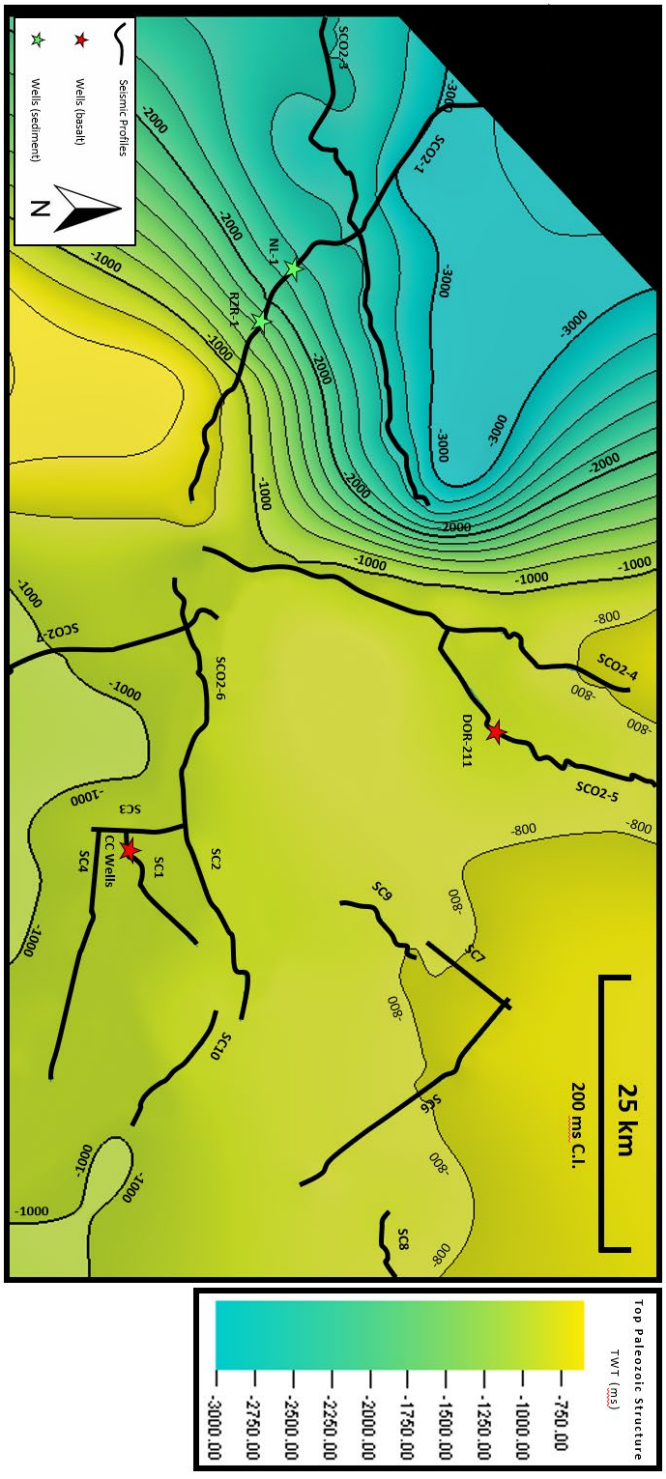

Fig. 10. Top of Paleozoic Suwannee basin structure map in the time domain. Note the presence of the Triassic Basin and its generally northwest trending dip indicated by the contour gradient increase along seismic line SCO2-1. The remaining Paleozoic structure is relatively flat-lying.

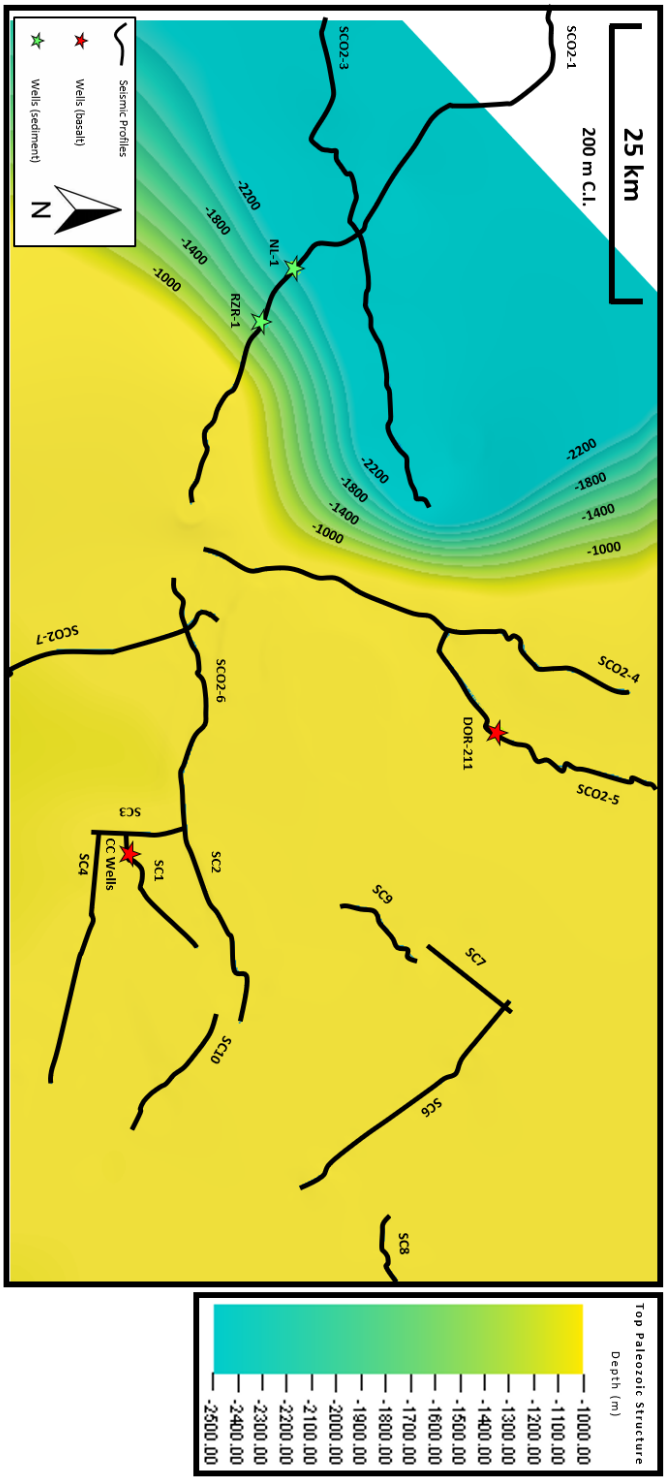

Fig. 11. Top of Paleozoic Suwannee basin structure map in the depth domain. Note the presence of the Triassic Basin and its generally northwest trending dip indicated by the contour gradient increase along seismic line SCO2-1. The remaining Paleozoic structure is relatively flat-lying.

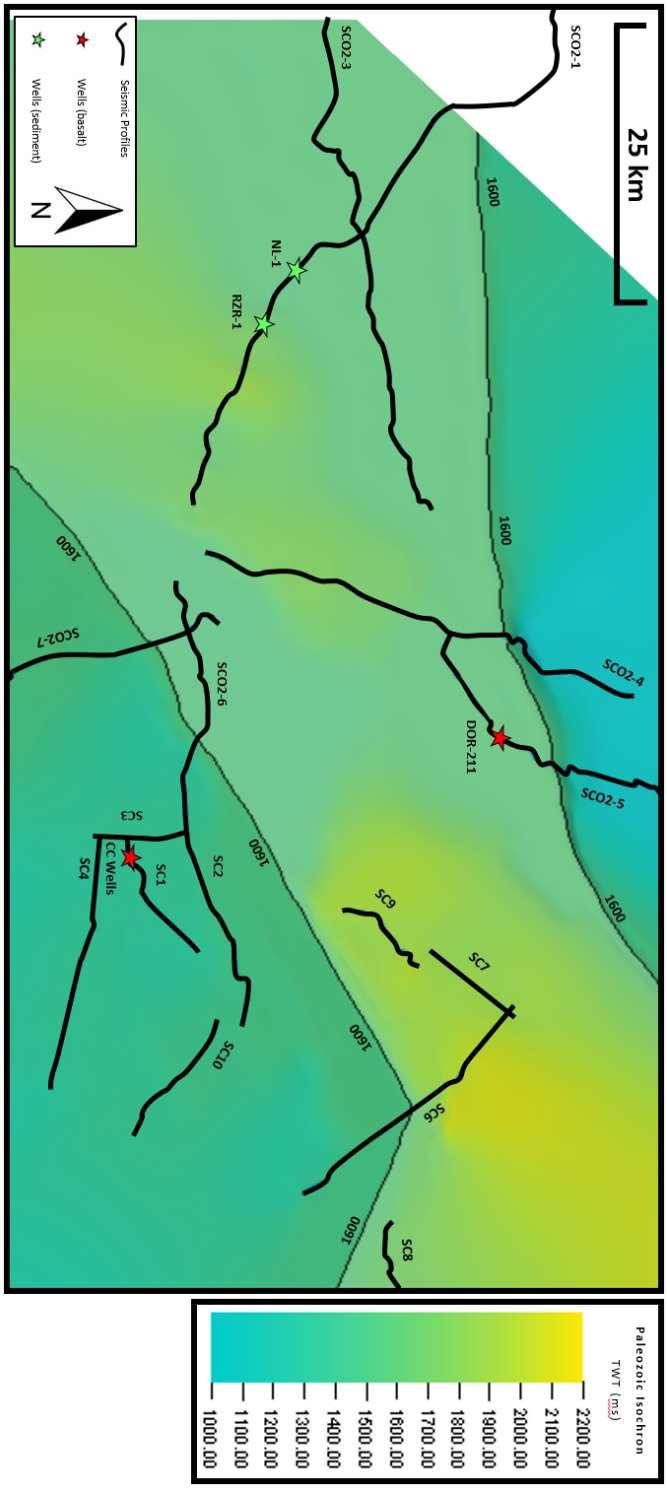

Fig. 12. Paleozoic Suwannee basin isochron map. Note the substantial thickness changes that occur at the northern, northwestern, and southern most portions of the map. These thickness changes are a result of faulting as seen on Figs. 3, 6, 7, 8, 9, and 17. The substantially thinned portions are also spatially coincident with magnetic highs seen on Fig. 18. We believe the thinned Suwannee basin section allows the basement to interact with the magnetic survey and produce the magnetic high anomalies that occur within the Study area

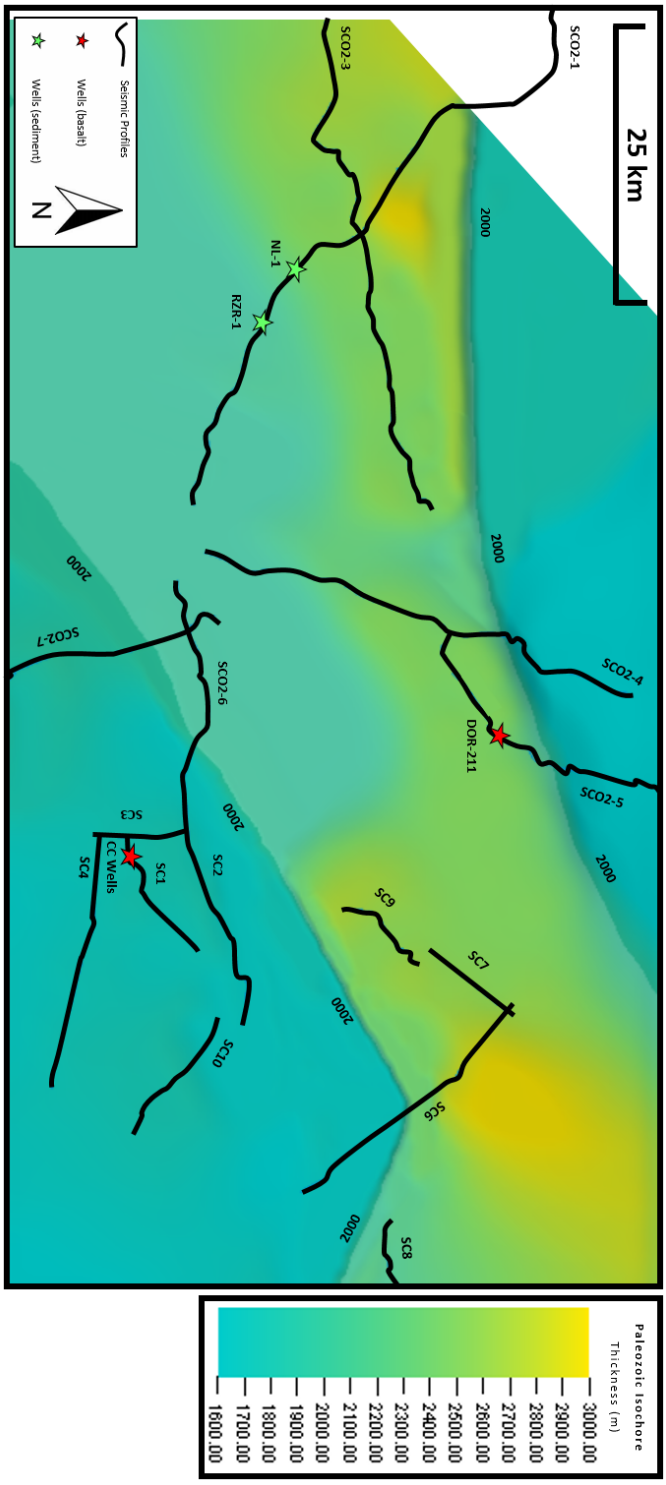

Fig. 13. Paleozoic Suwannee basin isochore map. Note the substantial thickness changes that occur at the northern, northwestern, and southern most portions of the map. These thickness changes are a result of faulting as seen on Figs. 3, 6, 7, 8, 9, and 17. The substantially thinned portions are also spatially coincident with magnetic highs seen on Fig. 18. We believe the thinned Suwannee basin section allows the basement to interact with the magnetic survey and produce the magnetic high anomalies that occur within the Study area

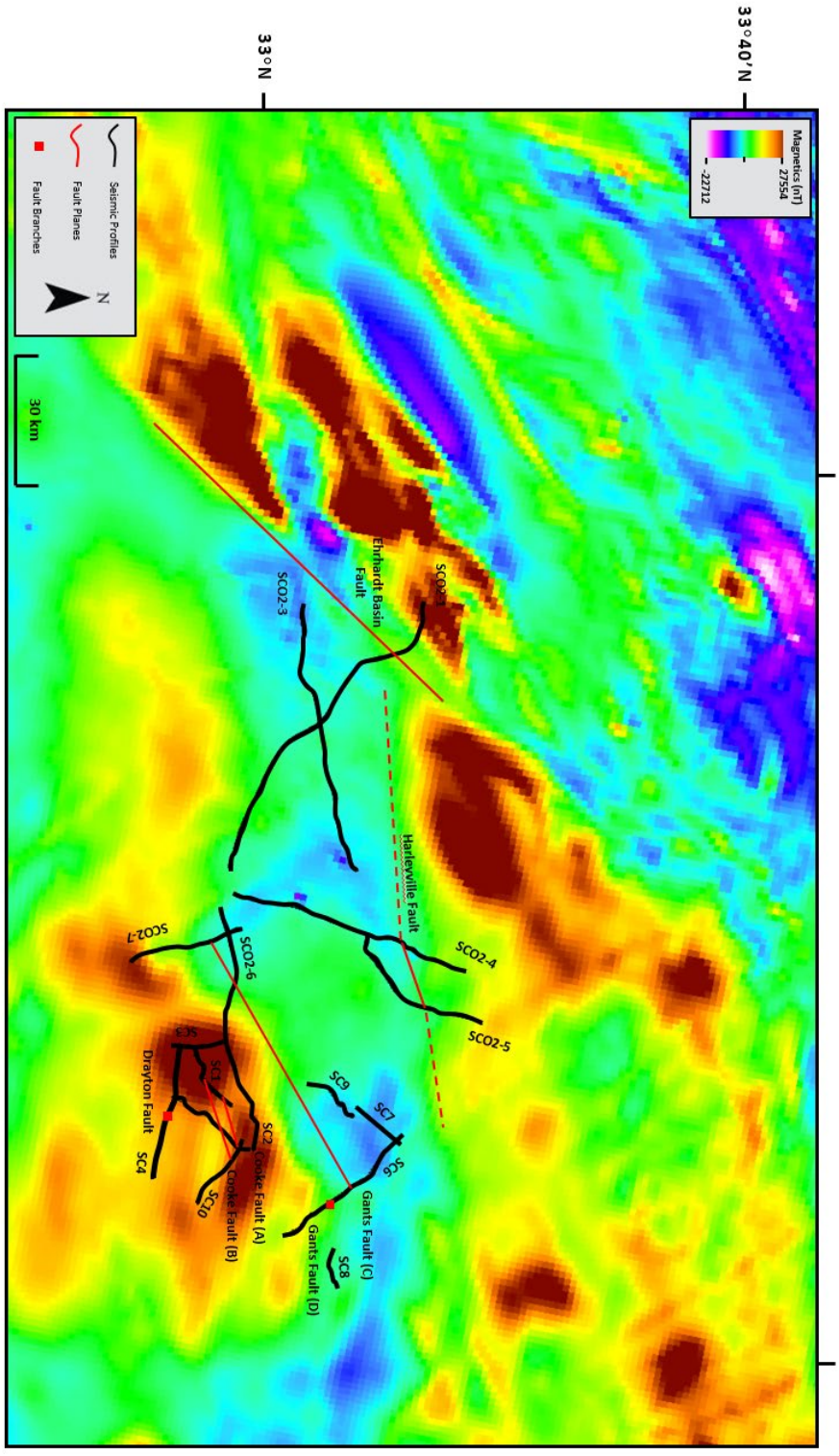

Fig. 14. Magnetic anomaly map showing location of faults in relation to magnetic features and the seismic dataset. Note the Ehrhardt basin fault bounding the Triassic basin seen on seismic profile SCO2-1, the newly interpreted Harleyville fault which bounds the northern magnetic high where substantial Paleozoic Suwannee basin thinning occurs, and Gants fault which bounds the southern magnetic high where substantial Paleozoic Suwannee basin thinning also occurs.

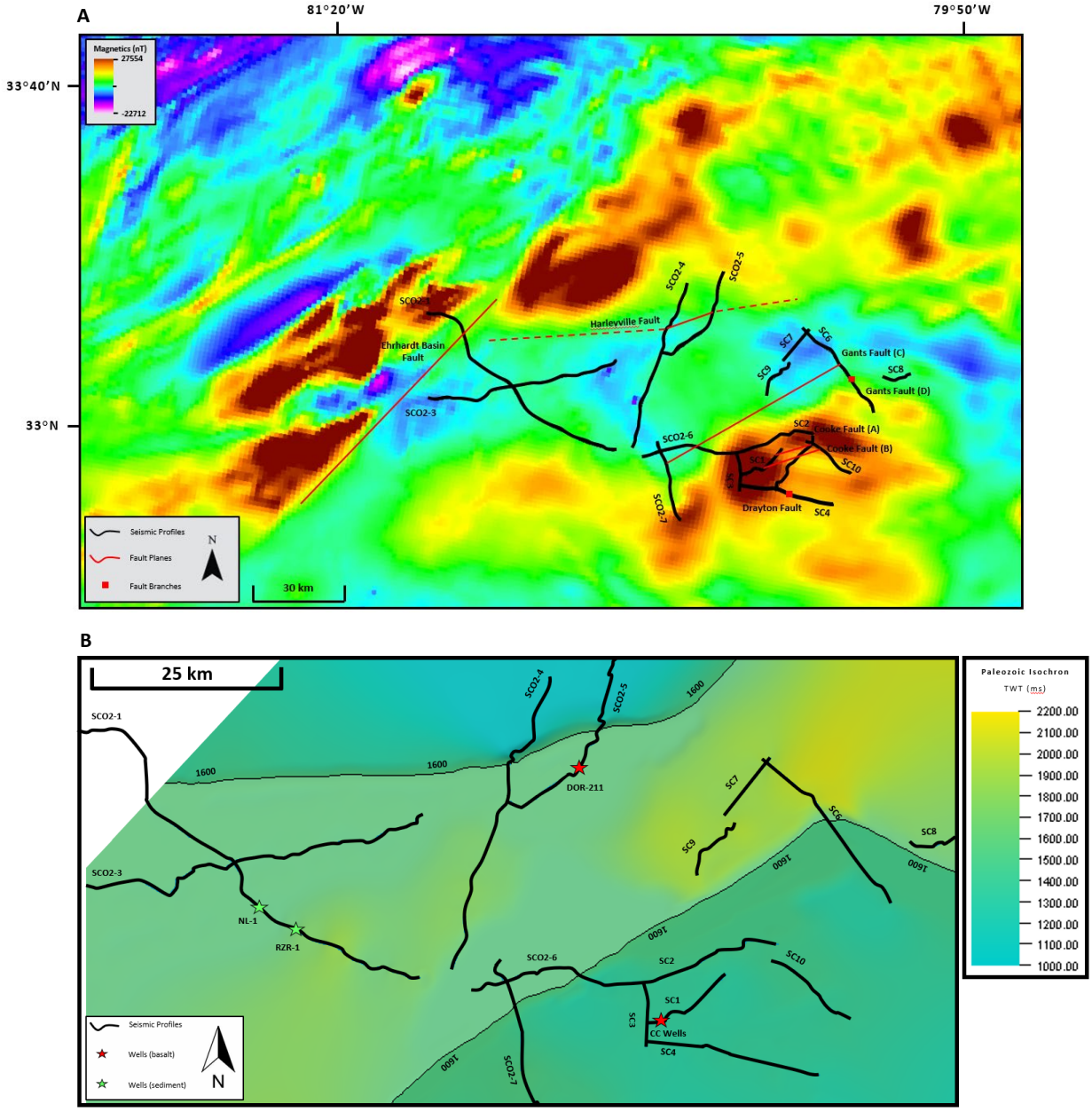

Fig. 15. (a) Magnetic anomaly map showing location of faults in relation to magnetic features and the seismic dataset, as seen previously. (b) Paleozoic Suwannee basin isochron map, as seen previously. Note the spatial correlation of substantially thinned Suwannee basin and magnetic highs as well as faults bounding both the magnetic highs and Suwannee basin thickness changes.

4.2 MPSSZ Seismicity

Throughout the SC and SCO2 seismic datasets, high angle faults were observed (Figs. 16, 17, 18, 19, and 20). Many of these faults were observed in (Hamilton et al., 1983) with some additional faults interpreted in this study. However, in the (Hamilton et al., 1983) study, the faults were not projected into the Suwannee basin sequence due to the skepticism that the sequence was present in their study. The presence of this sequence and the faults projecting into it implicates these faults may be related to the 1886 earthquake as well as more recent activity that occurs within the MPSSZ.

The faults are interpreted where we see a disruption of lateral continuity of reflector packages within the reflectivity profiles, an abrupt dip change within reflectors, and sudden amplitude loss (Figs. 16, 17, 18, 19, 20). Furthermore, attributes of the seismic profiles such as RMS amplitude, instantaneous phase, and cosine of phase assist in being able to isolate and better observe such characteristics within the seismic data. Hence, in the same location where the lateral disruption of seismic events occurs, we see abrupt changes in phase continuity on both the instantaneous phase and cosine of phase profiles (Figs. 16d, 16e, 17d, 17e, 18d, 18e, 19d, 19e, 20d, 20e).

Phase changes can be indicative of lateral pinch outs in bedding. However, those would be gradual phase changes. Here, where the interpreted fault branches are located, we see abrupt phase changes and lateral discontinuities. Both of these seismic signatures emphasize the presence of fault structure. In addition, both phase attributes allow us to observe abrupt dip changes within reflectors which is also indicative of fault presence. Lastly, the cross-cutting relationship of the faults relative to bedding planes instills an amplitude disruption within the reflectors as they interact with the fault planes (Figs. 16, 17, 18, 19, 20). Utilizing the RMS amplitude profiles (Figs. 16c, 17c, 18c, 19c, 20c), we can isolate the average amplitudes of reflectors within a time window and observe this lateral discontinuity of average amplitude

consistency across a given reflector. The RMS amplitude was utilized due to its ability to highlight amplitude on an absolute scale rather than a relative scale which is beneficial for observing amplitude anomalies.

Some of the interpreted fault branches can be correlated with each other to produce fault planes projecting in a two-dimensional space. When the branches are correlated, they are oriented NE-SW parallel to the Helena Banks fault (see Fig. 1 from Behrendt et al., 1983) (Fig. 21). When all of the fault planes, with the exception of the Harleyville and Ehrhardt basin fault planes, are projected they intersect the locus of major seismicity within the MPSSZ (see Fig. 1 from Hamilton et al., 1983). Thus, it is proposed that these structures are likely related to much of the seismicity within the region, including the major 1886 earthquake. However, it is impossible to make that claim with absolute certainty based off of what is observed in this dataset alone.

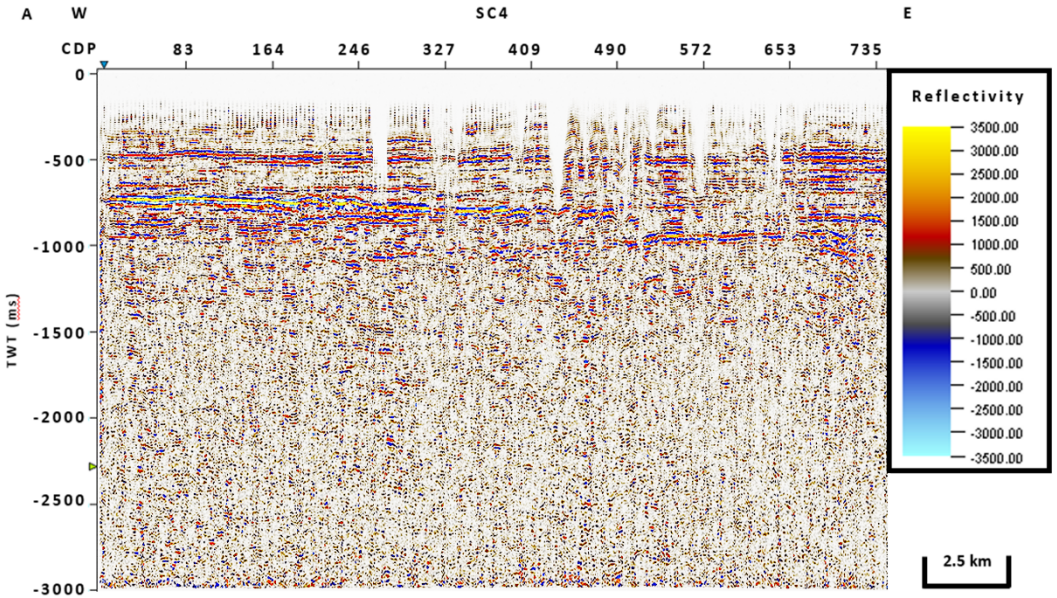
A
W
SC4
E
CDP
83
164
246
327
409
490
572
653
735
0
-500
-1000
-1500
-2000
-2500
-3000
TWT (ms)
Reflectivity
3500.00
3000.00
2500.00
2000.00
1500.00
1000.00
500.00
0.00
-500.00
-1000.00
-1500.00
-2000.00
-2500.00
-3000.00
-3500.00
2.5 km

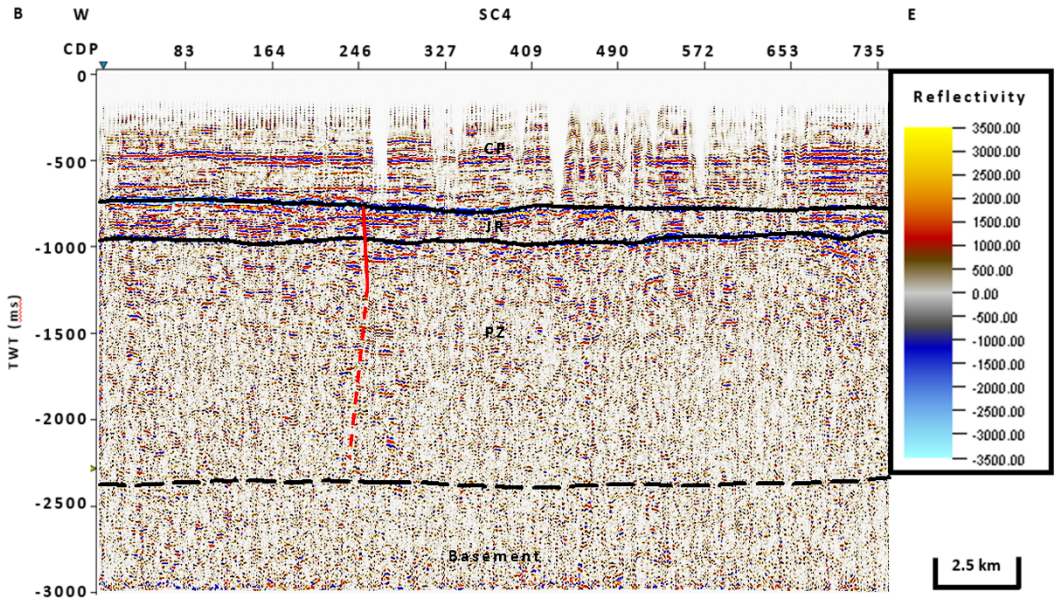
B
W
SC4
E
CDP
83
164
246
327
409
490
572
653
735
0
-500
-1000
-1500
-2000
-2500
-3000
TWT (ms)
CP
JR
PZ
Basement
Reflectivity
3500.00
3000.00
2500.00
2000.00
1500.00
1000.00
500.00
0.00
-500.00
-1000.00
-1500.00
-2000.00
-2500.00
-3000.00
-3500.00
2.5 km

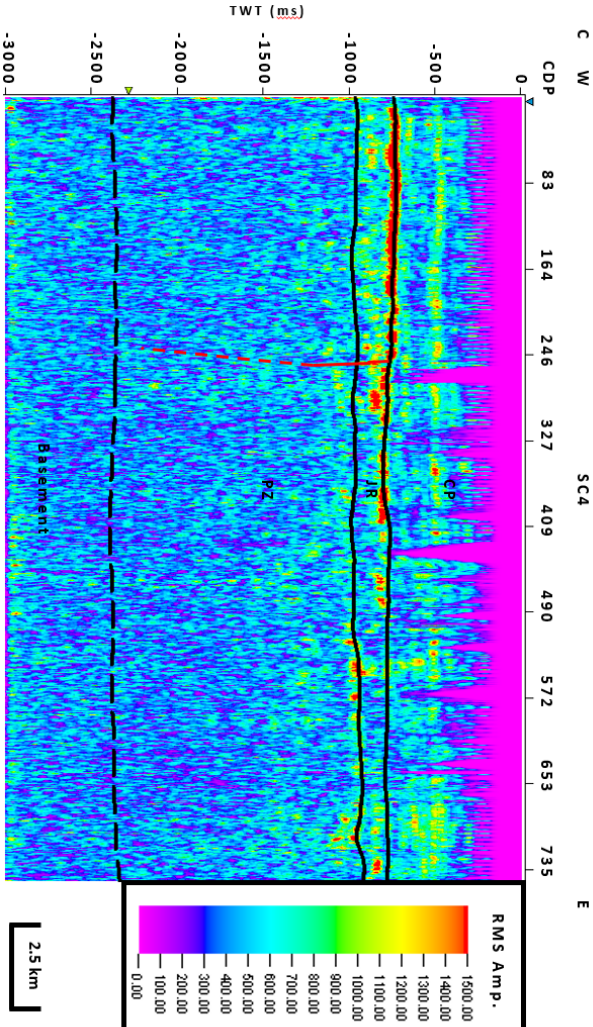
C
W
CDP
83
164
246
327
409
490
572
653
735
SC4
E
TWT (ms)
0
-500
-1000
-1500
-2000
-2500
-3000
CP
JR
PZ
Basement
RMS Amp.
1500.00
1400.00
1300.00
1200.00
1100.00
1000.00
900.00
800.00
700.00
600.00
500.00
400.00
300.00
200.00
100.00
0.00
2.5 km

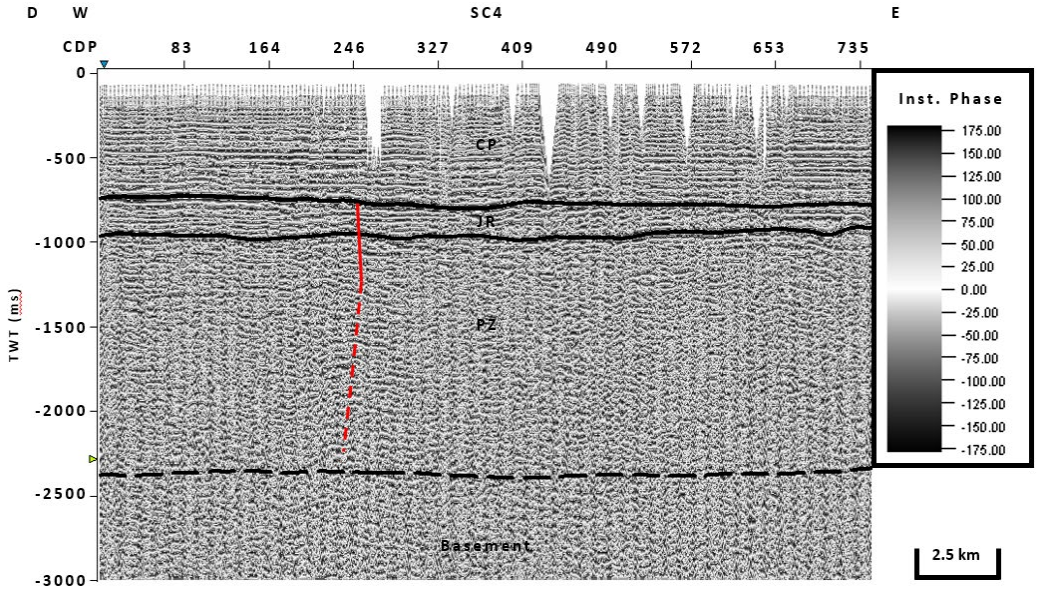
D
W
SC4
E
CDP
83
164
246
327
409
490
572
653
735
0
-500
-1000
-1500
-2000
-2500
-3000
TWT (ms)
CP
JR
PZ
Basement
Inst. Phase
175.00
150.00
125.00
100.00
75.00
50.00
25.00
0.00
-25.00
-50.00
-75.00
-100.00
-125.00
-150.00
-175.00
2.5 km

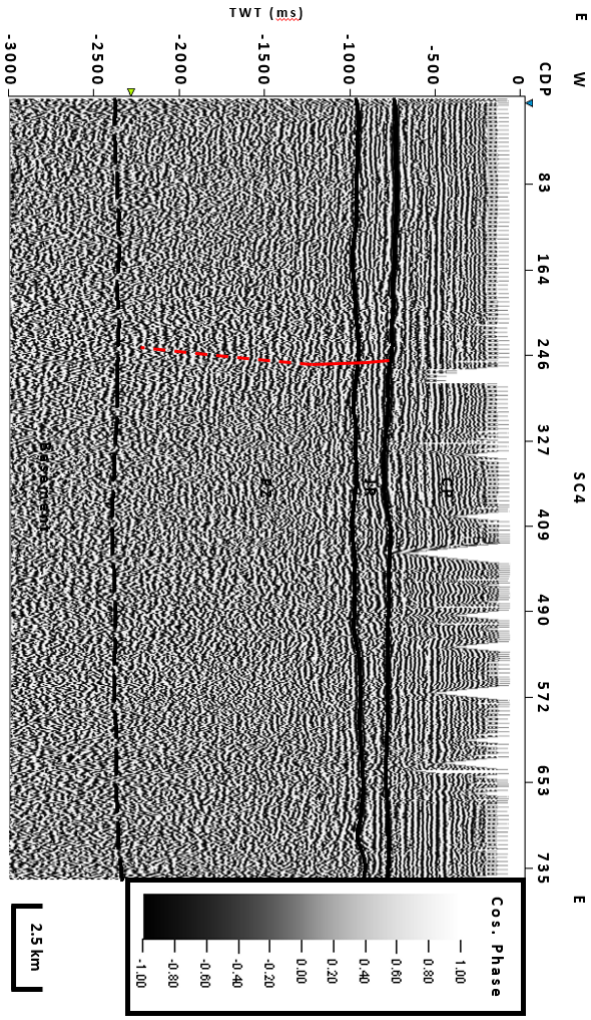

Fig. 16. Seismic reflectivity profile SC4 (a) and interpreted (b) and its associated attribute calculations: RMS amplitude (c); Instantaneous phase (d); and Cosine of phase (e). Each profile consistently exhibits features signifying the presence of the Drayton Fault branch previously interpreted by Behrendt et al. (1983). The solid line indicates the portion of the fault branch interpreted with high confidence. The dashed portions of the fault branch are interpreted with lower confidence. Note the disruption of lateral continuity and sudden amplitude loss within a and b, the sudden amplitude loss in c, and the abrupt disruption of lateral continuity and dip change in d and e all occurring at the location of the fault.

A
SW
SC1
NE
CDP
418
335
251
168
89
9
TWT (ms)
0
-500
-1000
-1500
-2000
-2500
-3000
Reflectivity
3500.00
3000.00
2500.00
2000.00
1500.00
1000.00
500.00
0.00
-500.00
-1000.00
-1500.00
-2000.00
-2500.00
-3000.00
-3500.00
2.5 km

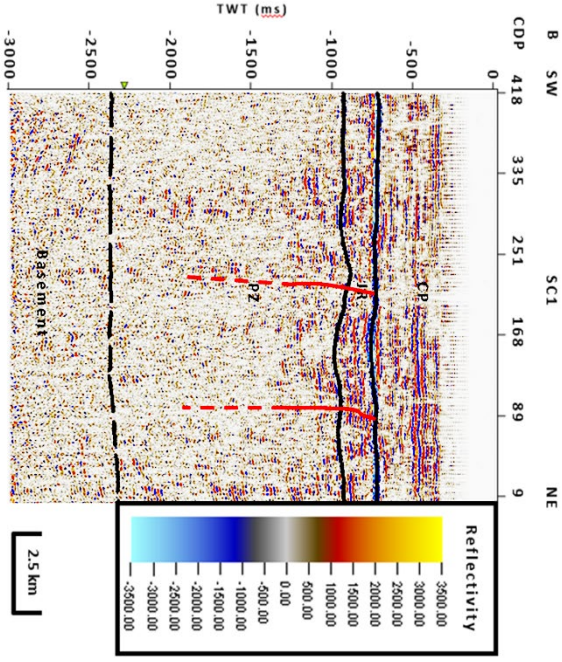
B SW SC1 NE
CDP 418 335 251 168 89 9
TWT (ms)
0
-500
-1000
-1500
-2000
-2500
-3000
CP
PZ
Basement
Reflectivity
3500.00
3000.00
2500.00
2000.00
1500.00
1000.00
500.00
0.00
-500.00
-1000.00
-1500.00
-2000.00
-2500.00
-3000.00
-3500.00
2.5 km

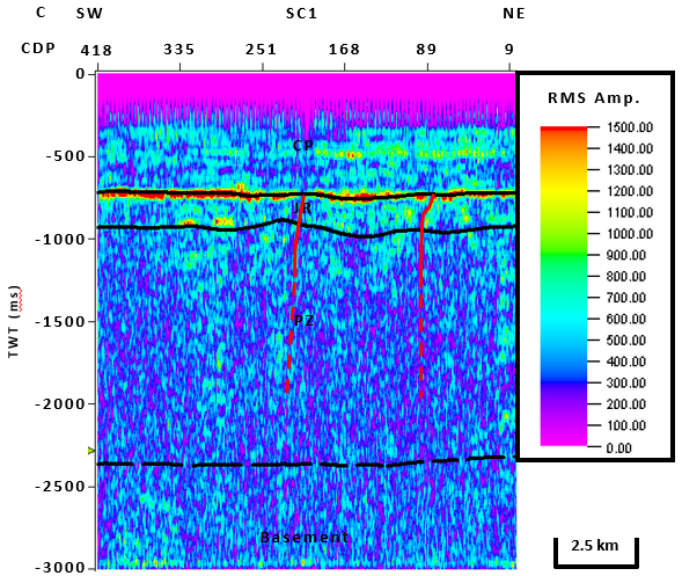
C
SW
SC1
NE
CDP
418
335
251
168
89
9
0
-500
-1000
-1500
-2000
-2500
-3000
TWT (ms)
CP
JR
BZ
Basement
RMS Amp.
1500.00
1400.00
1300.00
1200.00
1100.00
1000.00
900.00
800.00
700.00
600.00
500.00
400.00
300.00
200.00
100.00
0.00
2.5 km

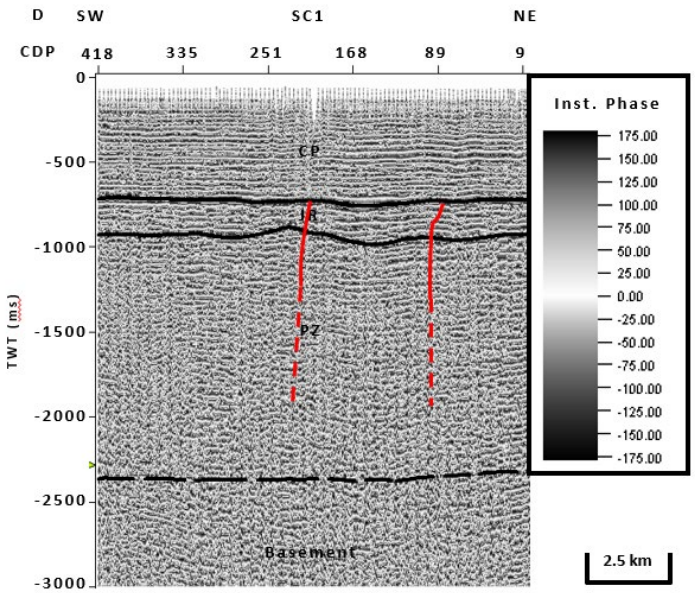
D
SW
SC1
NE
CDP
418
335
251
168
89
9
0
-500
-1000
-1500
-2000
-2500
-3000
TWT (ms)
CP
J
PZ
Basement
Inst. Phase
175.00
150.00
125.00
100.00
75.00
50.00
25.00
0.00
-25.00
-50.00
-75.00
-100.00
-125.00
-150.00
-175.00
2.5 km

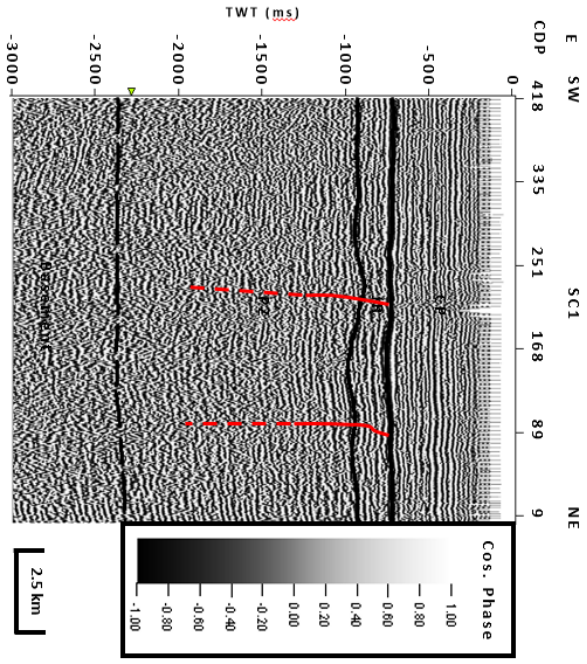

Fig. 17. Seismic reflectivity profile SC1 (a) and interpreted (b) and its associated attribute calculations: RMS amplitude (c); Instantaneous phase (d); and Cosine of phase (e). Each profile consistently exhibits features signifying the presence of the Cooke Fault branch previously interpreted by Behrendt et al. (1983). The solid line indicates the portion of the fault branch interpreted with high confidence. The dashed portions of the fault branch are interpreted with lower confidence. Note the disruption of lateral continuity and sudden amplitude loss within a and b, the sudden amplitude loss in c, and the abrupt disruption of lateral continuity and dip change in d and e all occurring at the location of the fault.

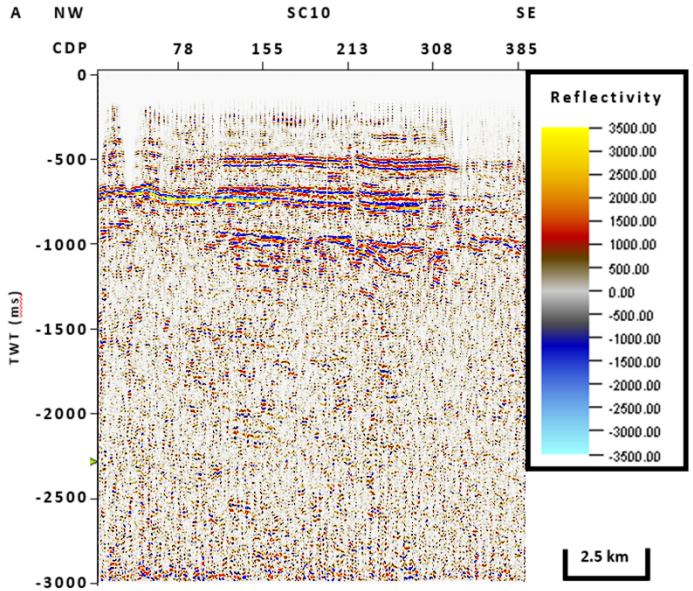
A
NW
SC10
SE
CDP
78
155
213
308
385
0
-500
-1000
-1500
-2000
-2500
-3000
TWT (ms)
Reflectivity
3500.00
3000.00
2500.00
2000.00
1500.00
1000.00
500.00
0.00
-500.00
-1000.00
-1500.00
-2000.00
-2500.00
-3000.00
-3500.00
2.5 km

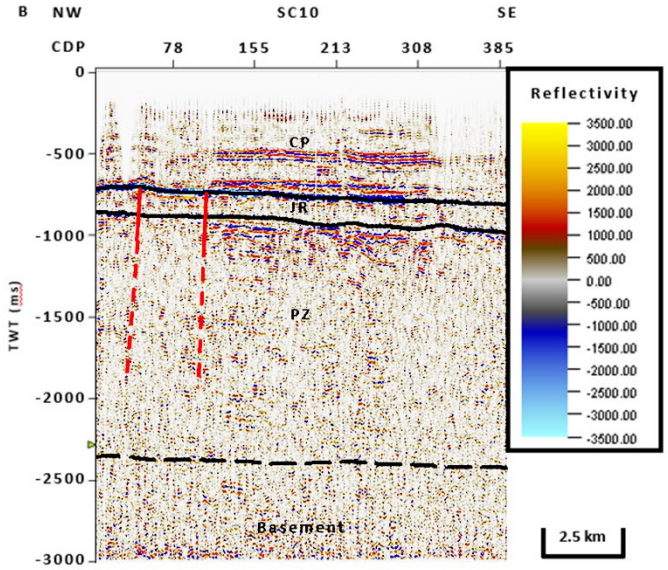
B NW
SC10
SE
CDP
78
155
213
308
385
0
-500
-1000
-1500
-2000
-2500
-3000
TWT (ms)
CP
JR
PZ
Basement
Reflectivity
3500.00
3000.00
2500.00
2000.00
1500.00
1000.00
500.00
0.00
-500.00
-1000.00
-1500.00
-2000.00
-2500.00
-3000.00
-3500.00
2.5 km

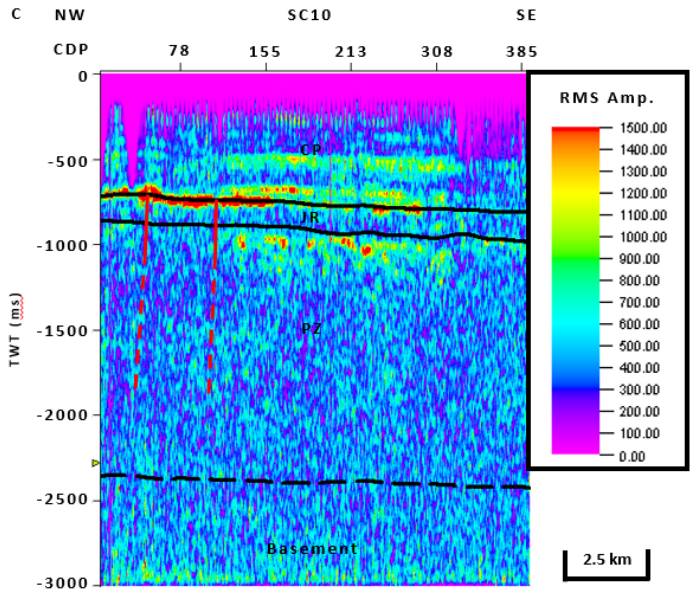
C
NW
SC10
SE
CDP
78
155
213
308
385
0
-500
-1000
-1500
-2000
-2500
-3000
TWT (ms)
CP
JR
PZ
Basement
RMS Amp.
1500.00
1400.00
1300.00
1200.00
1100.00
1000.00
900.00
800.00
700.00
600.00
500.00
400.00
300.00
200.00
100.00
0.00
2.5 km

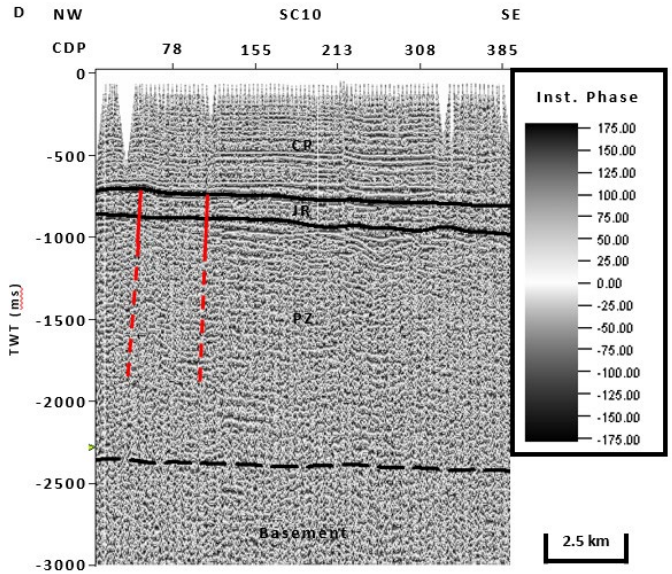
D
NW
SC10
SE
CDP
78
155
213
308
385
0
-500
-1000
-1500
-2000
-2500
-3000
TWT (ms)
CR
JR
PZ
Basement
Inst. Phase
175.00
150.00
125.00
100.00
75.00
50.00
25.00
0.00
-25.00
-50.00
-75.00
-100.00
-125.00
-150.00
-175.00
2.5 km

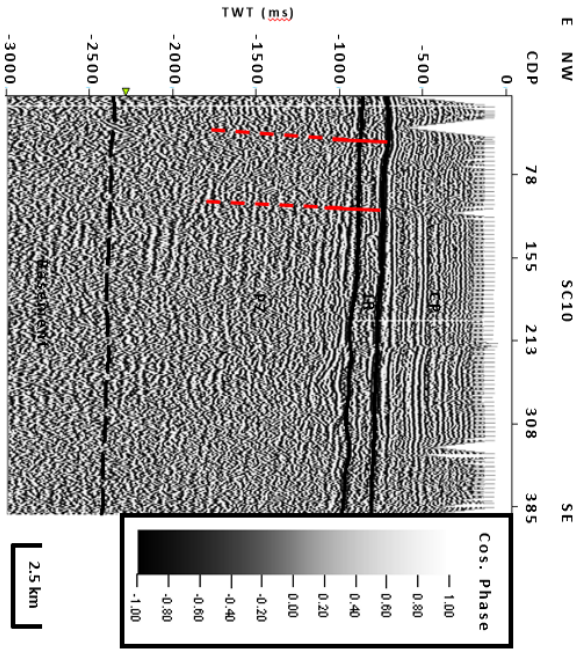

Fig. 18. Seismic reflectivity profile SC10 (a) and interpreted (b) and its associated attribute calculations: RMS amplitude (c); Instantaneous phase (d); and Cosine of phase (e). Each profile consistently exhibits features signifying the presence of the Cooke Fault branch previously interpreted by Behrendt et al. (1983). The solid line indicates the portion of the fault branch interpreted with high confidence. The dashed portions of the fault branch are interpreted with lower confidence. Note the disruption of lateral continuity and sudden amplitude loss within a and b, the sudden amplitude loss in c, and the abrupt disruption of lateral continuity and dip change in d and e all occurring at the location of the fault.

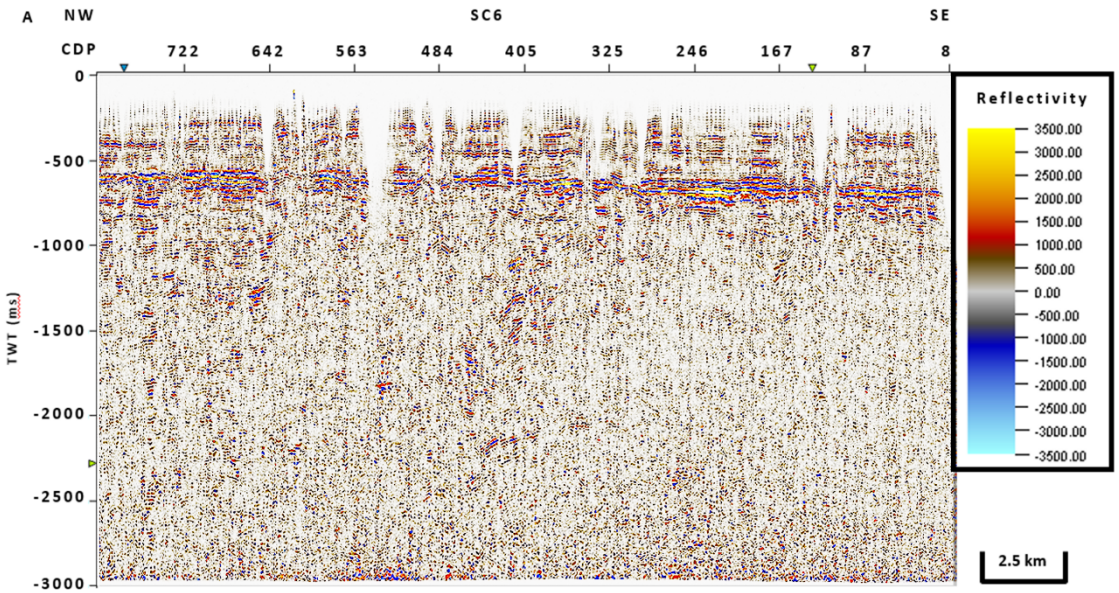
A
NW
SC6
SE
CDP
722
642
563
484
405
325
246
167
87
8
0
-500
-1000
-1500
-2000
-2500
-3000
TWT (ms)
Reflectivity
3500.00
3000.00
2500.00
2000.00
1500.00
1000.00
500.00
0.00
-500.00
-1000.00
-1500.00
-2000.00
-2500.00
-3000.00
-3500.00
2.5 km

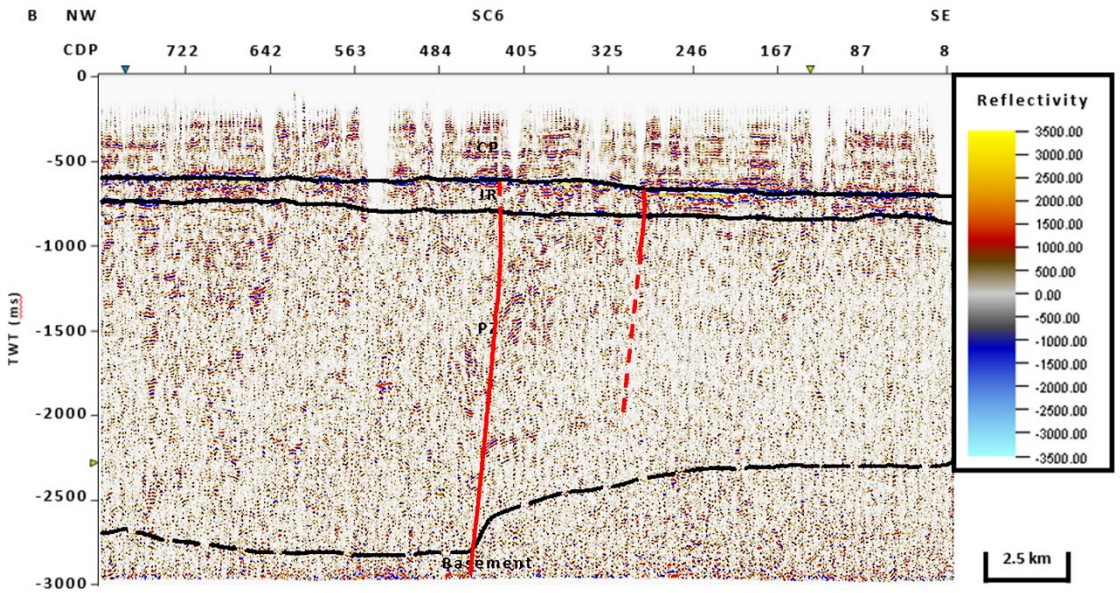
B NW
SC6
SE
CDP
722
642
563
484
405
325
246
167
87
8
0
-500
-1000
-1500
-2000
-2500
-3000
TWT (ms)
CP
IR
P
Basement
Reflectivity
3500.00
3000.00
2500.00
2000.00
1500.00
1000.00
500.00
0.00
-500.00
-1000.00
-1500.00
-2000.00
-2500.00
-3000.00
-3500.00
2.5 km

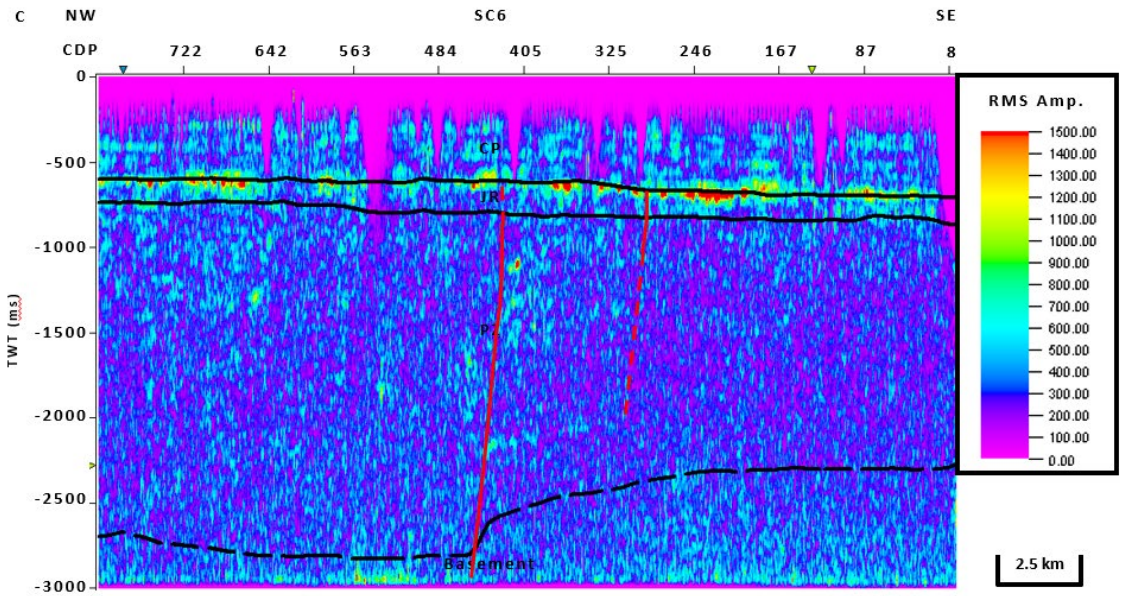
C
NW
SC6
SE
CDP
722
642
563
484
405
325
246
167
87
8
0
-500
-1000
-1500
-2000
-2500
-3000
TWT (ms)
CP
UK
P
Basement
RMS Amp.
1500.00
1400.00
1300.00
1200.00
1100.00
1000.00
900.00
800.00
700.00
600.00
500.00
400.00
300.00
200.00
100.00
0.00
2.5 km

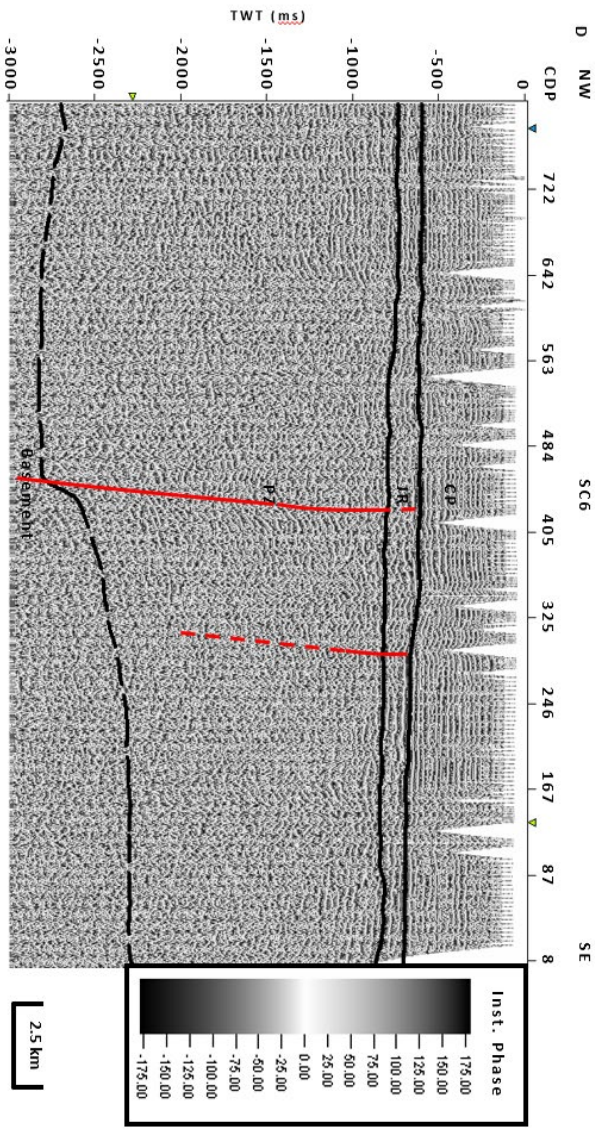
D
NW
SC6
SE
CDP
722
642
563
484
405
325
246
167
87
8
TWT (ms)
0
-500
-1000
-1500
-2000
-2500
-3000
CP
IRC
P7
Basement
Inst. Phase
175.00
150.00
125.00
100.00
75.00
50.00
25.00
0.00
-25.00
-50.00
-75.00
-100.00
-125.00
-150.00
-175.00
2.5 km

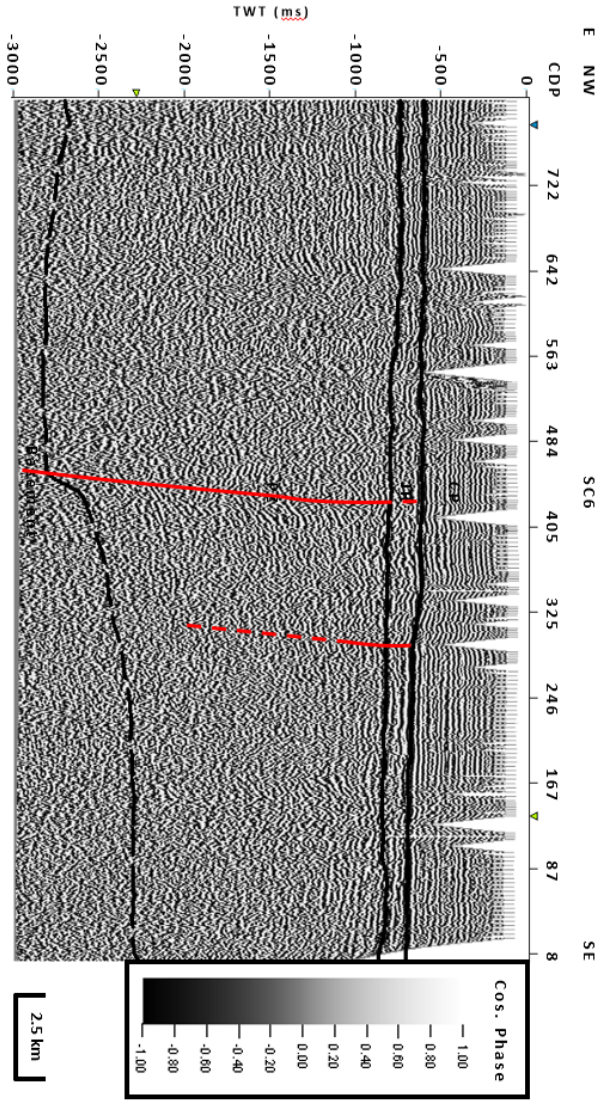

Fig. 19. Seismic reflectivity profile SC6 (a) and interpreted (b) and its associated attribute calculations: RMS amplitude (c); Instantaneous phase (d); and Cosine of phase (e). Each profile consistently exhibits features signifying the presence of the Gants Fault branch previously interpreted by Behrendt et al. (1983). The solid line indicates the portion of the fault branch interpreted with high confidence. The dashed portions of the fault branch are interpreted with lower confidence. Note the disruption of lateral continuity and sudden amplitude loss within a and b, the sudden amplitude loss in c, and the abrupt disruption of lateral continuity and dip change in d and e all occurring at the location of the fault.

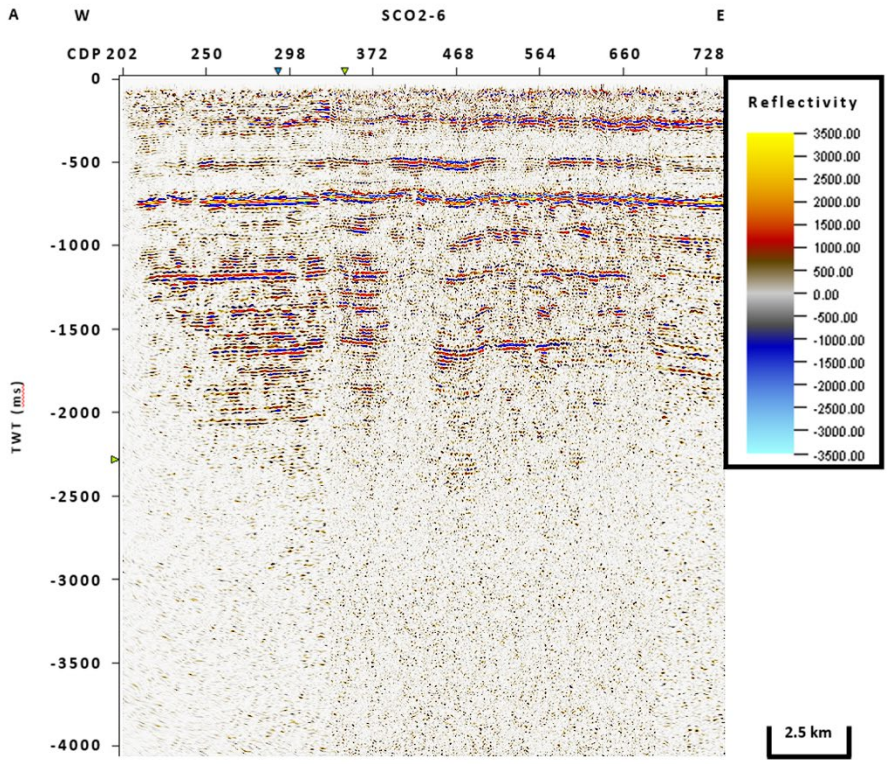
A
W
SCO2-6
E
CDP 202
250
298
372
468
564
660
728
0
-500
-1000
-1500
-2000
-2500
-3000
-3500
-4000
TWT (ms)
Reflectivity
3500.00
3000.00
2500.00
2000.00
1500.00
1000.00
500.00
0.00
-500.00
-1000.00
-1500.00
-2000.00
-2500.00
-3000.00
-3500.00
2.5 km

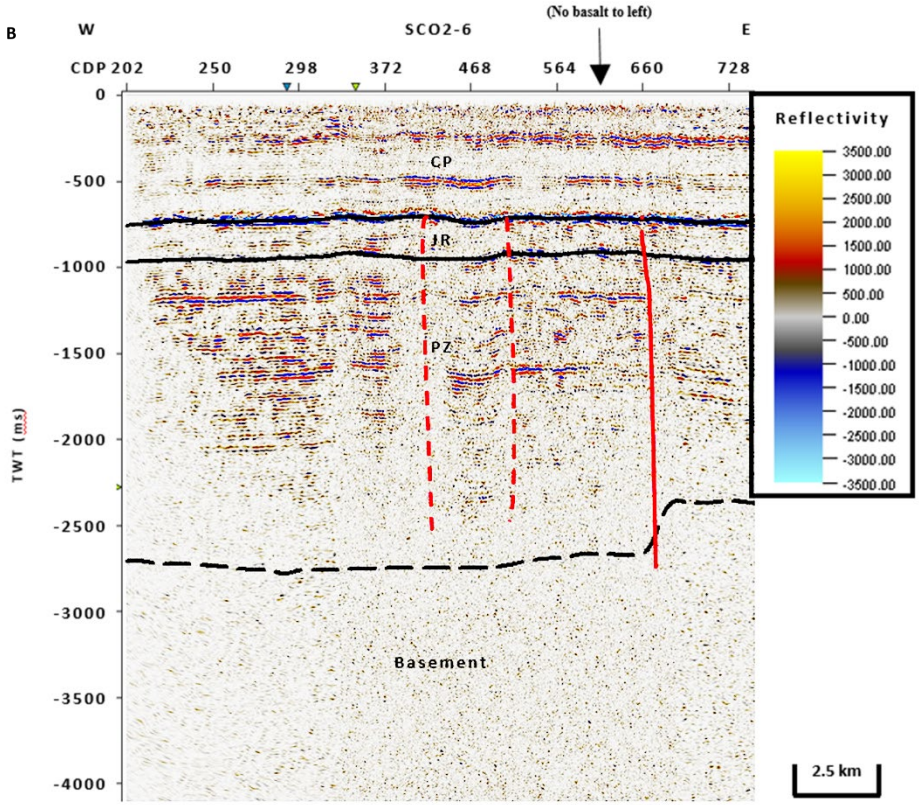
B
W
SCO2-6
E
(No basalt to left)
CDP 202
250
298
372
468
564
660
728
0
-500
-1000
-1500
-2000
-2500
-3000
-3500
-4000
TWT (ms)
CP
JR
PZ
Basement
Reflectivity
3500.00
3000.00
2500.00
2000.00
1500.00
1000.00
500.00
0.00
-500.00
-1000.00
-1500.00
-2000.00
-2500.00
-3000.00
-3500.00
2.5 km

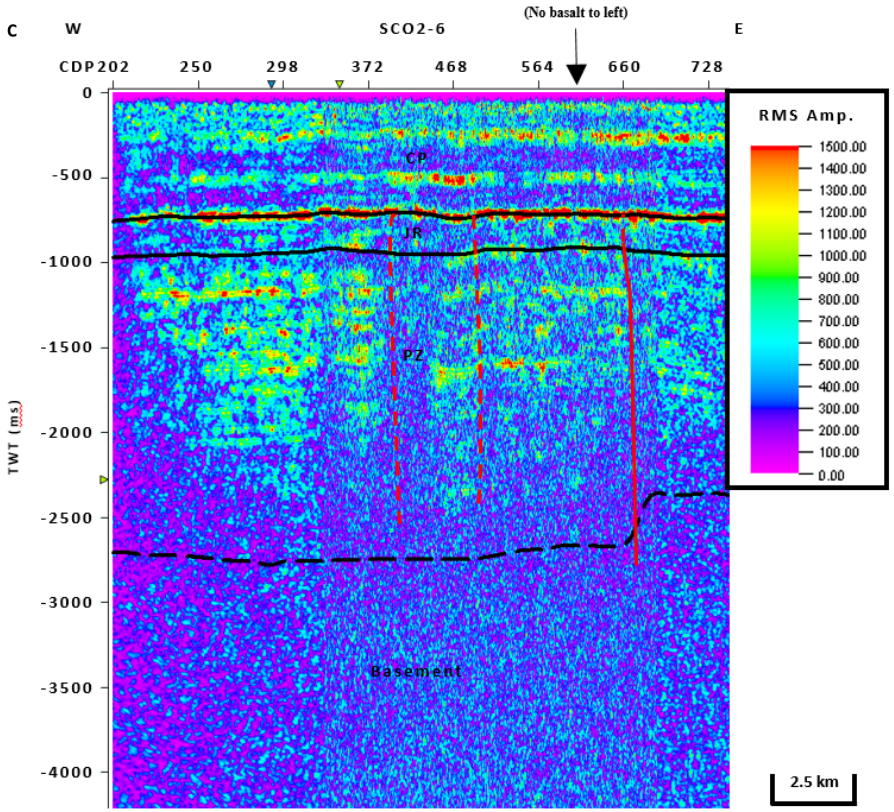
C
W
SCO2-6
E
(No basalt to left)
CDP202
250
298
372
468
564
660
728
0
-500
-1000
-1500
-2000
-2500
-3000
-3500
-4000
TWT (ms)
CP
JR
PZ
Basement
RMS Amp.
1500.00
1400.00
1300.00
1200.00
1100.00
1000.00
900.00
800.00
700.00
600.00
500.00
400.00
300.00
200.00
100.00
0.00
2.5 km

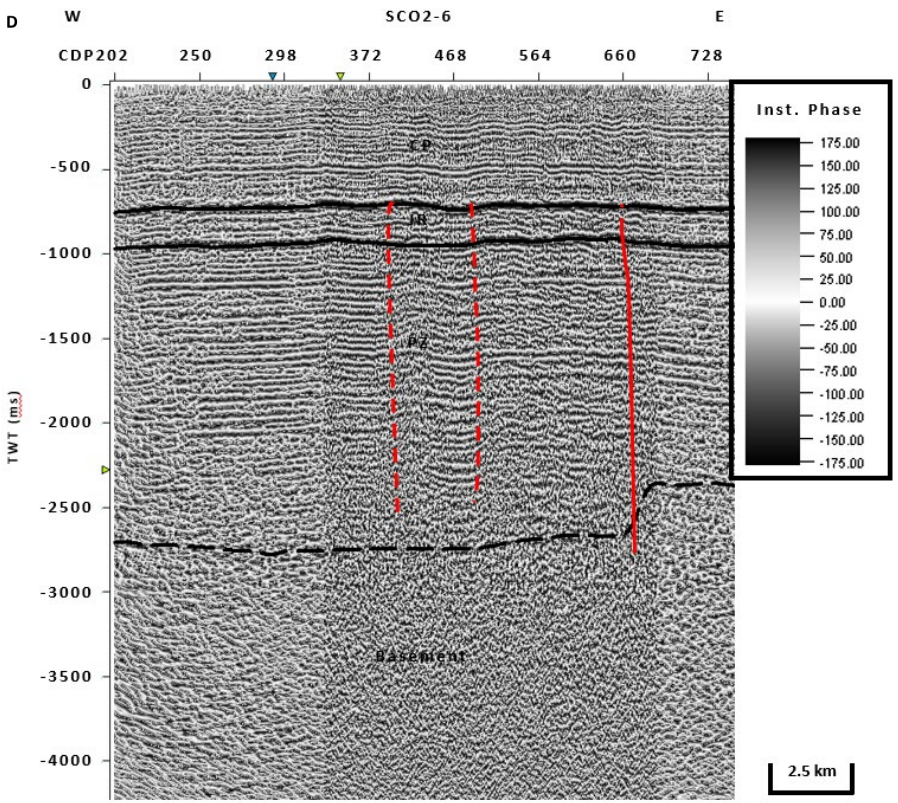
D
W
SCO2-6
E
CDP202
250
298
372
468
564
660
728
0
-500
-1000
-1500
-2000
-2500
-3000
-3500
-4000
TWT (ms)
EP
NB
PZ
Basement
Inst. Phase
175.00
150.00
125.00
100.00
75.00
50.00
25.00
0.00
-25.00
-50.00
-75.00
-100.00
-125.00
-150.00
-175.00
2.5 km

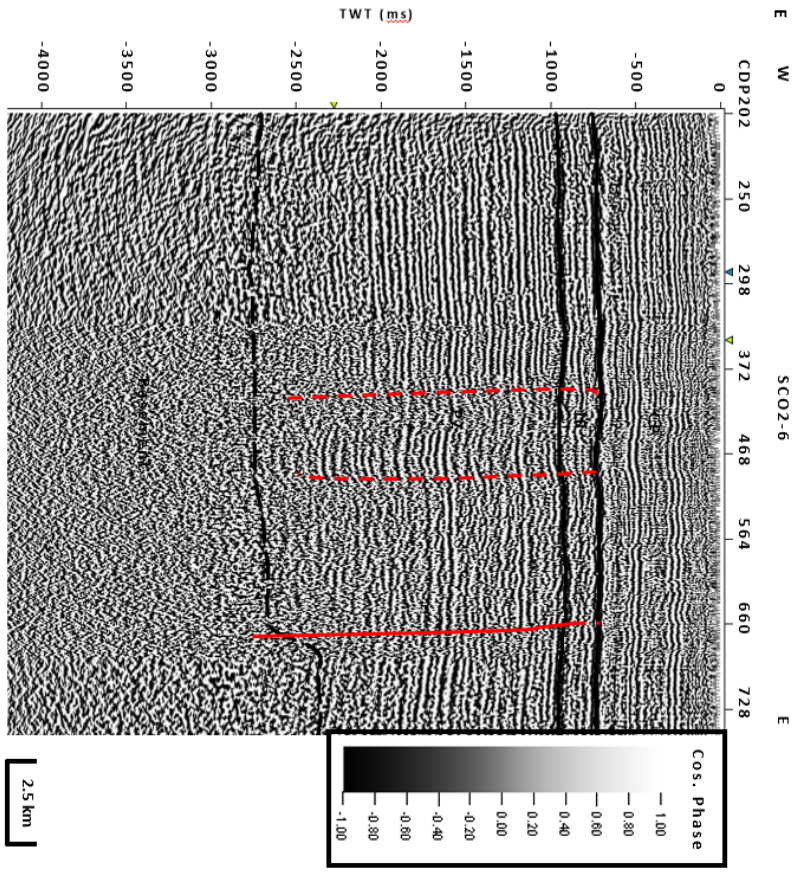

Fig. 20. Seismic reflectivity profile SCO2-6 (a) and interpreted (b) and its associated attribute calculations: RMS amplitude (c); Instantaneous phase (d); and Cosine of phase (e). Each profile consistently exhibits features signifying the presence of the Gants Fault branch previously interpreted by Behrendt et al. (1983). The solid line indicates the portion of the fault branch interpreted with high confidence. The dashed portions of the fault branch are interpreted with lower confidence. Note the disruption of lateral continuity and sudden amplitude loss within a and b, the sudden amplitude loss in c, and the abrupt disruption of lateral continuity and dip change in d and e all occurring at the location of the fault.

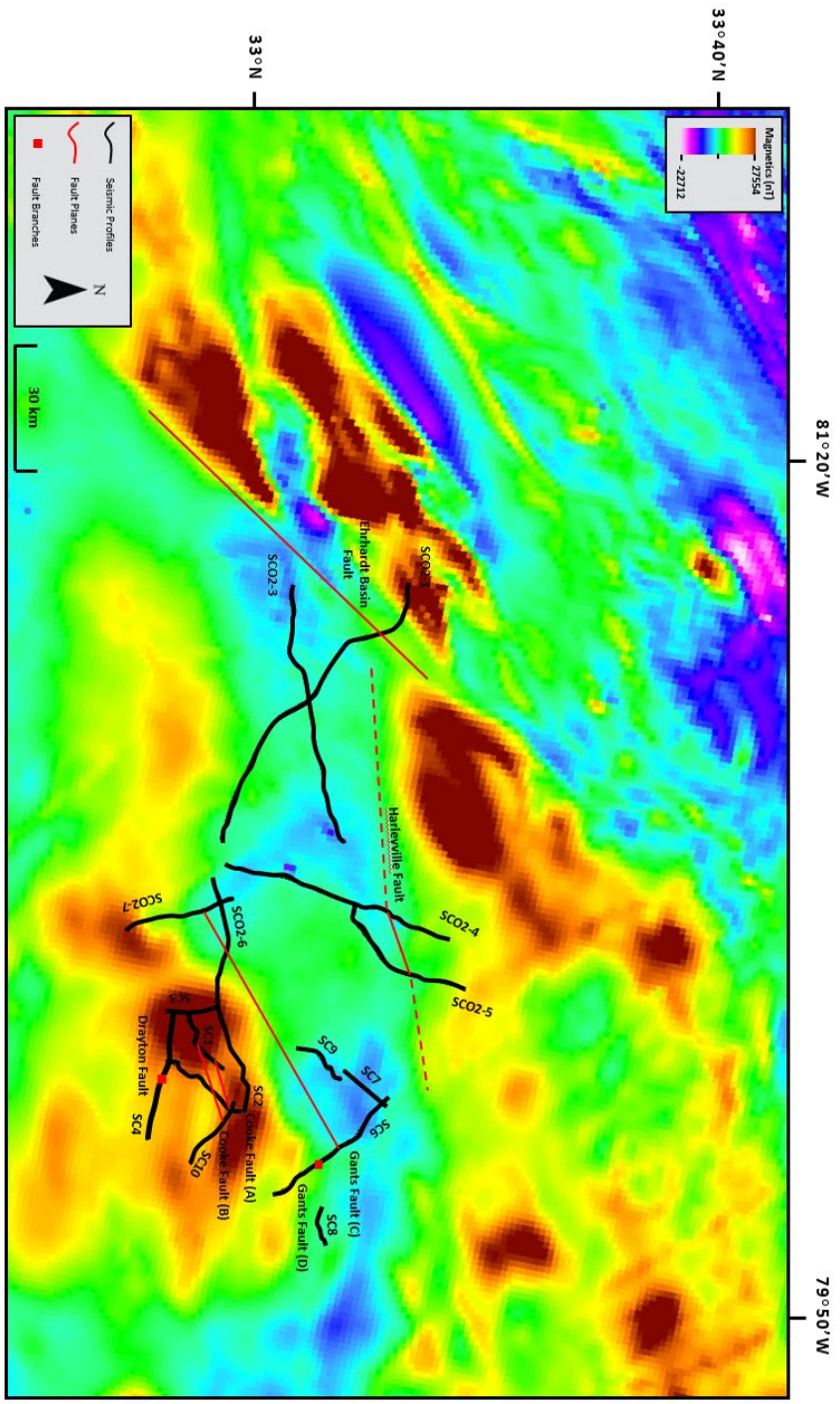

Fig. 21. Magnetic anomaly map, as previously seen, showing location of faults in relation to magnetic features and the seismic dataset. Note the Ehrhardt basin fault bounding the Triassic basin seen on seismic profile SCO2-1, the newly interpreted Harleyville fault which bounds the northern magnetic high where substantial Paleozoic Suwannee basin thinning occurs, and Gants fault which bounds the southern magnetic high where substantial Paleozoic Suwannee basin thinning also occurs. In regards to seismicity within the MPSSZ, the Gants, Cooke, and Drayton faults seem to be the most likely candidates.

CHAPTER V

CONCLUSIONS AND ADDITIONAL RESEARCH

The integration and synthesis of two seismic datasets, well data, refraction velocities, and seismic attributes aided in interpretation and correlation of the Suwannee basin sedimentary sequence. Furthermore, it aided in interpreting fault planes present on the seismic profiles. The Suwannee basin sedimentary sequence's presence throughout all 15 of the seismic profiles indicates the proposed position of the Suwannee Suture Zone by (Boote and Knapp, 2018) is likely the location of the Pangea supercontinent transcurrent fault, a large strike-slip boundary separating Gondwana from Laurentia. Furthermore, the sedimentary sequence's relative lack of deformation implies that the currently emplaced Suwannee basin strata was at a different location during the time of collision between Pangea and Gondwana. In other words, the sequence was likely emplaced in its current location by strike slip movement. The current interpretation implies evidence for the hypothesis that the Pangea supercontinent transcurrent fault is present roughly 40 km northwest of the study area described here.

In addition, the Suwannee basin's presence, characteristics, and interpreted faults within it have their own implications for the presence of magnetic highs seen on the magnetic anomaly map and seismicity that occurs within the MPSSZ. The high-angle fault presence within the analyzed seismic data, suggested by the disruption of lateral continuity of reflector packages within the

seismic profiles, an abrupt dip change within reflectors, and sudden amplitude loss, and their projected fault plane orientations trending toward the locus of earthquake activity within the MPSSZ suggests that these large-scale faults could be responsible for seismicity that occurs within the region. Furthermore, the fault planes are consistent with expected orientation of deformation resulting from the regional stress regime. The planes parallel the Helena Banks fault plane which has been substantiated by numerous studies. It promotes further research into structure within the epicentral region of seismogenic activity of the MPSSZ.

Some discrepancies with the analysis from this study include the loss of vertical resolution that occurs deep within the seismic profiles in both the SCO2 and SC datasets. In particular, in both the SCO2-1 and SCO2-3 lines, the Triassic basin sediment overlies the Suwannee basin sequence. Thus, greatly reducing the amount of seismic energy that is able to propagate and interact with those deeper targets. Furthermore, similar issues occur where the Jurassic basalt maintains a thick consistent presence. On a similar note, fault branch projections deep into the seismic sections can become somewhat ambiguous as additional factors begin to disrupt signal coherency, such as diabase presence causing noise interference, natural high-cut filtering, and amplitude loss. Additionally, there is no well control that penetrates deep enough to aid in interpretation of deeper propagating fault branches.

Additional research could include the processing and analysis of the SCO2 3D seismic volume. This volume would add data density and potentially further support or disprove the interpretation of the 2D seismic profiles. It would also prove helpful in connecting the gaps between some of the profiles, where there is no data. Newly acquired seismic data utilizing modern methods of acquisition may assist in the ability to better resolve deep within the Suwannee basin sequence, as well as fault branches and their planal projections. Furthermore, if additional seismic data were collected to the west, northwest of the study area then we may be able to define exactly where the boundary is that separates Paleozoic strata of Laurentian origin from that of Gondwanan origin.

Additional wells drilled throughout the concentrated study area would also provide higher vertical resolution in regards to lithologic boundaries and subtle sedimentary sequence changes that would assist in reconstructing the tectonic history of the region.

REFERENCES

Ackermann, H. D. (1983). Seismic refraction study in the area of the Charleston, South Carolina 1886 earthquake. *US Geological Survey Professional Paper*, *1313*, F1–F20.

Applin, P. L. (1951). Preliminary report on buried pre-Mesozoic rocks in Florida and states. *US Geological Survey Circular*, 91.

Arden Jr,, D. D. (1974). A geophysical profile in the Suwannee Basin, northwestern Florida. *Georgia Geological Survey Bulletin*, *87*, 111–112.

Austin Jr., J. A., Stoffa, P. L., Phillips, J. D., Oh, J., Sawyer, D. S., Purdy, G. M., … Makris, J. (1990). Crustal structure of the southeast Georgia embayment-Carolina trough; preliminary results of a composite seismic image of a continental suture(?) and a volcanic passive margin. *Geology*, *18*, 1023–1027.

Bakun, W. H., & Hopper, M. G. (2004). Magnitudes and locations of the 1811-1812 New Madrid, Missouri and the 1886 Charleston, South Carolina earthquakes. *Bulletin Seismological Society of America, 94*, 64-75.

Barnett, R. S. (1975). Basement structure of Florida and its tectonic implications. *Gulf Coast Association of Geological Societies*, *25*, 122–140.

Behrendt, J. C., & Hamilton, R. M. (1982). Record sections for multichannel seismic reflection data in the area of Charleston, South Carolina 1886 earthquake. *United States Department of the Interior Geological Survey*.

Behrendt, J. C., Hamilton, R. M., Ackermann, H. D., Henry, V. J., & Bayer, K. C. (1983). Marine multichannel seismic-reflection evidence for Cenozoic faulting and deep crustal structure near Charleston, South Carolina. *US Geological Survey Professional Paper, 1313,* J1-J29.

Boote, S. K., & Knapp, J. H. (2016). Offshore extent of Gondwanan Paleozoic strata in the southeastern United States: The Suwannee suture zone revisited. *Gondwana Research*, *40*, 199–210.

Boote, S. K., & Knapp, J. H. (2018). Preserved Neoproterozoic continental collision in southeastern North America: The Brunswick suture zone and Osceola continental margin arc. *Tectonics*, *37*, 1–17.

Braunstein, J. (1957). The habitat of oil in the Cretaceous of Mississippi and Alabama. *Mesozoic-Paleozoic Producing Areas of Mississippi and Alabama, Mississippi Geological Society*, *1*, 1–13.

Chapman, M. C., & Beale, J. N. (2008). Mesozoic and Cenozoic faulting imaged at the epicenter of the 1886 Charleston, South Carolina earthquake. *Bulletin of the Seismological Society of America*, *98*, 2533–2542.

Chapman, M. C., & Beale, J. N. (2010). On the geologic structure at the epicenter of the 1886 Charleston, South Carolina earthquake. *Bulletin of the Seismological Society of America*, 100, 1010–1030.

Chapman, M. C., & Beale, J. N. (2016). Modern seismicity and the fault responsible for the 1886 Charleston, South Carolina earthquake. *Bulletin of the Seismological Society of America*, 106, 364–372.

Chowns, T. M., & Williams, C. T. (1983). Pre-Cretaceous rocks beneath the Georgia coastal plain-regional implications: in Gohn, C.S., ed., studies related to the Charleston, South Carolina earthquake of 1886-tectonics and seismicity. *US Geological Survey Professional Paper*, *1313*, L1–L42.

Duncan, J. G. (1998). Geological history of an accreted terrane; Paleozoic stratigraphy of the north Florida basin, Suwannee terrane. *Ph.D. Thesis Florida State University*.

Dutton, C. E. (1989). The Charleston earthquake of August 31, 1886. *Ninth Annual Report of the U.S. Geological Survey to the Secretary of the Interior*, 203-528.

Gohn, G. S. (1983). Geology of the basement rocks near Charleston, South Carolina-data from detrital rock fragments in the lower Mesozoic(?) rocks in Clubhouse Crossroads Test Hole #3. *Geological Survey Professional Paper 1313-E*, E1–E22.

Hamilton, R. M., Behrendt, J. C., & Ackerman, H. D. (1983). Land multi-channel seismic reflection evidence for tectonic features near Charleston, South Carolina. *Geological Survey Professional Paper 1313-I*, I1–I18.

Hatcher Jr., R. D. (2010). The Appalachian orogen: a brief summary. *Geological Society of America Memoirs*, *206*, 1–19.

Heffner, D. M., Knapp, J. H., Knapp, C. C., & Akintunde, O. M. (2011). Preserved extent of Jurassic flood basalt in the South Georgia Rift: A new interpretation of the J Horizon. *Geology*, *40*.

Heffner, D. M. (2013). Tectonics of the South Georgia Rift. *Ph.D. Thesis University of South Carolina*.

Higgins, M. W., & Zietz, I. (1983). Geologic interpretation of geophysical maps of the pre-Cretaceous "basement" beneath the coastal plain of the southeastern United States. *Geological Society of America Memoirs*, *158*, 125–130.

Holbrook, W. S., Reiter, E. C., Purdy, G. M., Sawyer, D., Stoffa, P. L., Austin Jr., J. A., … Makris, J. (1994). Deep structure of the US Atlantic continental margin, offshore South Carolina, from coincident ocean bottom and multichannel seismic data. *Journal of Geophysical Research*, *99*, 9155–9178.

Horton, J. W., Drake, A. A., & Rankin, D. W. (1989). Tectonostratigraphic terranes and their Paleozoic boundaries in the central and southern Appalachians. *Geological Society of America Special Papers*, *230*, 213–245.

Johnston, A.C. (1996). Seismic moment assessment of earthquakes in stable continental regions – III. New Madrid 1811-1812, Charleston 1886 and Lisbon 1775. *Geophysical Journal International, 126,* 314-344.

King, P. B. (1961). Systematic pattern of Triassic dikes in the Appalachian region. *US Geological Survey Professional Paper*, *424-B*, B93–B95.

Koson, S., Chenrai, P., & Choowong, M. (2014). Seismic Attributes and Their Applications in Seismic Geomorphology. *Bulletin of Earth Sciences of Thailand*, *6*, 1–9.

Lizarralde, D., Holbrook, W. S., & Oh, J. (1994). Crustal structure across the Brunswick magnetic anomaly, offshore Georgia, from coincident ocean bottom and multi-channel seismic data. *Journal of Geophysical Research*, *99*, 21,721–741,757.

McBride, J. H., & Nelson, K. D. (1988). Integration of COCORP deep reflection and magnetic anomaly analysis in the southeastern United States: implications for origin of the Brunswick and East Coast magnetic anomalies. *GSA Bulletin*, *100*, 436–445.

Mueller, P. A., Heatherington, A. L., Wooden, J. L., Shuster, R. D., Nutman, A. P., & Williams, L. S. (1994). Precambrian zircons from the Florida basement: a Gondwanan connection. *Geology*, *22*, 119–122.

Mueller, P. A., Heatherington, A. L., Foster, D. A., Thomas, W. A., & Wooden, J. L. (2014). The Suwannee suture: Significance for Gondwana-Laurentia terrane transfer and formation of Pangea. *Gondwana Research*, *26*(1), 365–373.

Nelson, K. D., Arnow, J. A., McBride, J. H., Willemin, J. H., Huang, J., Zheng, L., & Kaufman, S. (1985). New COCORP profiling in the southeastern United States. Part I: Late Paleozoic suture and Mesozoic rift basin. *Geology*, *13*, 718–721.

Oh, J., Phillips, J. D., Austin Jr., J. A., & Stoffa, P. L. (1991). Deep-penetration seismic reflection images across the southeastern United States continental margin: continental lithosphere deep seismic reflections. *Geodynamics Series 22*, 225–240.

Pollock, J. C., Hibbard, J. P., & can Staal, C. R. (2012). A paleogeographical review of the peri-Gondwanan realm of the Appalachian orogeny. *Canadian Journal of Earth Sciences*, *49*, 259–288.

Poppe, L. J., Popenoe, P., Poag, C. W., & Swift, B. A. (1995). Stratigraphic and paleoenvironmental summary of the south-east Georgia embayment a correlation of exploratory wells. *Marine and Petroleum Geology*, *12*, 677–690.

Schilt, F. S., Brown, L. D., Oliver, J. E., & Coffmann, S. (1983). Subsurface structure near Charleston, South Carolina; results of COCORP reflection profiling in the Atlantic coastal plain, in studies related to the Charleston, South Carolina earthquake of 1886. *US Geological Survey Professional Paper 1313-H*, H1–H19.

Tauvers, P. R., & Muehlberger, M. R. (1987). Is the Brunswick magnetic anomaly really the Alleghanian suture? *Tectonics*, *6*, 331–342.

Thomas, W. A., Chowns, T. M., Daniels, D. J., Neathery, T. L., Glover, L., & Gleason, R. J. (1989). The subsurface Appalachians beneath the Atlantic and Gulf coastal plains. *The Geology of North America*, *F-2*, 447–458.

Thomas, W. A. (2010). Interactions between the southern Appalachian-Ouachita orogenic belt and basement faults in the orogenic footwall and foreland. *Geological Society of America Memoirs*, *206*, 897–916.

Traverse, A. (1987). Pollen and spores date origin of rift basins from Texas to Nova Scotia as early late Triassic; *Science, 236,* 1496-1472.

Weems, R. E. & Lewis, W. C. (2002). Structural and tectonic setting of the Charleston, South Carolina region: Evidence from the Tertiary stratigraphic record. *Geological Society of America Bulletin, 114,* 24-42.

Williams, H., & Hatcher, R. D. (1982). Suspect terranes and accretionary history of the Appalachian orogen. *Geology*, *10*, 536–550.

Wilson, J. (1966). Did the Atlantic open and then reclose? *Nature*, *211*, 676–681.

Yantis, B. R., Costain, J. K., Ackermann, H. D., & Coffmann, S. (1983). A reflection seismic study near Charleston, South Carolina. *US Geological Survey Professional Paper 1313-G*, G1–G20.

APPENDICES

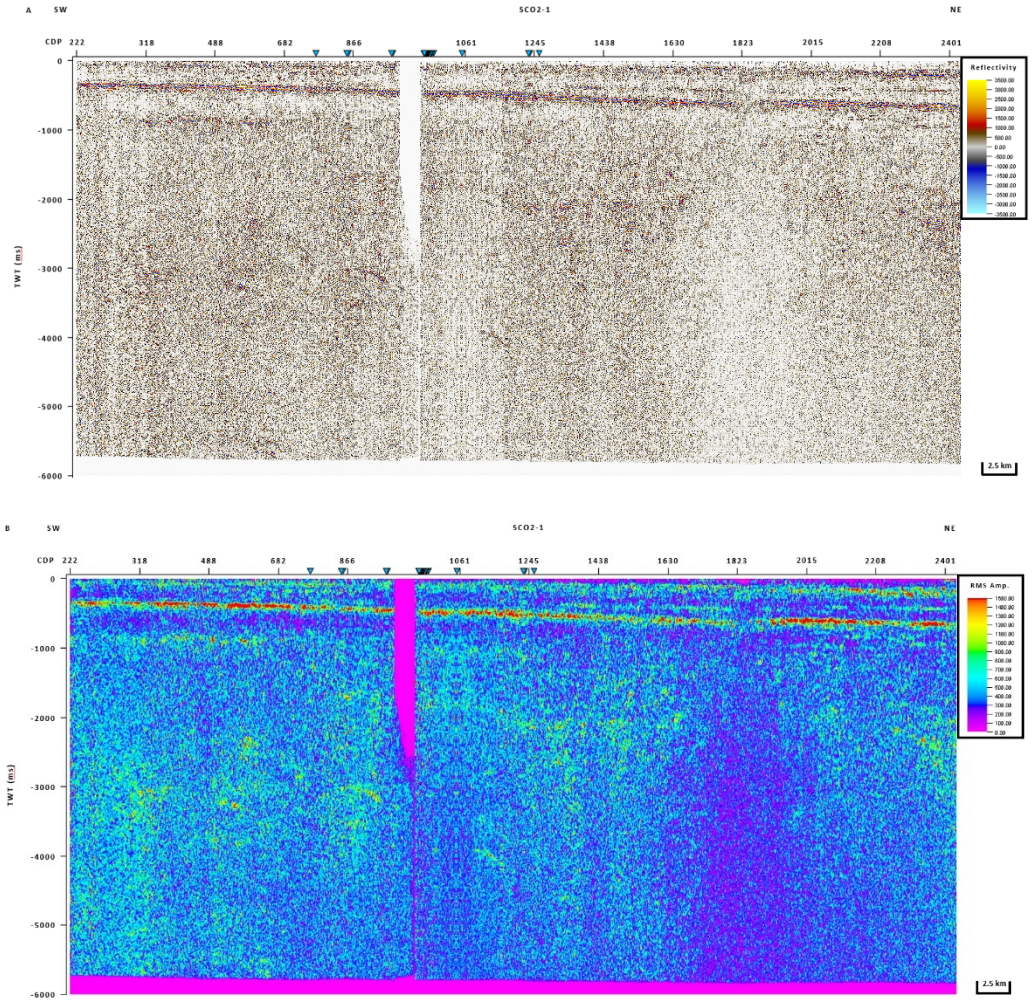
A
SW
SCO2-1
NE
CDP 222 318 488 682 866 1061 1245 1438 1630 1823 2015 2208 2401
0
-1000
-2000
-3000
-4000
-5000
-6000
TWT (ms)
Reflectivity
2.5 km
B
SW
SCO2-1
NE
CDP 222 318 488 682 866 1061 1245 1438 1630 1823 2015 2208 2401
0
-1000
-2000
-3000
-4000
-5000
-6000
TWT (ms)
RMS Amp.
2.5 km

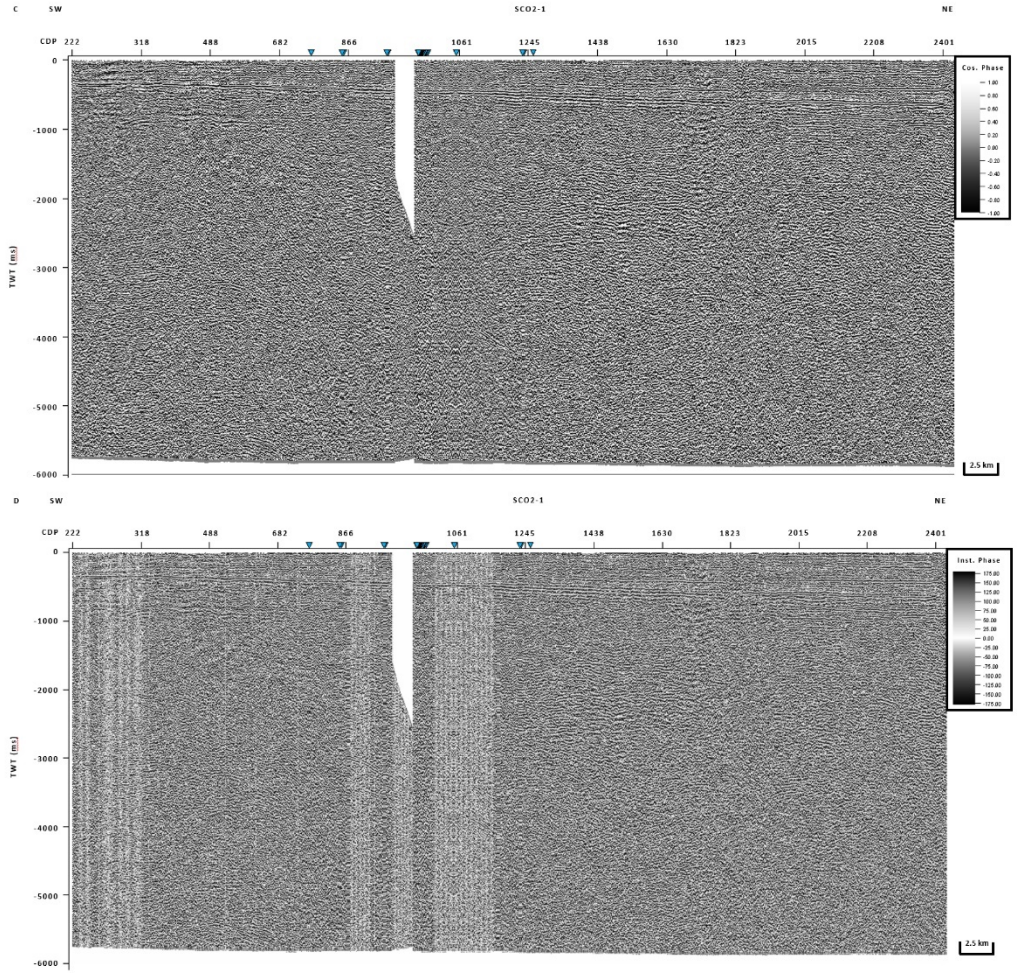

Fig. 22. Uninterpreted seismic reflectivity profile SC02-1 (a), RMS amplitude (b), cosine of phase (c), and instantaneous phase (d).

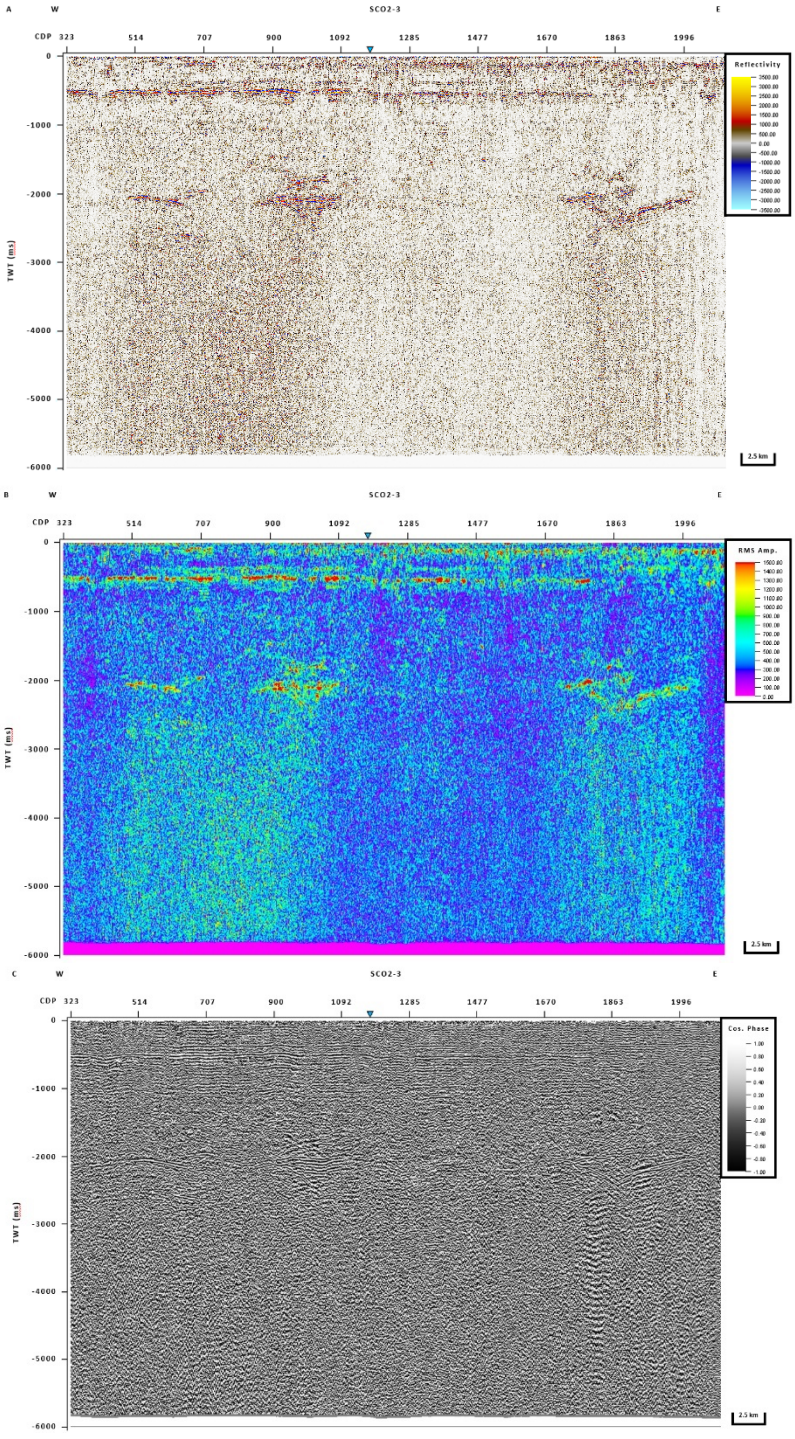
A
W
SCO2-3
E
CDP 323 514 707 900 1092 1285 1477 1670 1863 1996
0 -1000 -2000 -3000 -4000 -5000 -6000
TWT (ms)
Reflectivity
2.5 km
B
W
SCO2-3
E
CDP 323 514 707 900 1092 1285 1477 1670 1863 1996
0 -1000 -2000 -3000 -4000 -5000 -6000
TWT (ms)
RMS Amp.
2.5 km
C
W
SCO2-3
E
CDP 323 514 707 900 1092 1285 1477 1670 1863 1996
0 -1000 -2000 -3000 -4000 -5000 -6000
TWT (ms)
Cos. Phase
2.5 km

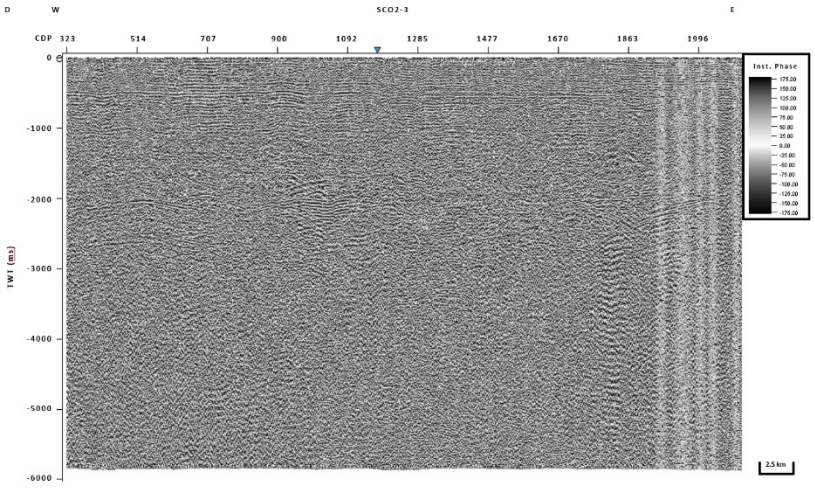

Fig. 23. Uninterpreted seismic reflectivity profile SC02-3 (a), RMS amplitude (b), cosine of phase (c), and instantaneous phase (d).

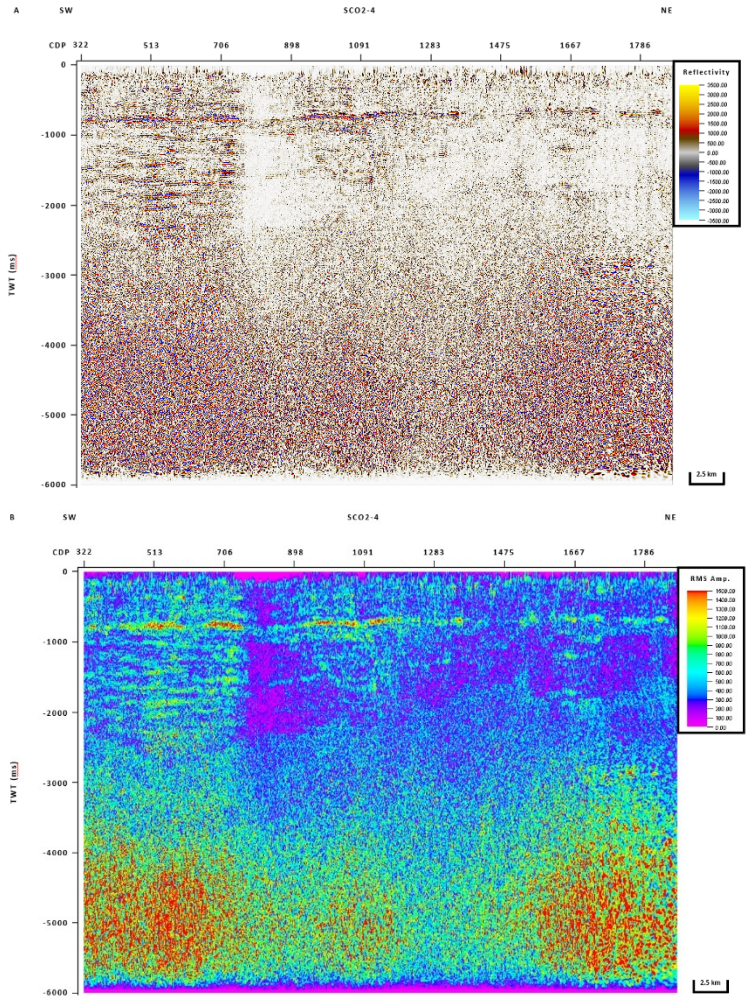

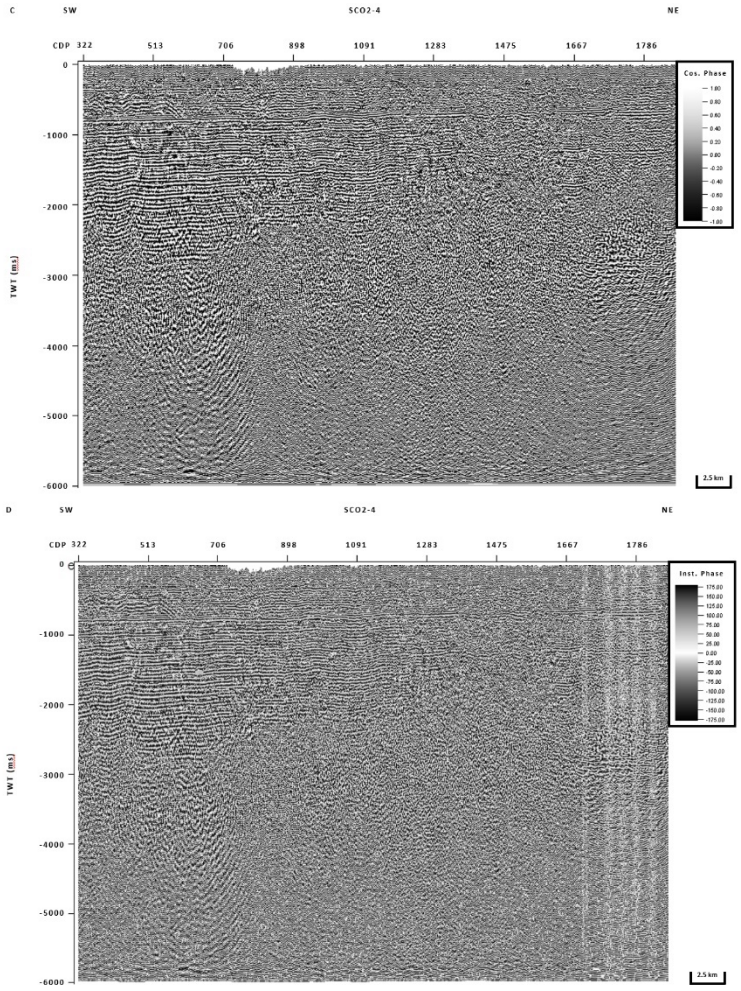

Fig. 24. Uninterpreted seismic reflectivity profile SC02-4 (a), RMS amplitude (b), cosine of phase (c), and instantaneous phase (d).

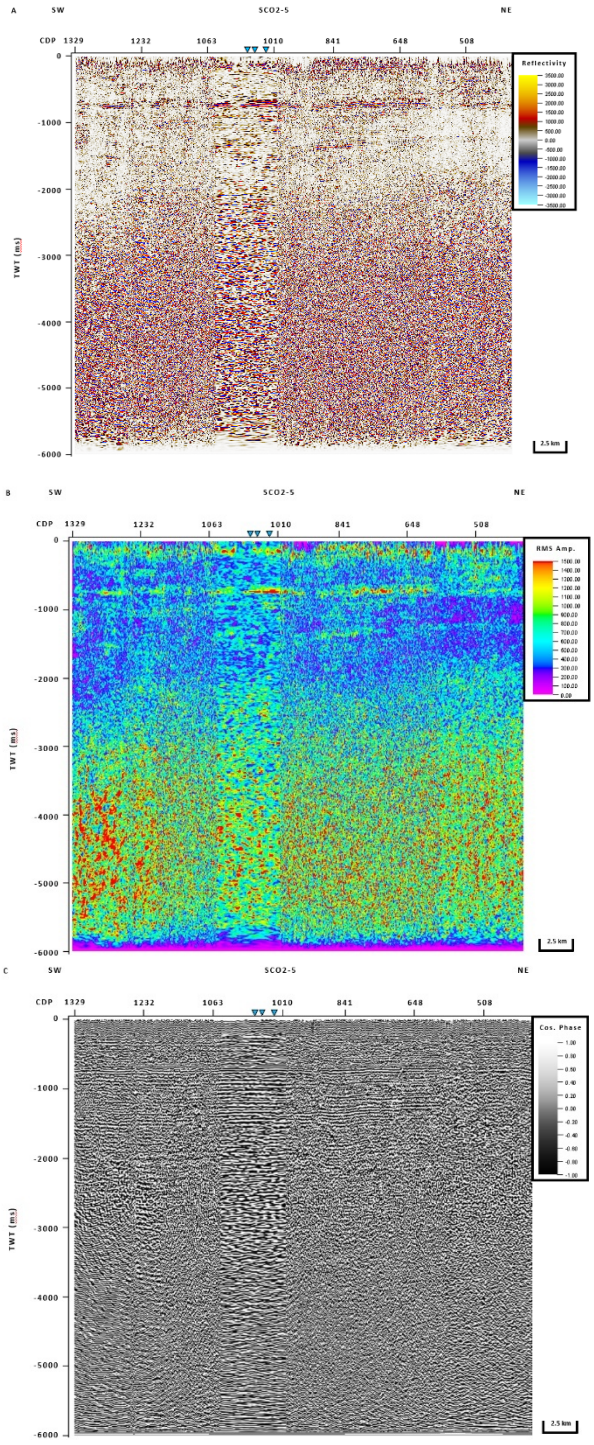
A
SW
SCO2-5
NE
CDP 1329
1232
1063
1010
841
648
508
Reflectivity
TWT (ms)
0
-1000
-2000
-3000
-4000
-5000
-6000
2.5 km
B
SW
SCO2-5
NE
RMS Amp.
C
SW
SCO2-5
NE
Cos. Phase

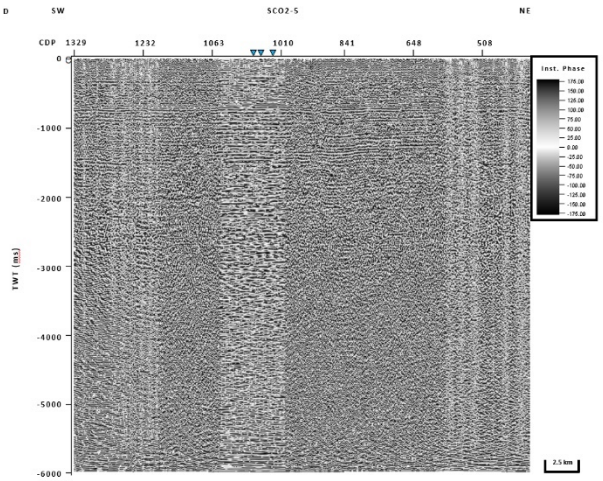

Fig. 25. Uninterpreted seismic reflectivity profile SC02-5 (a), RMS amplitude (b), cosine of phase (c), and instantaneous phase (d).

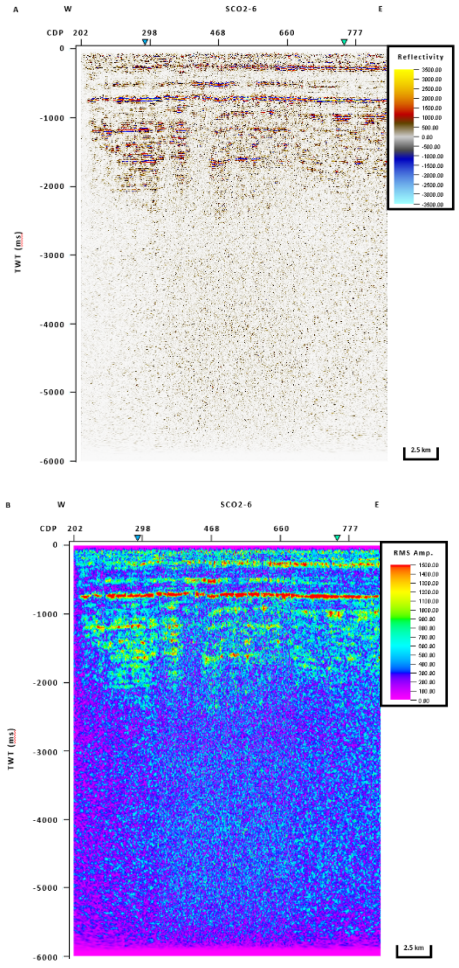

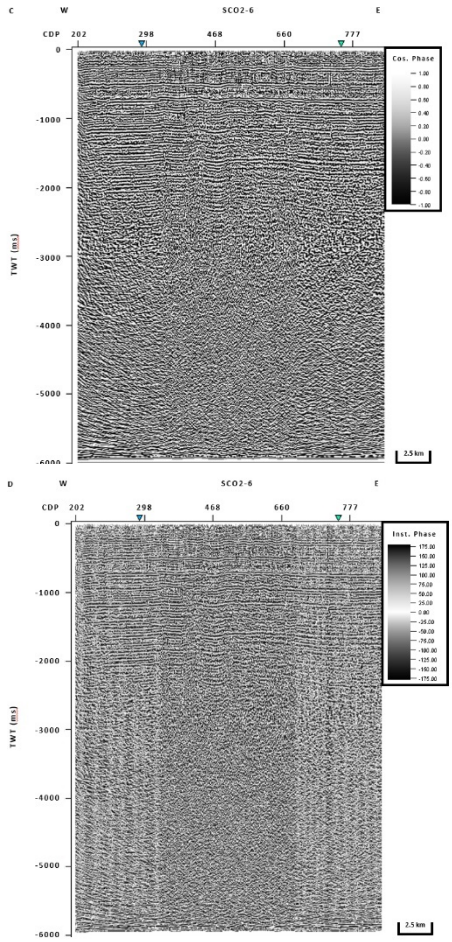

Fig. 26. Uninterpreted seismic reflectivity profile SC02-6 (a), RMS amplitude (b), cosine of phase (c), and instantaneous phase (d).

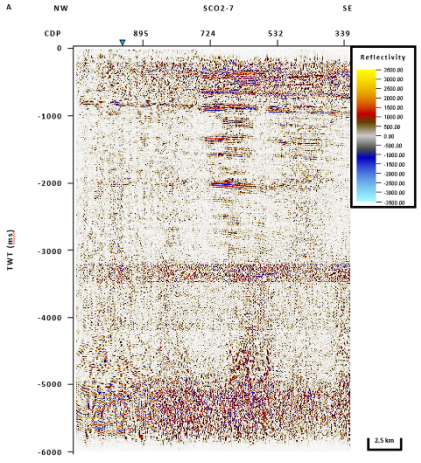

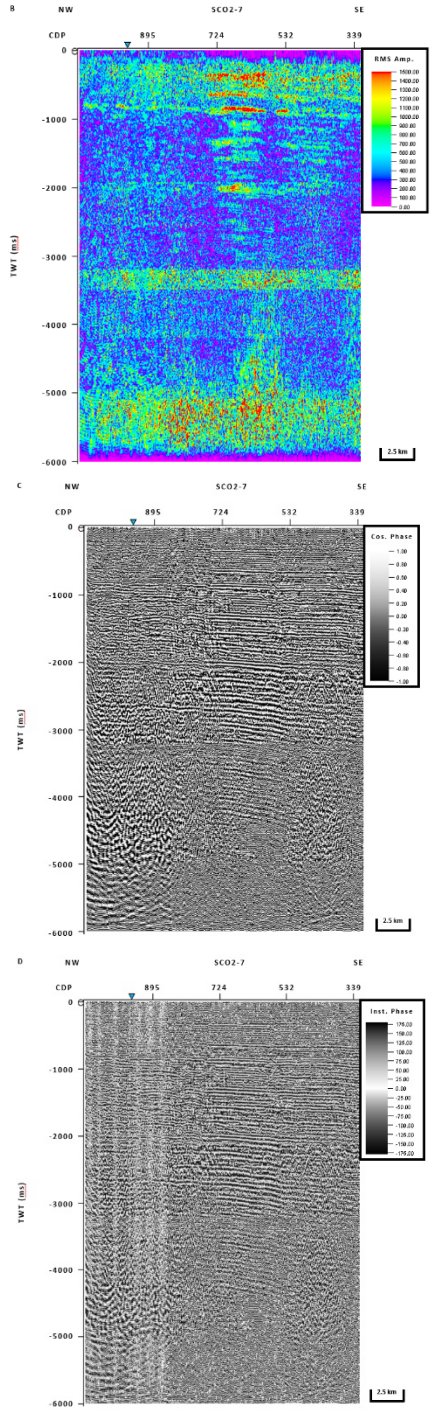

Fig. 27. Uninterpreted seismic reflectivity profile SC02-7 (a), RMS amplitude (b), cosine of phase (c), and instantaneous phase (d).

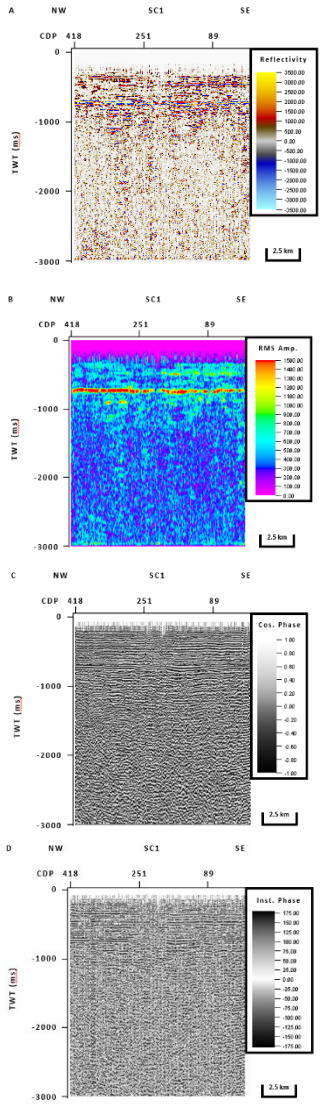

Fig. 28. Uninterpreted seismic reflectivity profile SC1 (a), RMS amplitude (b), cosine of phase (c), and instantaneous phase (d).

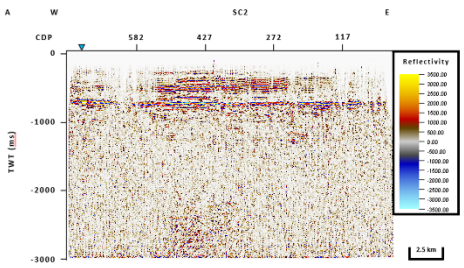

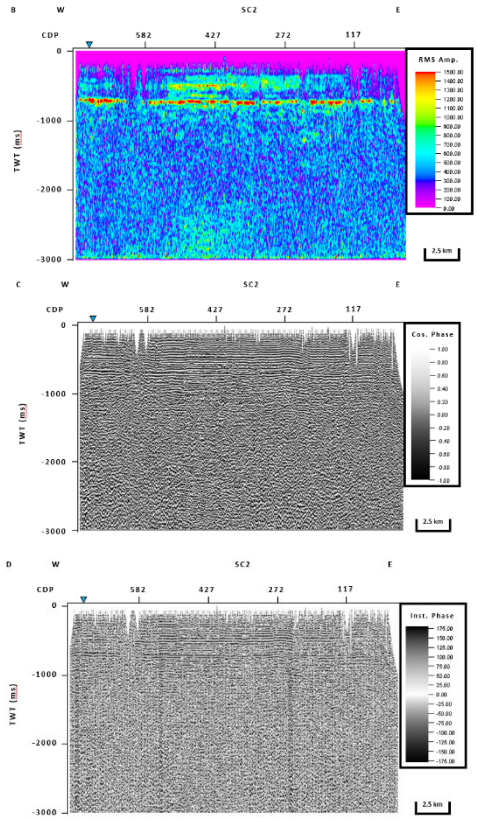

Fig. 29. Uninterpreted seismic reflectivity profile SC2 (a), RMS amplitude (b), cosine of phase (c), and instantaneous phase (d).

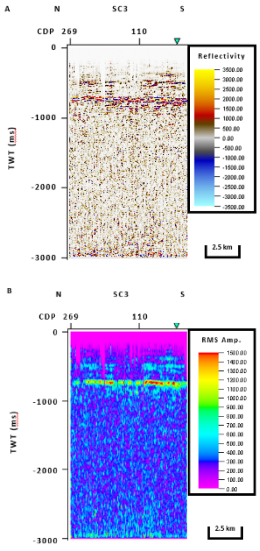

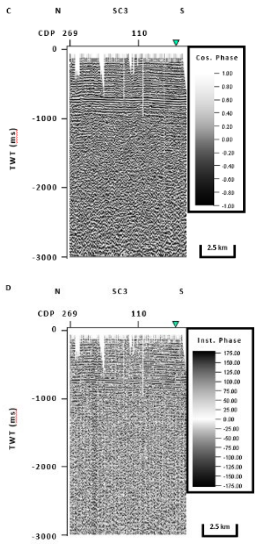

Fig. 30. Uninterpreted seismic reflectivity profile SC3 (a), RMS amplitude (b), cosine of phase (c), and instantaneous phase (d).

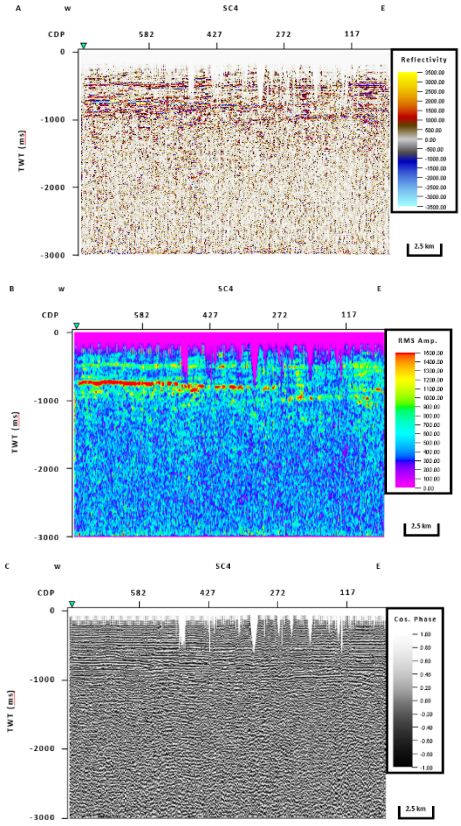

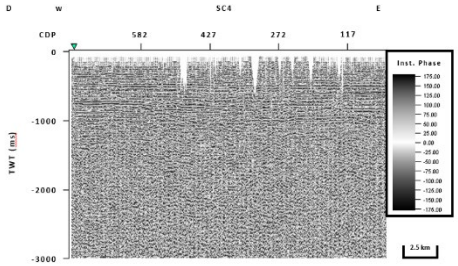

Fig. 31. Uninterpreted seismic reflectivity profile SC4 (a), RMS amplitude (b), cosine of phase (c), and instantaneous phase (d).

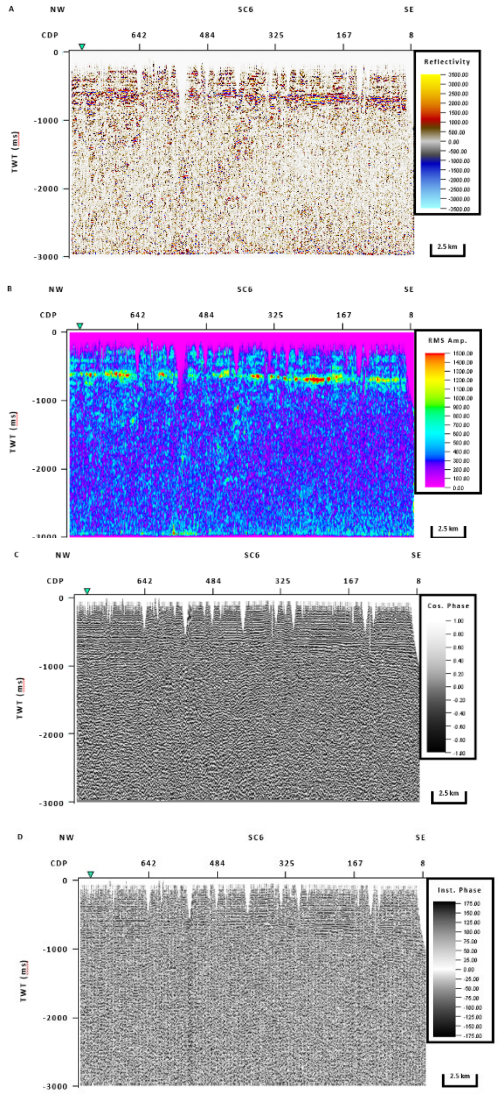

Fig. 32. Uninterpreted seismic reflectivity profile SC6 (a), RMS amplitude (b), cosine of phase (c), and instantaneous phase (d).

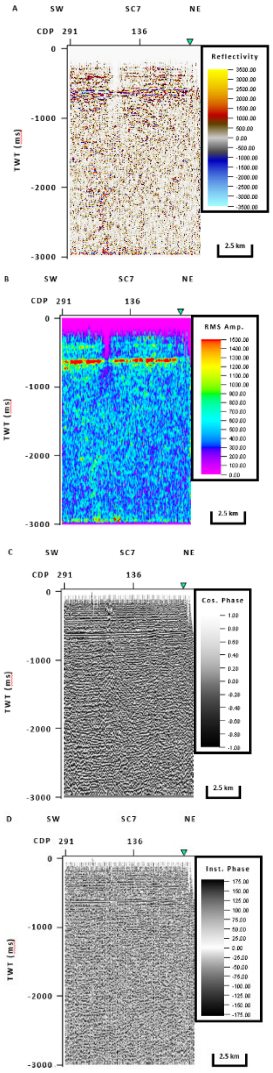

Fig. 33. Uninterpreted seismic reflectivity profile SC7 (a), RMS amplitude (b), cosine of phase (c), and instantaneous phase (d).

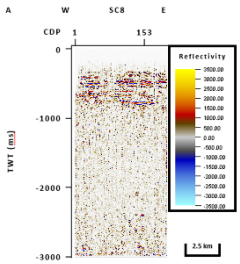

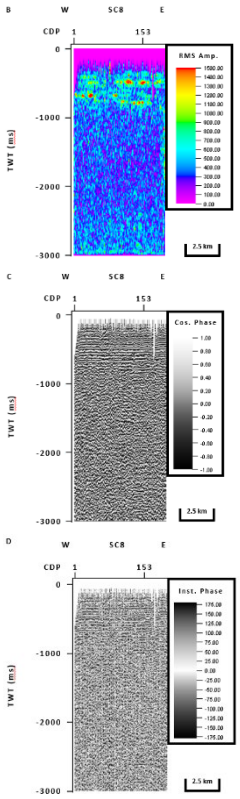

Fig. 34. Uninterpreted seismic reflectivity profile SC8 (a), RMS amplitude (b), cosine of phase (c), and instantaneous phase (d).

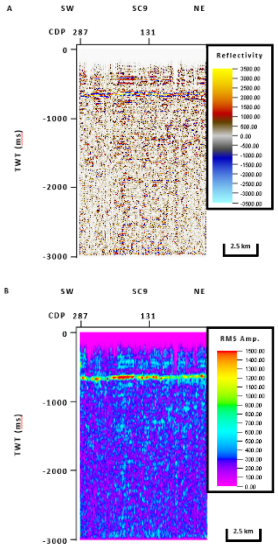

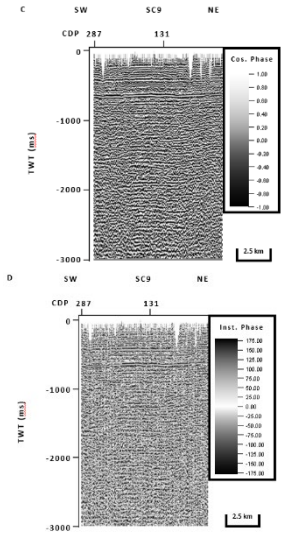

Fig. 35. Uninterpreted seismic reflectivity profile SC9 (a), RMS amplitude (b), cosine of phase (c), and instantaneous phase (d).

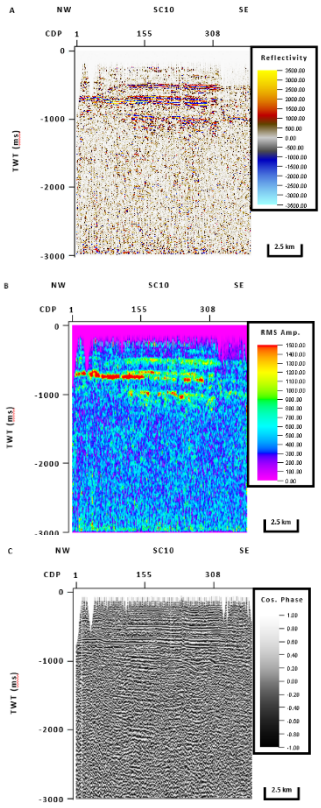

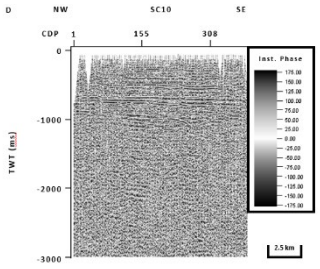

Fig. 36. Uninterpreted seismic reflectivity profile SC10 (a), RMS amplitude (b), cosine of phase (c), and instantaneous phase (d).

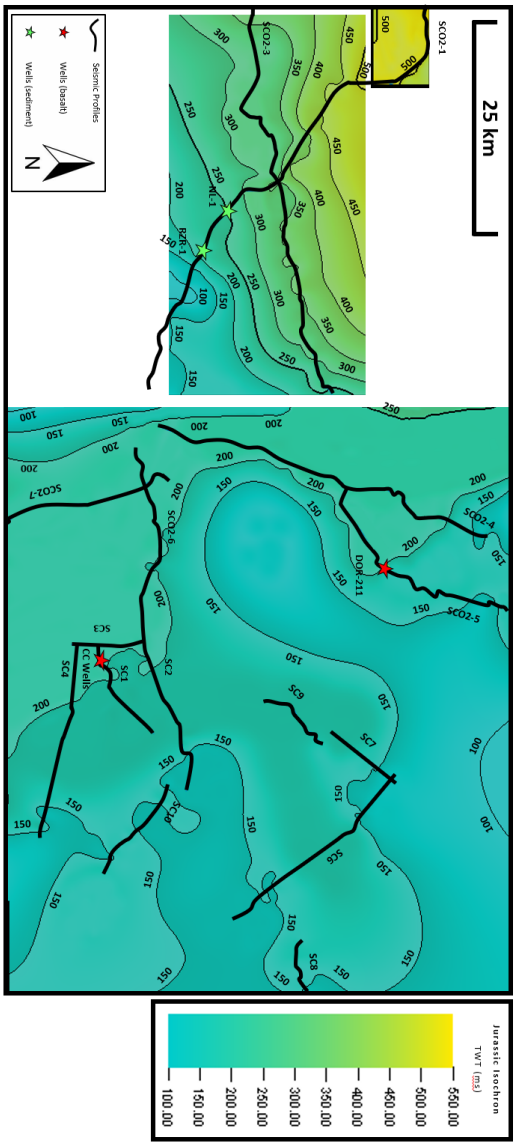

Fig. 37. Jurassic isochron map.

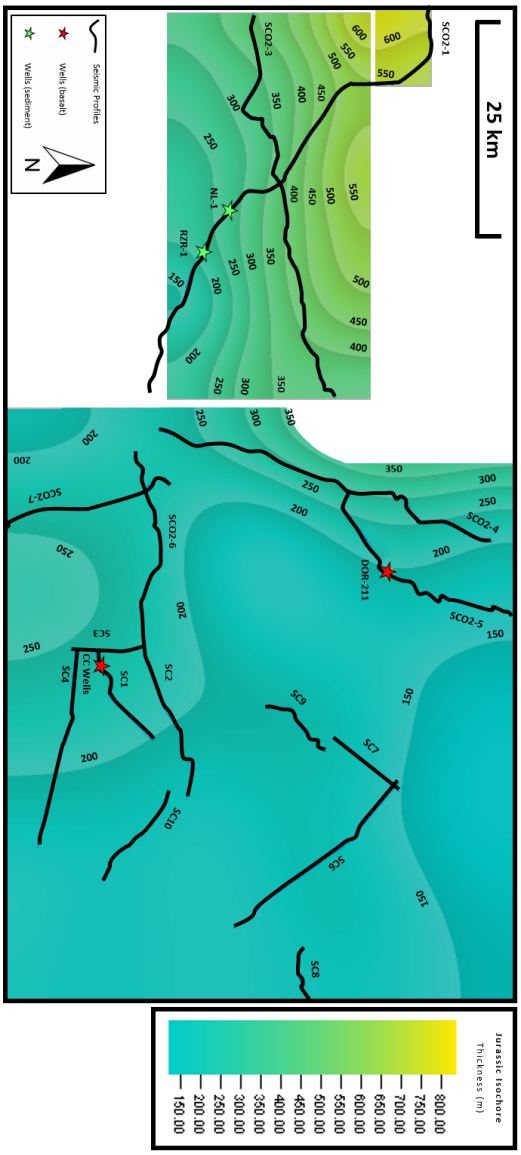

Fig. 38. Jurassic isochore map.

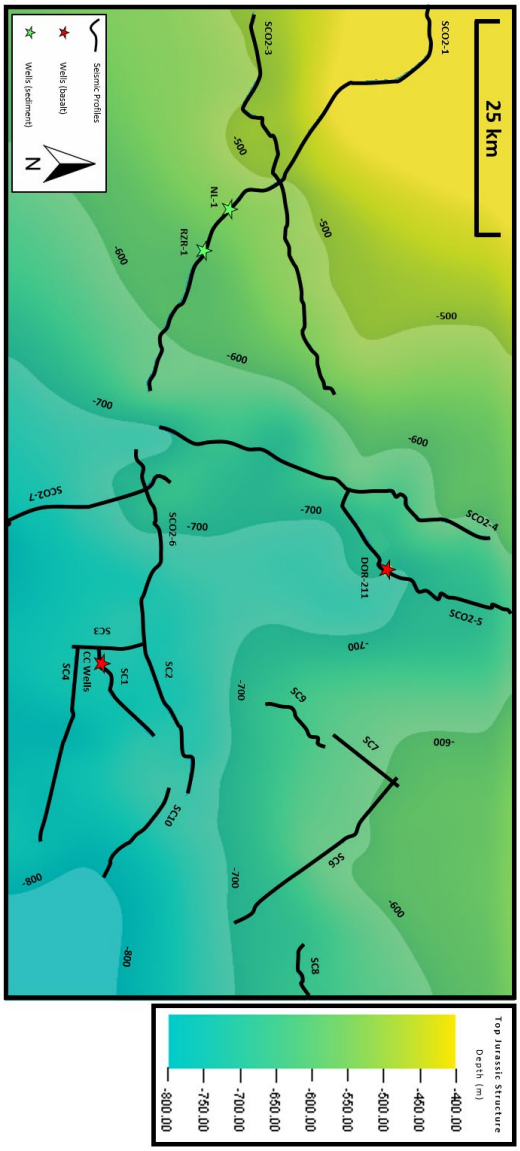

Fig. 39. Top of Jurassic structure map in depth.

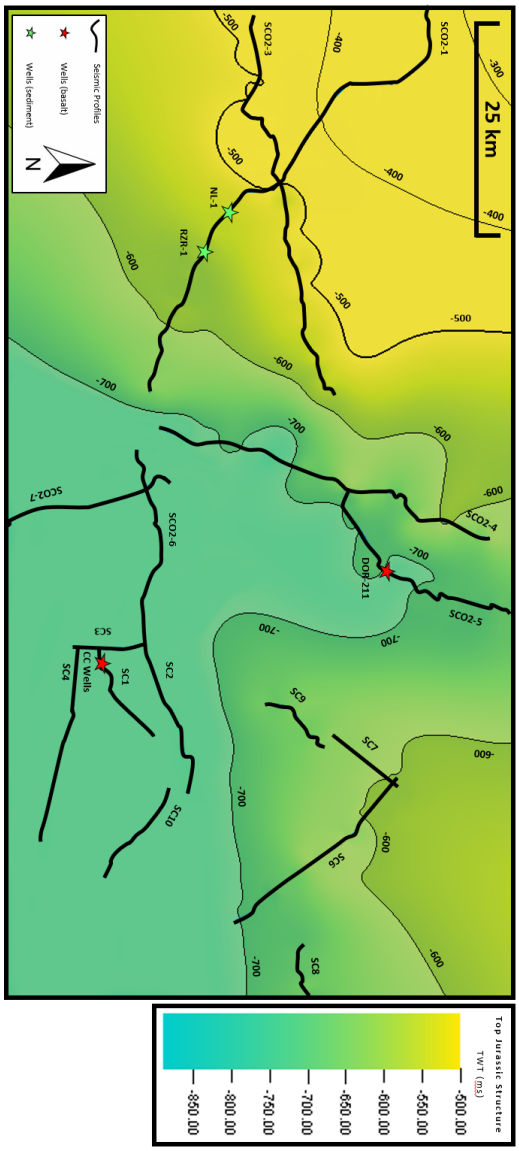

Fig. 40. Top of Jurassic structure map in two way time.

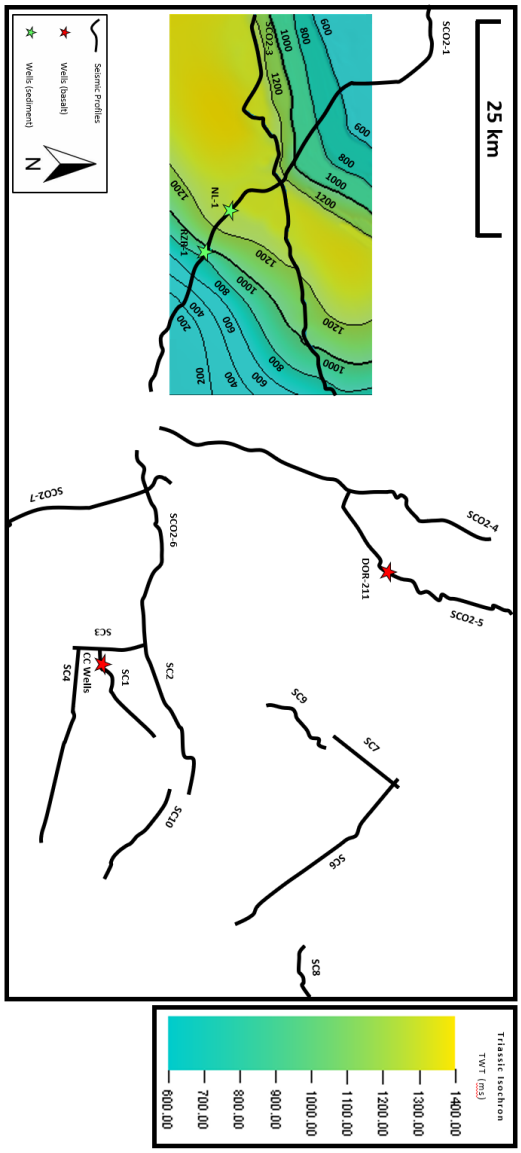

Fig. 41. Triassic isochron map.

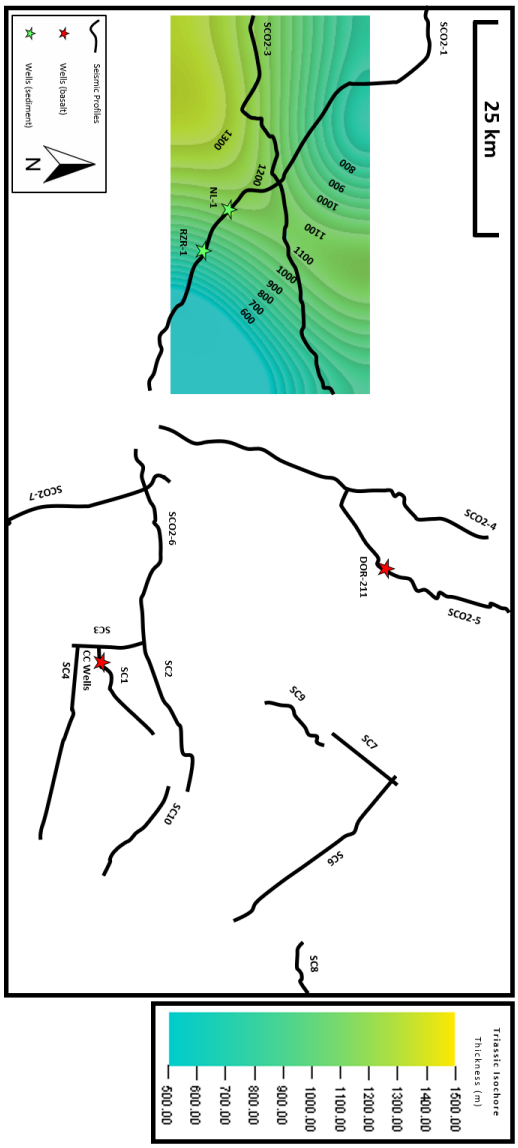

Fig. 42. Triassic isochore map.

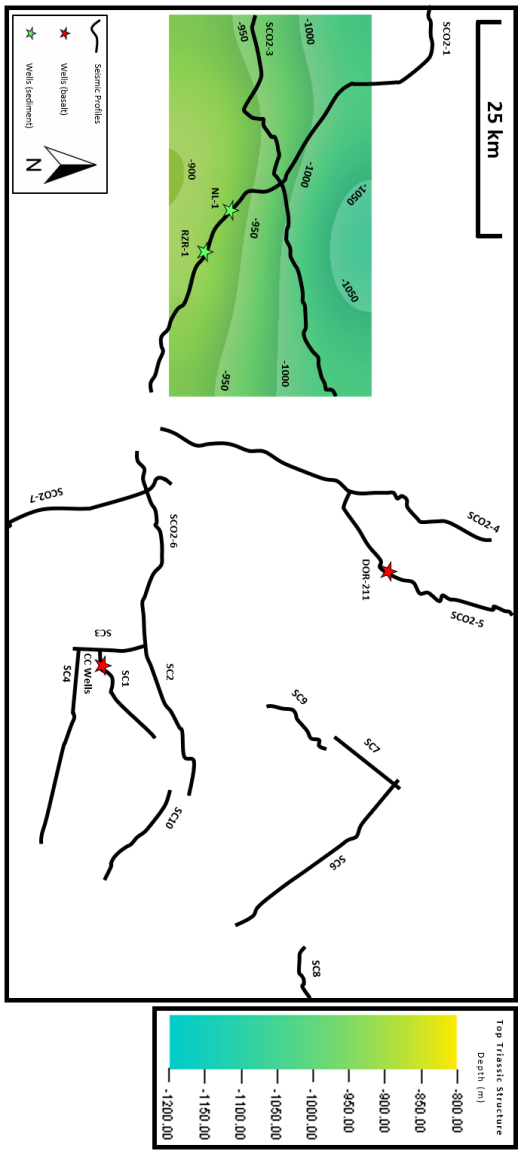

Fig. 43. Top of Triassic structure map in depth.

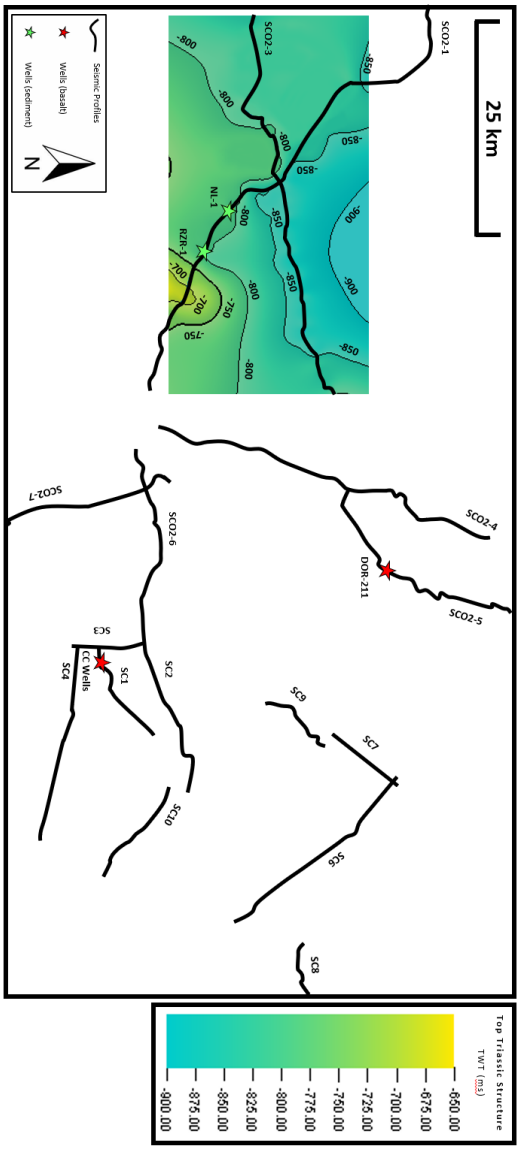

Fig. 44. Top of Triassic structure map in two way time.

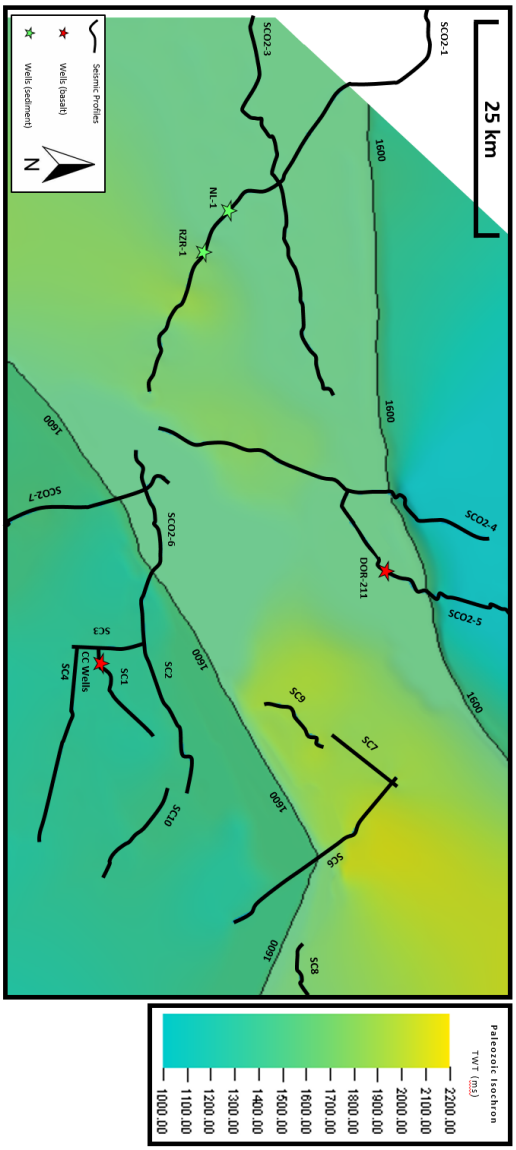

Fig. 45. Paleozoic Suwannee basin isochron map.

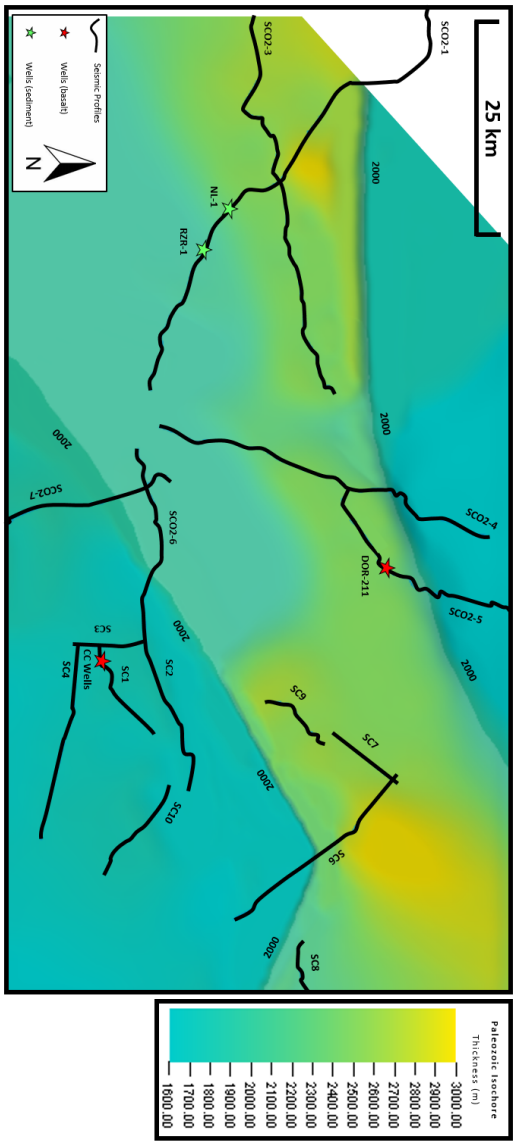

Fig. 46. Paleozoic Suwannee basin isochore map.

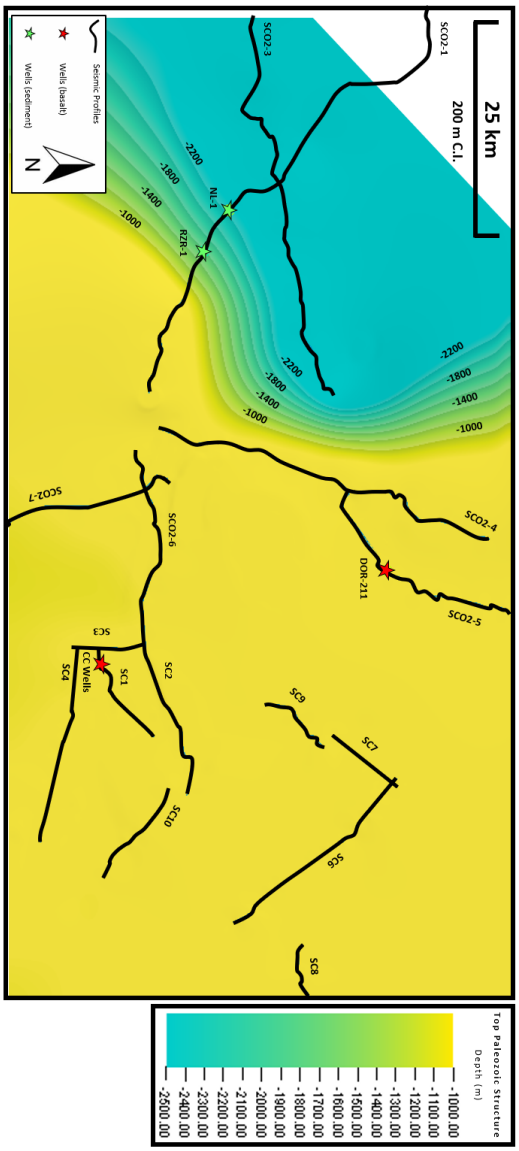

Fig. 47. Top of Paleozoic Suwannee basin structure map in depth.

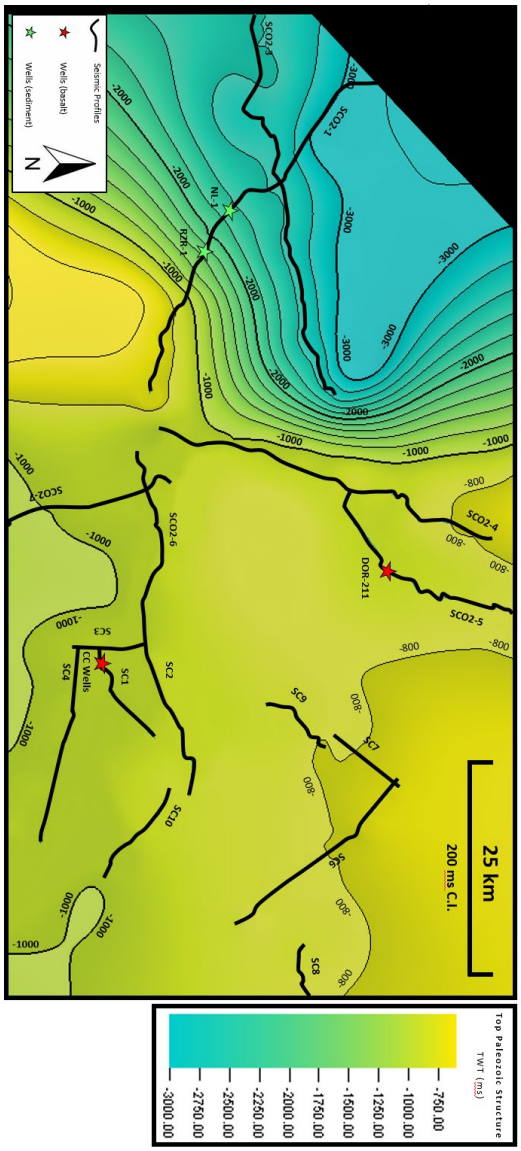

Fig. 48. Top of Paleozoic Suwannee basin structure map in two way time.

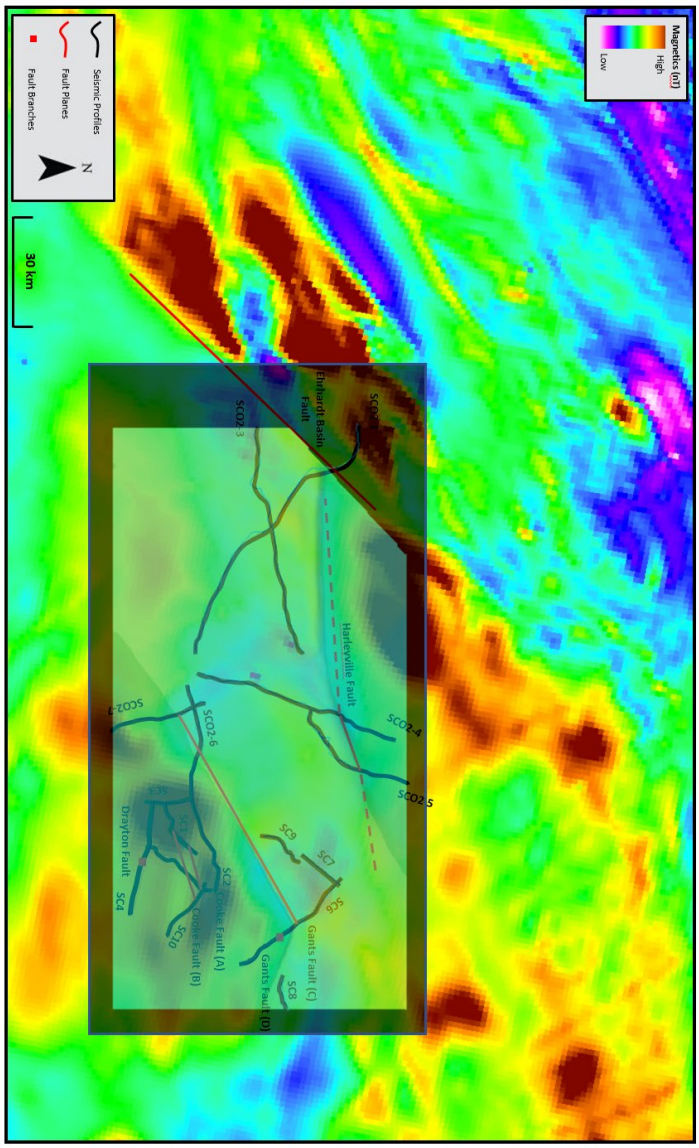

Fig. 49. Co-render of magnetic anomaly map with interpreted fault planes and Paleozoic Suwannee basin isochron map.

VITA

Michael Anthony Rohrer

Candidate for the Degree of

Master of Science

Thesis: RE-EVALUATION OF THE SCO2 AND SC SEISMIC REFLECTION DATASET, EASTERN SOUTH CAROLINA: IMPLICATIONS FOR TECTONIC EVOLUTION AND SEISMOGENIC ORIGIN

Major Field: Geology

Biographical:

Education:

Completed the requirements for the Master of Science in Geology at Oklahoma State University, Stillwater, Oklahoma in May, 2020.

Completed the requirements for the Bachelor of Science in Geophysics at Millsaps College, Jackson, Mississippi in 2018.

Experience:
Geophysics Intern – Concho Resources Summer 2019
Near-surface Integrated Geophysical Survey – 2017 to 2018

Professional Memberships:
Society of Exploration Geophysicists (SEG)